THE DEVELOPMENT OF HIGHLY SELECTIVE MODIFIED GLASSY CARBON ELECTRODE BASED ON ACTIVATED CARBON-IRON OXIDE/GRAPHENE FOAM FOR ELECTROCATALYTIC OXIDATION OF URIC ACID AND DOPAMINE

By

MPAKANYANE EDWIN TEBOHO

Student Number: 201300016

Thesis Submitted in Fulfilment of the Requirement for the Degree of

MASTER OF SCIENCE IN CHEMISTRY

at

The National University of Lesotho

Faculty of Science and Technology

Department of Chemistry and Chemical Technology

SUPERVISOR : PROF. M. SEKOTA

CO-SUPERVISOR : PROF. H. ALEMU

Declaration

I, Mpakanyane Teboho Edwin, hereby declare that the research work presented in this thesis, titled "***The Development of Highly Selective Modified Glassy Carbon Electrode Based on Activated Carbon-Iron Oxide/Graphene Foam for Electrocatalytic Oxidation of Uric Acid and Dopamine***", submitted to the National University of Lesotho, Faculty of Science and Technology, Department of Chemistry and Chemical Technology, is my own and has not been submitted for any other university's degree or examination. All sources have been quoted, indicated, and acknowledged through complete reference.

_____ *On the* _____ *Day of* _____ *2023*

Candidate

_____ *On the* _____ *Day of* _____ *2023*

Supervisor

_____ *On the* _____ *Day of* _____ *2023*

Co-supervisor

Dedication

This MSc research work is dedicated to

My late mother

(‘Me’ Mariam Mamonyaka Mpakanyane)

Abstract

This research study explores the application of nanomaterial-modified glassy carbon electrodes (GCE) for the voltammetric determination of dopamine and uric acid. The GCE was fabricated with iron oxide, activated carbon, and graphene foam. Energy Dispersive X-ray Spectroscopy (EDS), Fourier Transform Infrared spectroscopy (FT-IR), X-ray diffraction Spectroscopy (XRD), and Scanning Electron Microscopy (SEM) were used to examine the microporous activated carbon, iron oxide spherical structure (Fe_3O_4) particles that were attached to the graphene foam sheets. A drop-dry method was used for electrode modification. AC-Fe_3O_4/GF/GCE was electrochemically interrogated in the ferrocyanide redox probe using cyclic voltammetry. The current intensity and the reversibility of the redox probe were enhanced in the presence of the electrochemical sensor.

Differential pulse voltammetry technique (DPV) was employed for individual determination of uric acid under the optimized experimental conditions; pH 6, scan rate 50 mV s^{-1}, pulse width 0.05 s, pulse amplitude 0.05 V, and supporting electrolyte 0.1 M phosphate buffer solution. A detection limit of 2.55 µM was obtained with an analytical linear range of 5 - 1630 µM. All selected foreign species showed no significant interference with the electrochemical determination of uric acid. Furthermore, dopamine analysis was carried out on AC-Fe_3O_4/GF/GCE using DPV. The electrochemical sensing was also optimized at various analytical conditions and a detection limit of 1.47 µM was obtained in the linear dynamic range of 2.5 to 450 µM. Glucose, glutamic acid, l-lysine, and ascorbic acid are a few of the interfering species that exhibited almost no impact on dopamine detection.

In addition, the simultaneous determination of uric acid and dopamine was conducted successfully. They have been determined by differential pulse voltammetry, and the modified electrode exhibited a linearity relationship over a wide range of uric acid concentrations from 2.5 to 450 µM, with a detection limit of 1.75 µM, (s/n = 3). A linear trend for the current response for dopamine concentrations ranging from 5 to 400 µM, with a detection limit of 2.7 µM, has also been obtained. The results, therefore, demonstrated the sensor's superior electrocatalytic activity and its high selectivity for dopamine and uric acid even when some foreign species were present. The average

recoveries from the real sample analyses of the urine samples showed that the proposed sensor could be put to use in the real sample analysis.

The developed electrode was generally found to be highly selective and sensitive toward uric acid and dopamine. It has achieved better sensing performances with a very low detection limit, wider linear ranges, and short analysis times as compared to most previously reported modified electrodes for the same analytes. Furthermore, the developed electrode was validated successfully for real sample analysis in biological fluids. The proposed methods have many attractive features, such as low cost, simplistic electrode preparation procedure, easy renewability, long-term usability, and rapid analysis. The developed electrode also displayed good repeatability and selectivity towards interfering substances. It is a promising modified electrode for the electrochemical detection of other electroactive important compounds in biological systems.

Graphical Abstract

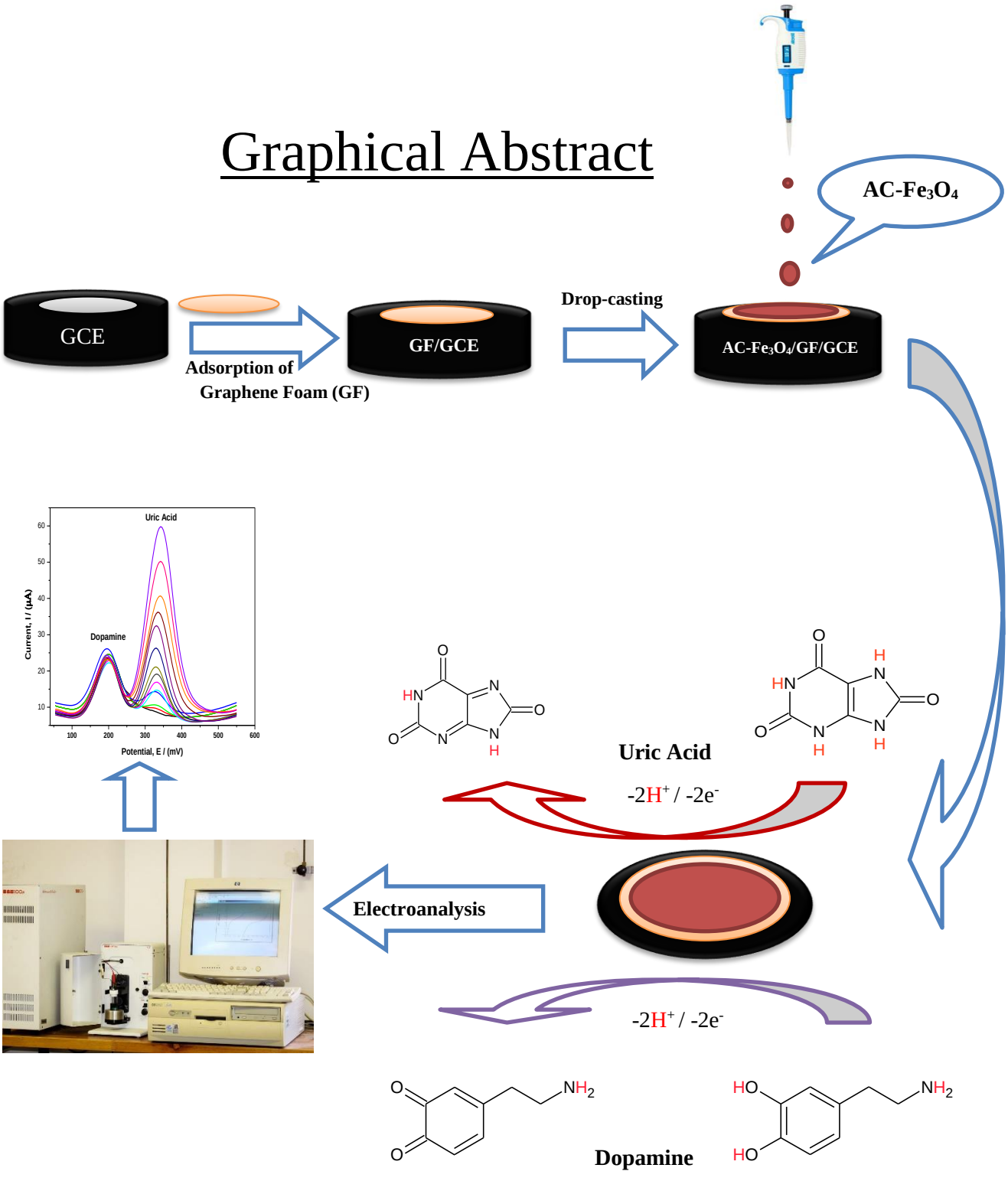

Acknowledgments

First and foremost, I wish to give my highest praise to God Almighty for laminating me with wisdom, love, blessings, and quantum understanding through this intellectual journey.

My deepest gratitude goes to Professor M. Sekota, my supervisor, for her insightful remarks, comments, and involvement throughout the master's research learning process and thesis writing. She also continues to support me in a variety of ways. Throughout this time, her patience, drive, and zeal, as well as her immense knowledge and advice, have been of assistance to me.

I would also like to express my gratitude to Professor H. Alemu, my co-supervisor, for his participation in this research project and thesis write-up. The study could not have been managed effectively without his active participation and input. I have gained a great deal from your instruction.

I would like to acknowledge the academic and technical staff in the Chemistry Department, and the members of the Inorganic research group for their patience and assistance in helping me to overcome the challenges that I encountered while working on this research project. I sincerely appreciate you.

My profound gratitude and thanks to Dr. P. Mafa, for his assistance with TEM, EDS, FT-IR, and XRD analysis. Indeed, I am grateful. Special thanks to Mr. L. Mafa, senior technician in the Department of Chemistry and Chemical Technology, for assisting with the reagents and equipment required to carry out this project successfully.

I want to say thanks to my fellow lab mates: Thank you, Mr. M. Mpopo, Ms. M. Kaneoa, Ms. M. Motheba, Mr. T. Rapelang, Mr. K. Makara, Mr. M. Hlongoane, Mr. T. Ramashamole, and Ms. S. Masiloane, for the discussions and fun we've had over the years.

Last but not least, I would like to thank my family, especially my mother for her emotional and moral support throughout my life and writing of this research work. My friends Mr. K. Khomo and Mr. P. Ramokhele merit a special mention.

Table of Contents

List of Abbreviations

AC	Activated carbon
Ag	Silver wire pseudo-reference electrode
Ag/AgCl	Silver/Silver chloride reference electrode
CE	Counter electrode
CV	Cyclic Voltammetry
DA	Dopamine
DPV	Differential Pulse Voltammetry
FT-IR	Fourier Transform Infrared
GCE	Glassy Carbon Electrode
GF	Graphene Foam
LoD	Limit of Detection
LoQ	Limit of Quantification
PBS	Phosphate Buffer Solution
RE	Reference Electrode
SEM	Scanning Electron Microscopy
SWV	Square-wave voltammetry
UA	Uric Acid
WE	Working electrode
XRD	X-ray diffraction

List of Symbols

A	Electroactive surface area (cm^2)
D	Diffusion coefficient ($cm^2 s^{-1}$)
E	Potential (V)
I_{pa}	Anodic peak current (µA)
I_{pc}	Cathodic peak current (µA)
n	Number of electrons
υ	Scan rate
V	Volts

List of Figures

List of Tables

List of Schemes

Chapter 1
Introduction

1.1 Uric Acid

Uric acid (UA), a nitrogen-containing heterocyclic compound of carbon, nitrogen, oxygen, and hydrogen, is one of the major antioxidants found in the human body [1]. According to the substance perspective, UA is known to have a molecular mass of 168.1103 $g.mol^{-1}$ with an atomic formula of $C_5H_4N_4O_3$ [2]. Uric acid is a biochemical compound that is only slightly soluble in water. Figure 1.1 depicts the structural formula of uric acid. Studies showed that UA is available in the greater part of creatures from microscopic organisms to people. Well-evolved creatures are known to contain uric acid essentially in blood and urine [3].

The kidney glomeruli filter a significant amount of uric acid, and approximately 90% of it is reabsorbed, indicating that it plays a significant physiological role. In the blood plasma, it functions as an antioxidant [2]. It is a decent cell reinforcement, peroxynitrite scavenger, and a strong reactive oxygen species scavenger (ROS). Uric acid, which serves as an antioxidant, is easily found in the cytosol of humans and mammals, particularly in the liver, nasal secretions, and vascular endothelial cells [4].

At physiological pH levels, uric acid is a weak acid with a pKa value of 5.75 and is mostly present as monosodium urate. Urate levels are significantly higher in humans (240 - 360 µM) than in other warm-blooded animals (30 - 50 µM in mice) as a result of uricase inactivation. Purine debasement in humans results in the formation of uric acid, but in other warm-blooded creatures, it is additionally degraded into allantoin by uricase, a catalyst that is generally found in the liver [5].

The degradation of purine nucleotides produces uric acid, which is a weak organic acid. Ingestion, the endogenous synthesis of purines from nonpurine precursors, and the reutilization of preformed purine compounds are all sources of purine nucleotides [6] [7]. Purine metabolism is mostly carried out in the intestine, liver, kidneys, and vascular endothelium. Nucleic acids derived from living and dying cells make up the majority of the purine found in endogenous sources, while dietary sources, animal proteins, and fructose catabolism make up the purine found in exogenous sources [7]. Uric acid production and elimination are in equilibrium in steady-state conditions.

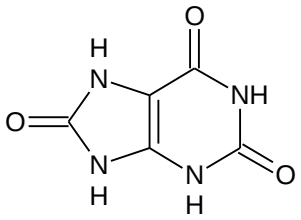

Figure 1.1: Structure of Uric Acid: (2, 6, 8 – Trihydroxypurine).

In humans, uric acid is an effective free radical scavenger, but it is also a sign of high levels of harmful oxidative stress caused by increased xanthine oxidase activity [8]. Not only it is important to keep UA levels at a healthy level because UA plays a crucial role in how the human body works, but also because higher or lower UA levels can cause or reveal a variety of diseases [3]. For instance, individuals have changed enormously their eating routines, and the purines they consume have likewise expanded, bringing about a huge increase in the rate of gout and hyperuricemia sicknesses.

The primary tool for determining various clinical contentions connected to the human body's level of uric acid is the clinical evaluation for uric acid [5], [9]. The concentration of UA contained in blood or pee is connected with the state of being of an individual and problems of UA are side effects of a few illnesses like gout and hyperuricemia [10], [11].

Gout, a common and painful rheumatic disease, is caused by the accumulation of monosodium urate monohydrate microcrystals, or uric acid, in various body parts. It is a painful type of fiery joint inflammation, that happens when uric acid levels get excessively high, which prompts the development of crystals that deposit themselves in the joints [12]. Most people who have gout need to take a medication that works to lower uric acid levels, like allopurinol, to avoid future flare-ups. To reduce their intake of foods high in purines, others alter their diet [13]. With high plasma uric acid levels, hyperuricemia is closely linked to cardiovascular and renal disorders.

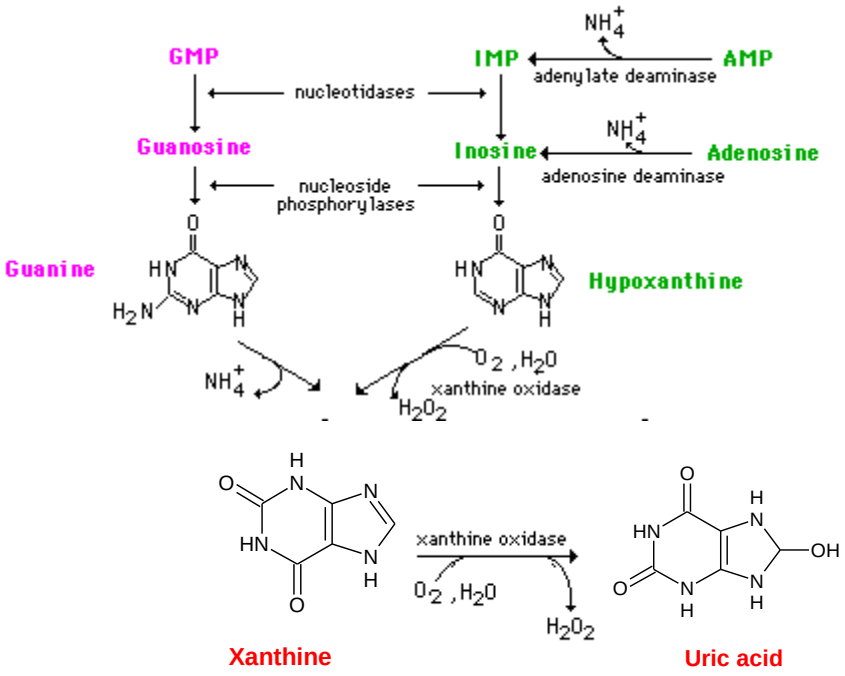

Figure 1.2: Purine nucleotide degradation and uric acid formation [14].

Figure 1.2 depicts the degradation of purine nucleotides which begins with nucleotidase activity in a reaction that releases phosphate from nucleotides and produces nucleosides, adenosine, and guanosine. For uric acid development, the xanthine oxidoreductase enzyme oxidizes hypoxanthine to xanthine, and lastly xanthine to uric acid. Figure 1.2 shows a comprehensive reaction mechanism for this biosynthetic procedure.

1.2 Dopamine

Dopamine (DA) is an organic molecule that has a catechol structure (a benzene ring with two hydroxyl groups), and one amine group that is attached to an ethyl chain. It has a molecular formula of $C_8H_{11}NO_2$ and a molecular mass of 153.1784 $g.mol^{-1}$. Figure 1.3 shows the 2-dimensional structure of dopamine.

Dopamine serves a wide range of well-defined functions in humans, such as controlling coordinated movement, metabolism, addiction, reward, and hormone secretion [15]. It is produced in the brain and used to send messages between nerve cells in the nervous system. Sometimes it is referred to as a chemical messenger. Learning, motivation, blood vessel function, attention, pain processing, kidney function, movement, and other aspects of human behavior are all impacted by dopamine [16].

Brain neurotransmission is a fundamental cycle for neuronal separation and development, as well as for the advancement of interneuronal correspondence and neuronal hardware [17]. Neurotransmitter issues are because of abnormal metabolism or transport of the biogenic amines, glycine, vitamin B6, and glutamic acid. The biogenic amines are practically significant groups of mind synapses and comprise catecholamines (dopamine, norepinephrine, and epinephrine) and serotonin. Dopamine and serotonin play key parts in the mind, including the control of headway, temperament, and conduct [18].

Dopamine is communicated in limited cerebrum regions associated with various integrative capabilities adding to computerized ways of behaving that are profoundly versatile. It can go about as a strong controller and integrator of various parts of the mind's capabilities.

Dopamine enters the bloodstream as a hormone and has a minor impact on the "fight-or-flight" mentality. The body's response to a perceived or actual stressful situation, such as the need to flee danger, is known as the "fight or flight" response. Dopamine deficiency can result in fatigue, lack of motivation, and unhappiness in humans [19]. Additionally, memory loss, difficulty concentrating, and issues with sleeping may occur. However, people may experience feelings of euphoria and energized if the level of dopamine is high.

It is equipped for directing human comprehension and feelings and exists as a primary catecholamine in the focal sensory system (CNS). The grouping of DA shifts under certain conditions, resulting in serious health and mental issues. Strange degrees of DA might bring about different neurological infections, like Parkinson's illness, Huntington's sickness, and schizophrenia [20], [21], and [22].

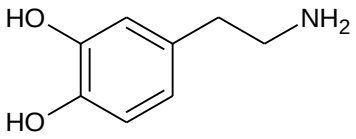

Figure 1.3: Dopamine structure: 4 - (2-aminoethyl) benzene-1, 2-diol.

A condition known as Parkinson's disease occurs when a portion of the brain deteriorates, resulting in more severe symptoms over time. Although this condition is most well-known for impairing balance, muscle control, and movement, it can also have a wide range of effects on the senses, thinking abilities, and emotional well-being [22]. Under normal circumstances, the brain uses chemicals known as neurotransmitters to control how the brain cells (neurons) communicate with each other. Parkinson's disease is the second most common age-related degenerative brain disease. One of the most important neurotransmitters, dopamine, is lacking in Parkinson's disease patients. Therefore, Parkinson's disease is characterized by slowed movements and trembling due to a deficiency of dopamine [23].

The term "schizophrenia" refers to a condition and a range of disorders that all involve hallucinations and delusions that are disconnected from reality. High levels of dopamine in particular brain regions may be the cause of some of the symptoms of schizophrenia. Although it is a serious condition that can be treated, many people with it can still live happy, and fulfilled lives. Lack of motivation is one of the other symptoms that may be brought on by a lack of dopamine in another part of the brain [24].

Drugs that imitate dopamine as the natural neurotransmitter are known as dopamine agonists. The brain's nerve cells respond comparatively to natural dopamine when dopamine agonists attach to and trigger their dopamine receptors. Parkinson's disease, depression, attention deficit

hyperactivity disorder, hyperprolactinemia, and low sex drive are all treated with dopamine agonists [20], [23].

Dopamine antagonists are medications that are attached to and inhibit dopamine receptors in the brain. This indicates that they prevent the subsequent nerve cells from receiving dopamine [23]. Dopamine antagonists are a common class of antipsychotics used to treat nausea, Schizophrenia, and bipolar disorder.

Figure 1.4 depicts a detailed biosynthetic pathway for neurotransmitter formation. Briefly, phenylalanine hydroxylase converts phenylalanine to tyrosine, tyrosine hydroxylase hydroxylates tyrosine to L-3, and 4-dihydroxyphenylalanine (L-DOPA). DOPA is then transformed into dopamine by aromatic amino acid decarboxylase. Dopamine-b hydroxylase hydroxylates dopamine to norepinephrine, which is methylated to epinephrine by phenylethanolamine N-methyltransferase [24].

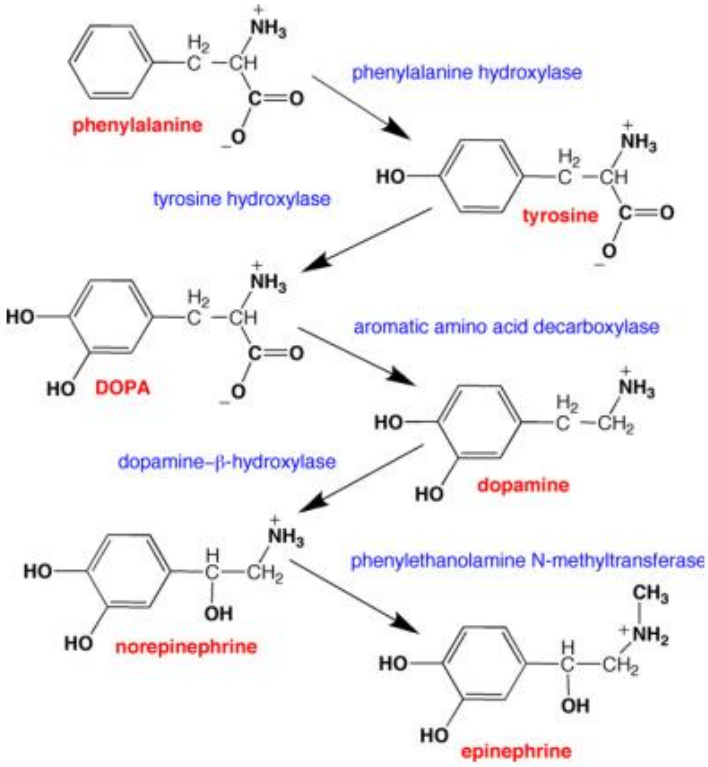

Figure 1.4: Biosynthetic pathway for neurotransmitters [24].

1.3 Problem Statement

High levels of both uric acid and dopamine in human body fluids are of great concern in pharmaceutical, clinical health, and medical research. These biological analytes require constant monitoring which is currently underprovided in medical health.

Dopamine and uric acid are generally viewed as vital atoms for physiological cycles in human digestion and they exist together in human body fluids. Along these lines, it is fundamental to foster particular and delicate techniques for their assurance in a logical application and analytic exploration [25].

Traditional methods for the detection of these biological analytes involve; a collection of samples, retrieval of the samples to a central laboratory, labor-intensive sample clean-up, expensive instrumentation, and pre-treatment steps followed by quantification. In addition to the lengthy and uneconomical steps involved, contamination of dopamine and uric acid may occur during the transportation of the samples from the field causing inaccurate analytical results.

Hence, it is desirable to develop a technique that enables rapid measurements for real clinical or biological samples. Electrochemical sensors present a promising alternative to conventional methods for the determination of dopamine and uric acid in either clinical or biological research due to their rapid and sensitive measurement protocol.

Therefore, the objective of this study is to develop an electrochemical method for the simultaneous determination of uric acid and dopamine using a glassy carbon electrode modified with activated carbon, iron oxide, and graphene foam composite.

However, to the best of our knowledge, no electrochemical method based on the application of (AC-Fe_3O_4/GF/GCE) modified glassy carbon electrode (GCE) has been reported for uric acid and dopamine determination.

Graphene foam with a two-dimensional layered structure has been successfully established as a new paradigm in the chemistry of nanomaterials in recent years due to its excellent thermal conductivity and electrical conductivity properties [26], [27]. It was found to effectively improve the surface area, electrocatalytic activity, conductivity, and stability of modified electrodes to

enhance electrochemical performance. Graphene foam coupled with activated carbon and iron oxide, could increase the surface area of the modified electrode due to their small particle sizes and paramagnetic properties, respectively [28], [29].

1.4 Aim of the study

The focus of this project is to develop a modified glassy carbon electrode based on activated carbon, iron oxide, and graphene foam that can provide synergic electrocatalytic activity for better detection, and selectivity towards uric acid and dopamine.

1.4.1 The specific objectives

- To synthesize, characterize, and fabricate glassy carbon electrodes with graphene foam (GF) and magnetite (iron oxide).
- To explore electrochemical sensing of the modified electrode towards an individual and simultaneous detection of uric acid and dopamine under optimized experimental parameters.
- To explore the linear range, determine the sensor’s limit of detection and limit of quantification for uric acid and dopamine.
- To study the impact of foreign substances and conduct real-sample analysis to determine the developed sensor's analytical application in biological samples.

1.5 Research Justification

Dopamine (DA) is a crucial member of the catecholamine family of neurotransmitters that have received a lot of attention in clinical research because it plays a crucial role in mammals' cardiovascular, metabolic, and central nervous system functions. The human body's homeostasis and metabolism systems are significantly regulated by the biomolecule compound uric acid (UA) [30].

Quantitative and subjective assurance of uric acid and dopamine is essentially valuable to give related data, particularly in the fields of drug, nursery, pathology, and clinical fields. In terms of detection limit and quantification of the amount of uric acid and dopamine, several techniques have been proposed that appear to be consistent and sensitive.

The analytical merits of the detection method determine how successful the process of detecting both dopamine and uric acid levels in a biological medium. The growing interest in green Chemistry has a significant impact on the selection of an appropriate method, even though analytical merits are relevant in determining the analytical method's applicability.

Therefore, it is pertinent to develop an environmentally friendly and effective analytical electrochemical method. Electrochemical techniques are inexpensive, simple to use, require small samples, have low detection limits, and produce the least amount of solvent waste possible. Because of these aspects, they are close to ideal analytical techniques for quantifying analytes in various matrices.

1.6 Thesis Outline

This thesis is presented in five chapters:

- **Chapter 1** presents the introduction, problem statement, aim and objectives, research justification, and thesis outline.

- **Chapter 2** This chapter summarizes an extensive related literature review on the electroanalysis of dopamine and uric acid. It also covers the fundamental concepts of electroanalytical methods.
- **Chapter 3** highlights the research design, method of modifying electrodes, and method of preparing solutions. Features the list of materials, equipment, and reagents used in this research. It also discusses different microscopic and spectroscopic characterization techniques used.
- **Chapter 4** contains results and discussions on the electroanalysis of dopamine and uric acid on the modified glassy carbon electrode. Moreover, detailed discussions of the synthesized materials used to modify electrodes.
- **Chapter 5** this chapter presents the general conclusions and recommendations for future work.

References

1. Durgapal, S., Jantwal, A., Upadhyay, J., Joshi, T., & Kumar, A. (2022). Uric acid. In *Antioxidants Effects in Health*, 505-516

2. Maiuolo, J., Oppedisano, F., Gratteri, S., Muscoli, C., & Mollace, V. (2016). Regulation of uric acid metabolism and excretion. *International Journal of Cardiology*, *213*, 8-14.

3. Wang, Q., Wen, X., & Kong, J. (2020). Recent progress on uric acid detection: a review. *Critical Reviews in Analytical Chemistry*, *50*, 359-375.

4. Mahomoodally, M. F., & MA-L, E. R. (2022). Uric acid. In *Antioxidants Effects in Health*, 167-176.

5. So, A., & Thorens, B. (2010). Uric acid transport and disease. *The Journal of Clinical Investigation*, *120*, 1791-1799.

6. Benedict, J. D., Forsham, P. H., & Stetten, D. (1949). The metabolism of uric acid in the normal and gouty human studied with the aid of isotopic uric acid. *Journal of Biological Chemistry*, *181*, 183-193.

7. Cortese, F., Giordano, P., Scicchitano, P., Faienza, M. F., De Pergola, G., Calculli, G., ... & Ciccone, M. M. (2019). Uric acid: from a biological advantage to a potential danger. A focus on cardiovascular effects. *Vascular Pharmacology*, *120*, 106565 (1-12).

8. Higgins, P., Ferguson, L. D., & Walters, M. R. (2011). Xanthine oxidase inhibition for the treatment of stroke disease: a novel therapeutic approach. *Expert Review of Cardiovascular Therapy*, *9*, 399-401.

9. Dong, J., Hu, Y., Zhu, S., Xu, J., & Xu, Y. (2010). A highly selective and sensitive dopamine and uric acid biosensor fabricated with functionalized ordered mesoporous

carbon and hydrophobic ionic liquid. *Analytical and Bioanalytical Chemistry*, *396*, 1755-1762.

10. Wang, C., Yuan, R., Chai, Y., Zhang, Y., Hu, F., & Zhang, M. (2011). Au-nanoclusters incorporated 3-amino-5-mercapto-1, 2, 4-triazole film modified electrode for the simultaneous determination of ascorbic acid, dopamine, uric acid and nitrite. *Biosensors and Bioelectronics*, *30*, 315-319.

11. Weng, Y. K., Rosli, A. R. M., & Yusoff, F. (2019). Magnetite graphene for electrochemical determination of uric acid. *Malaysian Journal of Analytical Sciences*, *23*, 407-422.

12. Chilappa, C. S., Aronow, W. S., Shapiro, D., Sperber, K., Patel, U., & Ash, J. Y. (2010). Gout and hyperuricemia. *Comprehensive Therapy*, *36*, 3-13.

13. Halabe, A., & Sperling, O. (1994). Uric acid nephrolithiasis. *Mineral and Electrolyte Metabolism*, *20*, 424-431.

14. Pasalic, D., Marinkovic, N., & Feher-Turkovic, L. (2012). Uric acid as one of the important factors in multifactorial disorders–facts and controversies. *Biochemia Medica*, *22*, 63-75.

15. Liu, Q., Gao, T., Liu, W., Liu, Y., Zhao, Y., Liu, Y., & Li, C. (2020). Functions of dopamine in plants: a review. *Plant Signaling & Behavior*, *15*, 1827782-8.

16. Marecos, C., Ng, J., & Kurian, M. A. (2014). What is new for monoamine neurotransmitter disorders? *Journal of Inherited Metabolic Disease*, *37*, 619-626.

17. Herlenius, E., & Lagercrantz, H. (2001). Neurotransmitters and neuromodulators during early human development. *Early Human Development*, *65*, 21-37.

18. Kurian, M. A., Gissen, P., Smith, M., Heales, S. J., & Clayton, P. T. (2011). The monoamine neurotransmitter disorders: an expanding range of neurological syndromes. *The Lancet Neurology*, *10*, 721-733.

19. Girault, J. A., & Greengard, P. (2004). The neurobiology of dopamine signaling. *Archives of Neurology*, *61*, 641-644.

20. Cao, X. H., Zhang, L. X., Cai, W. P., & Li, Y. Q. (2010). Amperometric sensing of dopamine using a single-walled carbon nanotube covalently attached to a conical glass micropore electrode. *Electrochemistry Communications*, *12*, 540-543.

21. Fernandes, S. C., Vieira, I. C., Peralta, R. A., & Neves, A. (2010). Development of a biomimetic chitosan film-coated gold electrode for determination of dopamine in the presence of ascorbic acid and uric acid. *Electrochimica Acta*, *55*, 7152-7157.

22. Thomas, T., Mascarenhas, R. J., Nethravathi, C., Rajamathi, M., & Swamy, B. K. (2011). Graphite oxide bulk modified carbon paste electrode for the selective detection of dopamine: A voltammetric study. *Journal of Electroanalytical Chemistry*, *659*, 113-119.

23. Lange, K. W., Nakamura, Y., Chen, N., Guo, J., Kanaya, S., Lange, K. M., & Li, S. (2019). Diet and medical foods in Parkinson's disease. *Food Science and Human Wellness*, *8*, 83-95.

24. Daubner, S. C., Le, T., & Wang, S. (2011). Tyrosine hydroxylase and regulation of dopamine synthesis. *Archives of Biochemistry and Biophysics*, *508*, 1-12.

25. Wang, H., Ren, F., Wang, C., Yang, B., Bin, D., Zhang, K., & Du, Y. (2014). Simultaneous determination of dopamine, uric acid and ascorbic acid using a glassy carbon electrode modified with reduced graphene oxide. *Rsc Advances*, *4*, 26895-26901.

26. Zhao, Y. H., Wu, Z. K., & Bai, S. L. (2015). Study on thermal properties of graphene foam/graphene sheets filled polymer composites. *Composites Part A: Applied Science and Manufacturing*, *72*, 200-206.

27. Yocham, K. M., Scott, C., Fujimoto, K., Brown, R., Tanasse, E., Oxford, J. T., & Estrada, D. (2018). Mechanical properties of graphene foam and graphene foam—tissue composites. *Advanced Engineering Materials*, *20*, 1800166 (1-9).

28. Ntakirutimana, S., Tan, W., Anderson, M. A., & Wang, Y. (2020). Editors' Choice—Review—Activated carbon electrode design: Engineering tradeoff with respect to capacitive deionization performance. *Journal of The Electrochemical Society*, *167*, 143501 (1-20).

29. Teja, A. S., & Koh, P. Y. (2009). Synthesis, properties, and applications of magnetic iron oxide nanoparticles. *Progress in Crystal Growth and Characterization of Materials, 55*, 22-45.

30. Sinha, A., Lu, X., Wu, L., Tan, D., Li, Y., Chen, J., & Jain, R. (2018). Voltammetric sensing of biomolecules at carbon-based electrode interfaces: A review. *TrAC Trends in Analytical Chemistry*, *98*, 174-189.

Chapter 2
Literature Review

2.1 Electrochemical studies of uric acid and dopamine at modified electrodes

Enzyme-based biosensors are popular sensing devices that have been introduced and are widely known to convert biological responses into readable analytical signals. They have good specificity and improve the selectivity and responsiveness of electrochemical detection of biological compounds [1]. The utilization of biosensors permits immediate, inexpensive, quick, and accurate measurement of uric acid or dopamine in real samples.

Screen-printed electrodes, for instance; have been utilized for the improvement of single-use, disposable sensors for clinical, environmental, and modern investigations [2]. This strategy has the benefits of straightforward development, high reproducibility, minimal expense, and a wide selection of materials. However, heaps of waste disposable sensors are produced and generate environmental pollution. In addition, the relative instability of enzyme-based biosensors and their sensitivity to pH, temperature, humidity, and other environmental factors have occasionally prompted researchers to look for enzyme-free approaches [3].

In recent years, new materials for sensing that can be deposited on an electrode's surface have been developed by researchers as a means of overcoming these challenges. Consecutively, these may increase the electrode's catalytic properties, resulting in a more stable, selective, and sensitive electrochemical sensor [4]. The electrochemical sensors act as redox mediators with a large specific surface area to improve the electrode's sensitivity and enhance the charge transfer.

Chemical sensors, in contrast to biosensors, contain components that are not biologically active, increasing their sensitivity and selectivity for analytes of interest. Modified electrodes are often utilized as sensing elements in electrochemical sensors. Different inorganic and organic materials with superior electrical conductivity and catalytic properties can be used to make these types of modified electrodes.

2.1.1 Electrochemical analyses of individual uric acid and dopamine

2.1.1.1 Electroanalysis of Dopamine

Dopamine is the most essential catecholamine neurotransmitter in the human central nervous system. It is found in the brain and vital for the renal, hormonal, and cardiovascular systems to function properly. High concentration levels of dopamine are connected with neurological problems, for instance, schizophrenia and Parkinson's illness, and variances of dopamine levels are critical in observing logical frameworks in the human mind [5]

Various materials have been used to fabricate electrodes for the electrochemical analyses of dopamine. Materials such as carbon-based nanomaterials [6], graphene and graphene oxide [7], [8], polymer films [9], [10], [11], [12], [13], metal nanoparticles [14], [15], [16], and metal oxides nanocomposite [17], [18] have been utilized in electroanalysis. These materials offer a large surface area, which increases the electrocatalytic activity and sensitivity toward the analytes of interest.

Metal oxide/carbon nanotube composites can be utilized for the electrochemical detection of dopamine. These composites have excellent mechanical properties, a large surface area, biocompatibility, and resistance to chemicals [19], [20]. Thus, Adekunle, S., et al. [21] used the edge-plane pyrolytic graphite electrode (EPPGE) modified with iron oxide (cubic spinel structure) coupled with single-walled carbon nanotubes for dopamine detection. The modified electrode exhibited an appreciable electrocatalytic activity with seven times more current response relative to bare (EPPGE), leading to the linear concentration range of 3.2 – 31.8 µM. Moreover, the electron transfer efficiency of ≈ 0.26 cm s^{-1} and 3.44 µA/ µM sensitivity were found. The detection limit of 0.36 µM was achieved using the square-wave voltammetry technique under optimum experimental conditions.

Similarly, MWCNTs/MoS_2 decorated with cobalt oxide polyhedrons demonstrated high significance in a physiological application for dopamine, as reported by Mani, V., et al. [22]. The developed composite showed good porosity, excellent electrocatalytic activity, high surface area, and sensitivity. In addition, the oxidation peak current was enhanced due to the presence of the modifier, and the superior detection limit of 13.45 nM was obtained in the linear range of 0.03 –

1950.2 µM, and 2150.2 – 5540 µM using an amperometric sensing platform. The sensor possessed good durability and was feasible for practical application in rat brains and human blood.

A new stable $Fe(CN)_6^{3-/4-}$/ poly (butyl viologen) thin film-modified platinum electrode was used as an electrochemical sensor and exhibited high stability, and electron transfer efficiency in the linear range of 20 µM – 1.25 mM using an amperometric technique suggested by Hsu, Chih-Yu, et al. [23]. The detection limit of 2.46 µm was obtained. Another composite tin-oxide-graphene/poly (4-amino benzene sulfonic acid) (TiO_2/GF/4-ABSA) electrochemical sensor has been studied by Xu, Chu-Xuan, et al. [24]. The mediated oxidation of dopamine at the modified glassy carbon electrode under optimized conditions (pH = 7) in CV showed very high current intensity compared to the unmodified glassy carbon electrode. The limit of detection of 0.1 µM was obtained in the linear dynamic range of 1 – 400 µM using the differential pulse voltammetry technique. The sensor demonstrated good reproducibility and high selectivity for dopamine in the presence of potentially interfering species such as Na^+, Cl^-, Cu^{2+}, CO_3^{2-}, and NO_3^-.

Conducting polymers are exceptionally common electrode modifiers that can be chemically or electrochemically deposited on bare electrode surfaces. The delocalization of the electrons in the polymeric backbone is caused by their extended π-conjugated structure, which alternates between single and double bonds. They are biocompatible and have excellent electrical conductivity.

They can likewise be combined with metal-oxide nanoparticles [25] or carbon-based nanomaterial [26] to form a stable defensive film, inhibit electrode fouling, and improve electrode selectivity towards target analytes. Polymers-based sensors have hydrophobic, hydrophilic, ion exchange, or electrostatic interaction properties, which makes them appropriate candidates for electroanalyses. A few important conducting polymers are; polyaniline (PANI), poly(o-aminophenol), poly(o-phenylenediamine), polythiophenes (PT), polymethyl thiophene (PMT), poly(3,4-ethylene dioxythiophene) (PEDOT), polypyrrole (PPY) [27].

Huong, Vu Thi, et al. [28] have developed an electrochemical sensor based on Nafion/single-walled carbon nanotubes/poly (3-methyl-thiophene)-glassy carbon electrode for dopamine detection in real sample analysis, (dopamine-hydrochloride drug injection). The Pharmaceutical injection (DA.HCl) was analyzed by the standard addition method, and the results proved the sensitivity of the modified electrode with less than 0.4% difference from the labeled concentration. The sensor displayed a superior electron transfer mechanism at the electrode surface (adsorption and diffusion modes), in the linear range of 1.5 – 20 µM and 20 – 120 µM using differential pulse voltammetry. Although the (Nafion/SWCNTs/PMT/GCE) showed a high specific surface area and adsorptive properties, the detection limit was not outlined.

In a research conducted by Xu, Guiyun, et al. [29], the preparation of an electrochemical sensor for the selective and oxidation of dopamine was investigated by electropolymerization of poly (3,4-ethylene dioxythiophene) (PEDOT) film coupled with carbon nanotubes at carbon paste electrode. In addition, Mathiyarasu, J., et al. [30], prepared a similar conducting polymer (PEDOT) and combined it with single-walled-carbon nanotubes at Pt-microelectrode. The modified electrodes are worth consideration due to charge interaction in the sensing mechanism. Again, high-affinity binding of dopamine to PEDOT-carbon-based nanostructures was observed as the enhanced peak current response was achieved using DPV.

Both modified electrodes improved redox reversibility, excellent catalytic properties in the linear range of 0.1 – 20 µM, and the detection limit of 20 nM [29] and 100 nM [30] respectively. However, the results indicated that the presence of miniaturized Pt-microelectrode modified with PEDOT/SWCNTs composite constitutes a promising device for in-vivo electroanalysis of dopamine compared to a modified carbon paste electrode.

Swamy, B. K., et al. [31] investigated the use of carbon fiber/single-walled-carbon nanotubes fabricated on microelectrode for dopamine detection using fast-scan cyclic voltammetry. Microelectrode modified with carbon-based nanomaterials displayed high selectivity towards dopamine and less fouling. However, the linear concentration range and the detection limit of dopamine were not shown.

Polymerconsolidated with metal particles show higher surface area-to-volume proportion and electric integration. The polymer framework additionally acts as the stabilizing medium that prohibits the agglomeration of metal particles during the use as the catalyst.

Therefore, Kumar, S., Senthil, et al. [32] described the preparation of gold-nanoparticles/PEDOT composite which showed a significant electrocatalytic effect on the oxidation of dopamine and improved peak-to-peak separation to ascorbic acid. The modified electrodes depict good reproducibility and stability of the developed sensor.

Furthermore, gold nanoparticles/PEDOT-GCE exhibited the detection limit of 2 nM within the linear range of 0.5 – 2 µM, and the oxidation peak current for dopamine detection was enhanced due to the large surface area of Au-nanoparticles.

C. Zanardi et al. and coworkers [33] developed a similar electrode sensor that showed preserved repeatability and reproducibility. Electroanalysis of DA was carried out in the concentration range of 1.5 – 40.9 ppm, however, the detection limit was not reported in their work.

In addition, AuNPs/PEDOT nanocomposite was described by Atta, Nada F., et al. [34] and used to modify Au-electrode and two linear ranges were obtained as 0.5 – 20 µM and 25 – 140 µM with the detection limits of 0.39 nM and 1.55 nM respectively. The electroanalysis was performed in the presence of sodium dodecyl sulfate (SDS). The modified gold electrode exhibited good electron transfer, and stable oxidation peak response over multiple cycles using cyclic voltammetry. The sensor displayed feasible practical application in the urine sample and a 98.5% - 101.4% recovery range was obtained.

In another study, S. Lupu et al. [35] prepared Prussian blue/PEDOT-Pt-electrode for electrochemical determination of dopamine as one type of neurotransmitter using differential pulse voltammetry, and gold disk microelectrode array using cyclic voltammetry [36]. The modified electrodes showed high catalytic activity for dopamine in the linear range and detection limit of 4 x 10^{-5} – 1 x 10^{-3} M (40 µM LoD) and 10 µM to 50 µM (4.3 µM LoD) respectively. Electrodes exhibited excellent electrocatalytic activity and stability in aqueous solutions. Oxidation peak current resolution was achieved in the presence of ascorbic acid, with high selectivity towards dopamine as the analyte of interest.

Mashhadizadeh, M. H., et al. [37] fabricated an electrochemical sensor by modifying Au-electrode with nickel hexacyanoferrate/ poly (1-naphthol) hybrid (NiHCF-PNH) composite for dopamine detection. The modified Au-electrode showed excellent electrocatalytic efficiency, easy preparation, facilitated oxidation reaction, and stability. The sensor also displayed high selectivity for dopamine in the presence of interfering species such as ascorbic and uric acid. Two linear concentration ranges were achieved (linear response from 0.1 – 4.3 µM and 4.3 to 9.6 µM) with the detection limits of 2.1 x 10^{-8} M and 0.02 µM. The polymer provides a channel for positively charged species thereby rebelling against negatively charged species and limiting interferences.
The negative redox peak potentials shift was observed demonstrating that the reaction was accompanied by protonation. Again, the semi-circle from the Nyquist plot was relatively small, indicating the conductivity and high catalytic activity of the electrode, thus facilitating charge transfer.

Moreover, a platinum electrode was modified with Pd-nanoparticles combined with poly (3-methyl-thiophene) film and an electrochemical investigation of dopamine was performed using differential pulse voltammetry (DPV), reported by Atta, N. F., et al. [38]. The Pd-modified electrode exhibited a dramatic catalytic effect with the enhancement of peak current response compared to a bare-Pd electrode from cyclic voltammograms.

A negative peak potential shift in cyclic voltammetry showed that the developed hybrid film possesses excellent electrocatalytic properties. High catalytic active sides of the sensor film favor the sensing of dopamine in the linear range of 0.05 – 1 µM with a 9 nM detection limit. The results demonstrate a better sensitivity of 1.37 µA/µM, and high percentage recoveries, indicating the sensor's applicability in real sample analyses.

Copper-electrode coated with PEDOT layers for selective dopamine determination was prepared by Stoyanova, A., et al. [39], and showed the largest oxidation peak current signal towards dopamine when compared with unmodified Cu-electrode. During the measurements, differential pulse voltammetry was carried out in the concentration ranges of 6 nM – 2 µM and 1 to 5 nM. However, large Cu crystals found suffered from surface destruction along the crystalline edges when subjected to electroanalysis measurements. On the other hand, small (~ 0.5 µm) Cu crystals deposited on the PEDOT-electrode improve large surface coverage and thus provide high sensitivity and stability of the modifier.

A graphene–polyaniline nanocomposite film electrochemical aptasensor for dopamine measurement was described by Dui, Su, et al. [40]. Due to the synergistic effect of graphene and polymer, the resulting sensor had a better peak current response, electron transfer activity, and high conductivity for dopamine electroanalysis. The electrochemical aptasensor had a detection limit of 0.002 nM with a 0.007 - 90 nM linear range.

In addition, a sensor was acquired by electropolymerization of p-amino benzene thiol, trailed by its doping with gold nanoparticles for the amperometric detection of dopamine in human serums, and showed high responsiveness and selectivity with a linear dynamic range of 0.02 µM to 0.54 µM and detection limit of 7.8 nM [41].

2.1.1.2 **Electroanalysis of uric acid**

In the human body, uric acid can be found in biofluids such as urine and blood [42]. The inert purine metabolism produces this biological compound as its final product. Numerous diseases, including gout, hyperuricemia, diabetes, high cholesterol, high blood pressure, and kidney disease, have been linked to high concentrations of uric acid in the human body [43]. As a result, UA concentration monitoring in biological fluids may be utilized as an early warning system to avoid abnormal levels.

For electrochemical detection of UA, zinc oxide, gold nanoparticles, and reduced graphene oxide-based materials have also received a lot of attention from researchers in recent years. M. Eryigit et al. [44] and Y. Xue et al. [45] have developed an electrochemical sensor based on reduced graphene oxide/zinc oxide (rGO/ZnO) nanocomposite on indium tin oxide (ITO) electrode and poly (diallyldimethylammonium chloride) gold nanoparticles-graphene nanosheets (PDDA-AuNPs/GNs) – on GCE electrode, respectively.

According to M. Eryigit, et al. [44], the rGO sheets can form a uniform thin film on the surface of ITO and provide specific active sites for uric acid oxidation, promoting the formation of well-distributed zinc oxide nanosphere-like particles on the surface of rGO sheets. This proved the synergistic effects between the zinc oxide nanostructures and rGO. Again, ZnO/rGO had a huge surface area and electroactive sides, which led to the improvement of synergist exhibitions toward the oxidation of UA. At the ZnO/rGO-GCE electrode, the linear range of 1 – 400 µM for UA and 150.7 µA/µM sensitivity were obtained.

On the contrary, Y. Xue et al. [45] investigated the (PDDA-AuNPs/GNs) electrochemical sensor and found that the modified electrode had lower peak potentials (negative shift) and higher peak currents than the bare GCE using cyclic voltammetry. In addition, the composite of (PDDA-AuNPs/GNs) enhanced the electrochemical oxidation reaction of UA, as evidenced by the sharpness of the peaks and the decrease in the overpotential. The calculated LoD was 0.1 µM, and the peak currents of UA increased linearly with a concentration between 0.5 µM and 20 µM.

The α-Fe_2O_3 nanoflowers were dispersed on a GCE surface and exhibited the capacity of the modified electrode (α-Fe_2O_3/GCE) to oxidize UA at a lower potential (480 mV) compared to unmodified GCE (600 mV), investigated by Suresh, R., et al. [46]. The developed sensor was tested using chronoamperometry (CA), and a linear concentration ranging from 7.9 µM to 67 µM was obtained. Although the selectivity and detection limit were not reported, the sensor did exhibit some stability. Uric acid's oxidation peak potential was shifted to a lower potential, indicating the modifier's effectiveness on the electrode surface.

Ghanbari, K. H. and Hajian, A. et al. [47] considered the synergistic electrocatalytic impact of (Au/ZnO/PPY/RGO) - modified glassy carbon electrode for the electrochemical determination of UA. The linear range that was obtained by DPV in a solution of 0.1 M phosphate buffer at a pH of 7.0 was between 1.0 µM to 680 µM, with a 0.09 µM LoD. Over and above that, the proposed sensor was utilized for measurement in human serum and urine samples with 95.5% to 102% recoveries. In addition, in the presence of ascorbic acid and epinephrine, it exhibited excellent electrocatalytic activity and good selectivity for uric acid.

Conducting polymers are another promising material that could be used as a platform for sensors. They share electronic characteristics with metals.

Reddy Y. Veera Manohara, et al. [48] and associates have manufactured poly (dipicolinic acid)/SiO_2@Fe_3O_4 by electropolymerization on the carbon paste electrode for uric acid determination.

They outlined that the poly (DPA)/SiO_2@Fe_3O_4 - CPE electrode showed increased peak current intensity towards the UA contrasted with the unmodified CPE in the neutral phosphate buffer solution (pH 7), because of the satisfactory behavior of the nanocomposite.

Moreover, the poly (DPA)/SiO_2@Fe_3O_4 nanocomposite had a large surface area, which speeds up electron transport and provides a good sensing signal. By interacting with uric acid through C=O bonds, the composite fiber's electrocatalytic behavior improves, activating NH groups and accelerating electronic charge transfer kinetics. The peak current of UA at poly (DPA)/SiO_2@Fe_3O_4 film gave a decent linear response in the range of 1.2 - 8.2 µM with a detection limit of 0.4 µM, at S/N = 3 using differential pulse voltammetry.

In further studies, Dai, H., et al. [49] investigated the electrocatalytic oxidation of UA on the surface of a glassy carbon electrode using polytetraphenylporphyrin, polypyrrole, and graphene oxide by differential pulse voltammetry (DPV). To determine UA, a 0.1 M phosphate buffer solution with a pH of 7.0 was chosen as the best-supporting electrolyte.

This method can easily be used to selectively detect uric acid in the presence of other interfering species in real samples. Again the modified electrode that was proposed demonstrated excellent electrocatalytic activity toward the oxidation of uric acid within the linear range of 5 to 200 mM and a detection limit of 1.15 mM. The developed sensor exhibited good reproducibility and stability

Arona et al. [50] reported that due to the appropriate behavior of the nanocomposite's fiber structure, the polyaniline/multi-walled carbon nanotubes (PANI/MWCNTs) electrochemical modifier produced peak currents toward the UA at a higher intensity than the bare indium tin oxide (ITO)-coated glass in a pH of 6.5 buffer solution. Uricase from (Bacillus fastidious) was covalently immobilized onto glutaraldehyde-modified MWCNT-Pani/ITO. The sensor had a large surface area, which sped up electron transport and contributed to a better sensing signal.

Strong π-π stacking between PANI and the uricase biosensor contributed to the enhancement of the electrocatalytic behavior of the Uricase-MWCNTs-Pani/ITO electrode fiber. At S/N = 3, the UA peak currents at the uricase-MWCNTs-Pani fiber electrode showed a good linear response between 0.02 to 0.8 μM and a sensitivity of 8.38 μA/μM. The uricase-MWCNTs-Pani composite created a more favorable microenvironment, which improved enzyme stability and substrate affinity.

Uric acid detection with polymers and gold nanoparticle-modified electrodes has been the subject of numerous studies. Poly (diallyldimethylammonium chloride) functionalized on reduced graphene oxide/gold nanoparticles mixed with polyoxometalates clusters modified electrode was developed and reported by Bai, Zhenyuan, et al. [51]. The electrocatalytic properties of the nanoparticles and reduced graphene oxide, in addition to the abundant electron cloud in the polymer-polyoxometalates clusters, contributed to the enhanced catalytic activity of the modified electrode.

The uric acid concentrations were measured in the linear range of 2.5 x 10^{-7} M to 1.5 x 10^{-4} µM, with a low detection limit of 0.08 µM using differential pulse voltammetry. The modified electrode was validated for the determination of uric acid in human urine and good recovery results with the percentage range of 95.24% to 103.13%.

2.1.2 Simultaneous determination of uric acid and dopamine

In most human body fluids, dopamine and uric acid are conventionally coexisting, and their redox potentials are almost identical. As a result, researchers are immensely interested in simultaneous detection, which is much more important than individual detection. Materials based on metals/metal oxide, polymers, and carbon nanostructure have been reported on the electroanalyses of these types of analytes and also to achieve peak-to-peak resolution.

To simultaneously measure uric acid and dopamine concentrations, some polymeric materials, such as polypyrrole [52] and overoxidized polymer films [53], [54], have been utilized.

Tang, J., et al. [55] proposed a modified electrode from Co (II)-based zeolitic imidazolate framework supported on graphene oxide film and it was claimed to have good sensitivity, stability, and low LoD with the values of 50 nM and 100 nM in the linear dynamic range of 0.2 – 80 µM and 0.8 – 200 µM for dopamine and uric acid respectively, in comparison with GO-modified electrode. Due to the synergistic effect of the high electrical conductivity of GO and porosity of ZIF-69, the modified electrode had excellent catalytic performance for both uric acid and dopamine. Also, the sensor showed good stability and reproducibility and satisfying recoveries for simultaneous detection of UA and DA in human urine samples.

Ensafi A. A. et al. [56] developed a simultaneous electrochemical sensor using poly (sulfonazo III) film and employed it for electroanalyses of uric acid and dopamine in the presence of ascorbic acid as a potential interfering species. The sensor showed excellent electrocatalytic activity towards the oxidation of DA and UA in the linear range of 0.2 – 100.0 µM for uric acid and 0.05 – 470.0 µM for dopamine with the detection limits of 0.11 µM and 0.03 µM respectively using differential pulse voltammetry. Again, the modified GCE exhibited high sensitivity relative to bare-GCE and good selectivity in matrix samples. The sensor did not only improved the current response for both uric acid and dopamine but also peak-to-peak resolution.

Furthermore, poly (acid chrome blue K) has been used by Zhang, Rui, et al. [57] as a redox mediator or electrochemical sensor for the simultaneous detection of dopamine and uric acid. Under optimized experimental conditions, the sensor manifested good catalytic activity properties, enhanced oxidation peak currents, and a broad linear range of 1.0 – 200 µM for DA and 1.0 – 120.0 µM for UA with the same detection limit of 0.5 µM for both UA and DA. Based on the semicircular impedance spectrum, a small semicircle of a modified GCE indicated that electron transfer resistance at the electrode/electrolyte interface decreased after the modification. Hence the increased peak current signals under (DPV) voltammograms were observed with improved peak-to-peak potential separation of (166 mV).

In other studies, K. C. Lin et al. [58] and S. R. Jeyalakshmi et al. [59] have fabricated multiwalled-carbon nanotubes poly-(3,4-ethylene-dioxythiophene) (MWCNTs-PEDOT) composite and poly (3,4-ethylene dioxythiophene) (PEDOT) film on glassy carbon electrodes and used for simultaneous determination of dopamine and uric acid. K. C. Lin et al [58] reported that (the MWCNTs-PEDOT) electrode exhibited high peak current intensity toward DA and UA relative to the bare electrode at a pH of 7 (phosphate buffer solution). The electrochemical analyses were performed using differential pulse voltammetry and good linear ranges of ($1 \times 10^{-5} – 3.3 \times 10^{-4}$ M for DA and $1 \times 10^{-5} – 2.5 \times 10^{-4}$ M for UA) were obtained with the same LOD of 1×10^{-5} M for both UA and DA. (MWCNTs-PEDOT) provided a high surface area which accelerated the electron transfer and contributed to the good sensing platform.

S. R. Jeyalakshmi et al [59] have also investigated the performance of PEDOT film on the surface of the electrode. The peak currents of dopamine and uric acid linearly increased with the concentration in the ranges of (20 – 80 µM, for DA and 20 - 130 µM, for UA) and the calculated LODs were 1.4 µM and 1.2 µM respectively. The cyclic voltammetry results showed enhanced oxidation-reduction peaks of both DA and UA compared to bare GCE. The film stands out as the detecting material due to its phenomenal synergist capacities and extraordinary properties.

In addition, well-distinguished peak potentials with clear peak separation were obtained, and the modified electrodes demonstrated good stability and reproducibility. The PEDOT film exhibited lower LODs than when coupled with multi-walled carbon nanotubes.

R. Manjunatha et al. and co-workers [60] developed a high sensitivity and selective electrochemical sensor based on polystyrene sulfonate-wrapped multiwalled carbon nanotubes-graphite electrode for electrochemical detection of both UA and DA. Due to the electrostatic interaction of the polymer and the analytes, the oxidative peak current of uric acid and redox peaks of dopamine were enhanced in cyclic voltammetry.

Over and above that, the modified graphite electrode disclosed a superior electrocatalytic effect, and the linear ranges of 1 – 120 µM for UA and 1 – 150 µM for DA were obtained from DPV curves. Although the electrode demonstrated magnificent stability, improved peak-to-peak resolution, and significant catalytic activity towards DA and UA, the detection limits were not indicated.

Conducting polymers coupled with nanoparticle structure increased the electroactive surface area of the bare electrodes, creating more active sides for electroactive species. Besides that, the composite-based possesses properties such as lowering the electron transfer resistance between the electrode/electrolyte interfaces thereby increasing the electrocatalytic efficiency of the modified electrode.

Consequently, J. Mathiyarasu et al. [61] and his group prepared PEDOT incorporated with gold nanoparticles and fabricated the glassy carbon electrode for voltammetric studies of dopamine and uric acid. Nanoparticles-polymeric composite displayed excellent electrocatalytic effect, synergistic chemical and physical properties of the sensor for DA and UA detection in the linear concentrations of 20 – 80 µM for DA and 20 – 130 µM for UA with the detection limits reported to be in the range of micro-molar concentrations.

Moreover, differential pulse voltammetry was employed during the analyses, and well-defined oxidation peak potentials were obtained. The conducting polymeric film with high porosity easily entrapped Au-nanoparticles thereby increasing the electroactive surface area of the modified electrode and enhancing the sensitivity relative to the polymer film only.

Harish S. et al [62], and Yu, Shiji et al [63] proposed PEDOT-based sensor platforms, that is; PEDOT/palladium composite and (PEDOT) polymer were successfully fabricated on glassy carbon and nickel/silicon microchannel plate electrodes respectively. The mediators exhibited an appreciable catalytic activity for the simultaneous determination of DA and UA and a large surface area to volume ratio.

In addition, the modified electrode exhibited a high current response for DA and UA as compared to when electrodes were modified with only the polymer film (PEDOT). The results, therefore, cement the fact that nanoparticles indeed improve the electrocatalytic efficiency of the redox reaction. Their work showed that modified electrodes do not suffer from fouling due to by-products of either DA or UA.

The DPV curves revealed a linear relationship between the peak currents and the analytes concentration over the range of 0.5 – 1 µM for DA and 7 – 11 µM for UA with 0.5 µM and 7.0 µM detection limits respectively [62]. However, Yu, Shiji et al. work presented 12 - 48 µM for Da and 36 – 216 µM linear concentrations ranges with the detection limit of 1.5 µM and 2.7 µM respectively. A wide linear range was obtained from Ni/Si-MCP-PEDOT but with palladium nanoparticles, only limited linear concentration ranges were found for both DA and UA. These proved that Nickel/silicon microchannel plate electrodes have better catalytic efficiency when coupled with conducting polymeric film (PEDOT).

C. Wang et al. [64] have developed a modified (GCE) electrode based on non-covalent iron (III)-porphyrin/MWNTs. Differential pulse voltammetry (DPV) and cyclic voltammetry (CV) were used to measure the Fe(III)P/MWCNTs electrode's sensor performance in 0.1 M of phosphate buffer solution (PBS) at pH 4.0. In the presence of AA and nitrite ions, the detection limit for DA and UA were 0.09 µM and 0.30 µM in the linear dynamic range of 0.70 µM – 3.60 mM and 5.80 µM – 1.30 mM respectively.

They found that composite improved the electrode's electroactive surface area, good biocompatibility, and high sensitivity in the presence of ascorbic acid and nitrite ions. The combination of the Fe(III)-porphyrin complex and MWCNTs had a dramatic impact on bare electrode behavior by improving electron transfer efficiency and thereby widening the linear range of the modified electrode with an order of 10^3.

T. Q. Xu et al. [65] in another study utilized DPV to investigate the electrocatalytic oxidation of UA and DA on the surface of a glassy carbon electrode modified with Pt-nanoparticles and reduced graphene oxide. To determine UA and DA, a phosphate buffer solution with a pH of 7.0 was chosen as the best-supporting electrolyte. Within the linear range of 10 – 130 µM (UA), and 10 – 170 µM (DA), detection limits of 0.45 µM for UA, and 0.25 µM for DA were obtained.

Therefore, the proposed modified electrode demonstrated excellent electrocatalytic activity for the oxidation of UA and DA, and high reproducibility for the simultaneous determination of DA and UA. Uric acid and dopamine can be detected selectively in real samples with ease using this method. In addition, Pt-NPs/RGO-GCE demonstrated that is not subject to surface fouling by oxidation of electroanalyses.

Graphene possesses thermal and electrical conductivity, incredible mechanical performances, and a high specific surface area that can uphold the adsorption and diffusion process of dopamine and uric acid. The high surface area of graphene/size-selected Pt-nanoparticles serves as an electroactive surface for the oxidation of dopamine and uric acid. Sun, Chia-Liang, et al [66] reported that the addition of platinum nanoparticles could have accelerated the electron transfer rate, and lowered the detection limit.

Graphene/Pt-GCE displayed a high sensitivity toward the DA, and UA oxidation with the linear concentration ranges of 0.03 - 8.13 µM and 0.05 - 11.85 µM, with a limit of detections of 0.03 µM, and 0.005 µM, respectively. These electroanalyses were carried out on an amperometric platform. The altered electrode surface has been shown to have distinct oxidation peaks of UA and DA that are well-separated and highly selective for the simultaneous detection of these species.

Meanwhile, Wan, Xuan, et al [67] investigated that manganese (IV) oxide (MnO_2) porous nanoflowers and reduced graphene oxide (rGO) as GCE modifier (MnO_2NFs/rGO) exhibited high conductivity and good electroactive surface area towards electro-oxidation of UA and DA. The proposed sensor was utilized to analyze human blood samples, achieving recovery percentages ranging from 104.9% to 105.6%, demonstrating its suitability for the analysis of complex samples. Again, the linear Sweep Voltammetry (LSV) was used during the analyses, and the calculated limit of detections of 0.036 μM and 0.029 μM for DA and UA, respectively were found. The most promising candidates for determining DA and UA simultaneously from various samples rely on the application of nanocomposite-modified electrodes.

Thus, the literature demonstrated that a variety of nanomaterials, including metals, metal oxides, carbon materials, polymers, and a combination of these materials, were excellent at increasing the selectivity and sensitivity of modified electrodes. In particular, the nanomaterials demonstrated their capacity to promote electron transfer reactions on the electrode and enhance the detection of distinctive oxidation peaks.

Furthermore, modified electrodes have also indicated that, under normal conditions, they can be used to detect uric acid or dopamine, with detection limits as low as micromolar or nanomolar and selectivity for the desired analyte in the presence of foreign substances. They have also revealed a degree of maturation that is sufficient to allow them to be used in real analytical applications. As a result, the technology has captivated us to carry out research based on the development of electrochemical sensors using graphene foam, activated carbon (carbon materials), and iron oxides.

2.2 Graphene foam (GF) nanomaterials as electrode modifier

A foam is a material in which a gas can be trapped in its solid pockets-like structure. Graphene foam is prepared by growing a network of carbon atoms using a chemical vapor deposition method on a 3-dimensional nickel foam substrate. The graphene foam is very strong and conductive and has been applied in different areas such as purification/absorption material, battery cells, sensors, and supercapacitors [68], [69], [70]. Some other exceptional properties include high mechanical strength, high electrical conductivity, and surface area [71], [72], [73].

For electroanalytical applications, the macroporous structure of graphene foam has received enormous applications in which electrical conductivity is needed most, such as in electrode modification. Graphene foam tends to improve electron transport and electrolyte diffusion during electrocatalysis [74].

Graphene macroporous structure is generally prepared from the self-assembled method of graphene oxide [75], [76], [77], or the growth of graphene foam on a porous metal template such as nickel foam [78], [79]. Although graphene oxide is relatively cheap and scalable in production, however; its oxidation and exfoliating processes impose defects into the graphene structure thereby disrupting the delocalized sp^2 bonds, and adversely affecting its properties [80], [81], [82]. In contrast; a template such as nickel substrate is used in chemical vapor deposition during graphene foam preparation. The reason behind this is that nickel substrate had been reported to have an average pore size of about 50 μm [70], [83].

The application of graphene foam coupled with other nanomaterials as electrode modifiers has been explored in electrochemical sensing in recent years. For instance, the developed electrochemical sensors based on graphene foam composite have been reported towards electrochemical detection of dopamine [84], [85], [86], [87] and simultaneous detection of dopamine and uric acid [88], [89], [90]. Electrodes such as indium tin oxide/3-dimensional graphene foam, and 3-dimensional graphene foam as a monolithic showed a high sensitivity and excellent selectivity for electrochemical detection of biological compounds [85], [90].

Zinc oxide nanosheet balls anchored onto graphene foam [86] gave the detection limit of 0.01 μM in the linear range of 1 μM – 80 μM for dopamine electroanalysis. Three-dimensional reduced graphene oxide (3D-rGO) materials have been prepared by template-assisted self-assembly and applied for dopamine electroanalysis and a 0.17 μM detection limit was obtained in the linear range of 5 μM – 1mM [87]. A three-dimensional graphene foam-based metal-free composite as an electrochemical sensor was fabricated on the surface of the electrode and used for dopamine and uric acid analysis. The detection limits were determined to be 0.21 μM for DA and 1.27 μM for UA in the linear dynamic ranges of (1 – 80) μM and (5 – 500) μM respectively [88].

The literature, therefore, shows a comparable detection limit in the range of (1 – 80) μM which shows that the modifiers had an impact on the surface of the bare electrode. Reduced graphene

material, on the other hand, reveals that the material has a significant impact on the behavior of the electrode as the modified electrode gave a wide linear range of 5 μM – 1 mM [88]. They also show high selectivity towards dopamine and uric acid in the presence of some foreign species. Nevertheless, most of the reported work did not reveal the electroactive surface area of the modified electrode relative to the bare electrode. Again, the migration or diffusion coefficients of dopamine and uric acid calculations were not carried out to show how active sides of the modified electrode enhance the migration of electroactive species from the electrolyte solution.

The incorporation of graphene foam with other nanoparticles, carbon-based materials, or transition metal oxides as composites for electrochemical analysis of different analytes, had significantly improved the electrocatalytic activity of the modified electrodes. Therefore the utilization of graphene foam as an electrode modifier based on the literature has activated our appetite for the development of an electrochemical sensor for this research project.

2.3 Metal-oxide nanomaterials as electrode modifier

Nanoscience has been worldly used and applied in research areas such as pharmaceutical, biological, engineering, medicine, environmental, and material science. Nanomaterials possess good physical properties due to their exceptionally small particle size and shape which increases their high surface area. Nanoparticles can be defined as solid particles in size ranging from 1 – 1000 nm.

Magnetite (Fe_3O_4) demonstrates unparalleled magnetic properties due to the mobile electron between iron (II) and iron (III) in the cubic sites [91]. Moreover, their superparamagnetic leads to extremely high relativity, biocompatibility, and easy synthesis and functionalized on the electrode surfaces for target molecules [92], [93]. The cubic spinel structure of the magnetite with oxygen anions creates a face-centered cubic, with iron (cations) located at the interstitial tetrahedral points (T_d) and octahedral sites (O_h) [94].

Nanoparticles have received tremendous application in electroanalysis research. The use of transition metals such as cobalt (Co), nickel (Ni), and iron (Fe) have a mixed-valence character that promotes their properties in electroanalytical chemistry [95], [96]. Iron oxide (magnetite) is

one of the metal oxides that has been widely used in electroanalysis due to its excellent magnetic property, chemical stability, and high electron transfer efficiency [97], [98], [99].

Several nanomaterials in which magnetite is combined or coated on other materials have been reported to enhance the current signal and improve the electrode sensitivity and selectivity when used as electrochemical sensors. Fe_3O_4@APTES for dopamine, Fe_3O_4-based nanocomposites for heavy metal ion detection, Fe_3O_4 nano-flakes for ascorbic acid electrocatalysis, magnetite nanoparticles bonded to carbon quantum dots as an electrochemical sensor for NADH and magnetic iron oxide/reduced graphene oxide for paracetamol analysis have been used in electrochemical studies [100], [101], [102], [103], [104].

The sensors improved the sensitivity and selectivity of the modified electrodes in the presence of interfering species such as glucose, ascorbic acid, cations, and anions. A differential pulse voltammetry technique was employed for dopamine and uric acid analysis using the modified electrodes and the detection limit was found to be 34.3 nM dopamine, 2.9 µM dopamine [105], and 0.29 µM uric acid [106] was used. The average linear range of 1 – 200 µM was obtained.

These results cement the fact that iron oxide with its properties showed some potential electrochemical features and improved the electron transfer kinetics. This triggered our interest to explore its electrocatalysis when used on glassy carbon electrodes and its impact on redox reversibility. However, more experimental analysis on the electroactive surface area and the diffusion coefficient of electroactive analytes towards a modified electrode needs to be explored.

The captivating properties of iron oxide as an example of transition metal oxide have attracted our attention for exploring its features towards the electroanalysis of biological compounds. Magnetite or (iron oxide) will be used as one of the candidates used to develop a composite for glassy carbon electrode modification in this work.

2.4 Activated carbon as electrode modifier

Activated carbon is one carbon-based material with a high degree of porosity and surface area due to small particle size. It has received numerous applications in the environmental, and industrial compound removal and modification of different compounds [107]. This material possesses some functional groups such as quinone, phenol, and carboxyl groups which makes it a suitable candidate for adsorbing concomitants. In addition, elements like oxygen, sulfur, sodium, and nitrogen can be also present in the form of functional groups or chemical atoms in the activated carbon structure [108].

These properties make it extremely attractive for use as a support material in the electroanalysis sensor for electrode modification. Development of electrochemical sensors based on copper oxide nanoparticles, titanium oxide, nickel-cobalt oxide@reduced graphene oxide, and palladium nanoparticles incorporated with activated carbon had improved the stability and electrical conductivity of the sensor towards detection of various electroactive species [109], [110], [111] and [112].

The developed nanocomposite possessed a highly porous structure due to the presence of activated carbon and had improved the surface area which allowed better ion transport in supercapacitor devices [108].

The fascinating qualities of graphene foam, activated carbon, and iron oxide have attracted us to explore their features as electrochemical sensors for sensing some selected biological compounds. The composite of graphene foam-iron oxide/activated carbon can therefore be utilized to modify glassy carbon electrodes in this research work.

The intended study is to explore the effect of the electroactive surface area of the modified electrode, improve the separation of oxidation peak potential overlap of dopamine and uric acid, and determine the diffusion coefficient of the analytes towards the electroactive sides of the modified electrode.

2.5 Voltammetry techniques

In voltammetry, the electroactive entity's concentration is altered by oxidation or reduction at the surface layer of the indicator electrode, which can be made of gold, platinum, glassy carbon, or mercury. The current response is plotted as a function of the applied potential.

A dropping mercury electrode takes the place of the flat surface electrodes in polarography. Between the dropping mercury electrode and the reference electrode, a potential program that changes continuously is applied, and the changes in current that result are plotted against the voltage that was applied. The analyte's qualitative value can be estimated using half-wave potential, while its quantitative value can be estimated using wave height.

Voltammetry has been adjusted to a few examination applications including both inorganic and natural analytes in ecological, drugs, food sources, medical, clinical exploration, and metallurgical samples.

Electroanalytical methods have certain advantages over other analytical methods, these include; precision, sensitivity, fastness, and cheapness [113]. The electrochemical evaluation allows the determination of various oxidation states of an element in a solution, and not only the total concentration of the element. Electroanalytical methods can produce large characterization data, including chemical kinetics data, with extremely low detection limits.

Depending on the nature of the analyte under study, various electrochemical methods are used for analysis. Some of these methods can be hyphenated to enhance the quantitative and qualitative analysis of the sample. In an electrochemical analysis, several measuring parameters need to be adjusted such as choosing the type of electrodes, supporting electrolyte, pH, electrolytic cell, temperature, and others.

Voltammetry methods which are known as (controlled-potential methods) are based on monitoring of current changing of the estimated sample depending on applied potential (against the potential of the reference electrode) at the working electrode.

Electrochemical techniques have been very helpful in the elucidation of processes and mechanisms of oxidation and reduction of electroactive species [114], such as cyclic voltammetry, differential-pulse, stripping voltammetry, and square wave voltammetry [115]-[118].

2.5.1 Cyclic Voltammetry (CV)

Cyclic voltammetry is the most widely used technique for qualitative information about electrochemical reactions, that is, about the thermodynamics of redox processes, and coupled chemical reactions or adsorption processes [119]. Cyclic voltammetry usually is the first electrochemical technique performed for the study of a novel electrochemically investigated compound. The basis of CV (Figure 2.1) is a recording of current depending on potential (that ramps linearly versus time) applied to a working electrode in a triangular shape [120]. The voltammogram thus represents observing the current that flows between electrodes at a given potential.

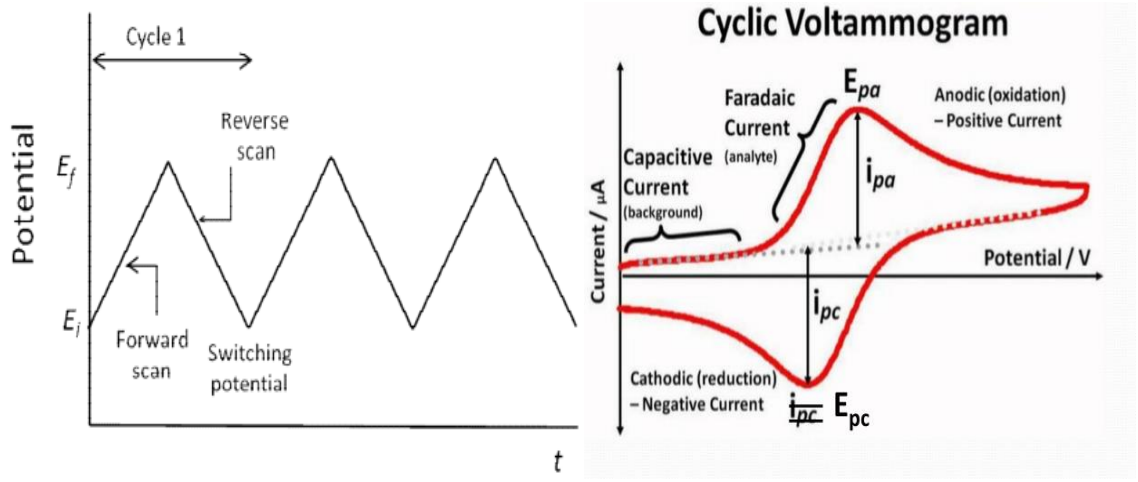

Figure 2.1: (**a**) Potential-time excitation signal in CV experiment. (**b**) Typical cyclic voltammogram for an O + ne − ↔ R redox process [121].

The lines in Figure 2.1 (a) are called voltammograms or cyclic voltammograms. The x-axis represents a parameter that is imposed on the system, here the applied potential (E), while the y-axis is the response, here the resulting current (i) passed. The current axis is sometimes not labeled (instead a scale bar is an inset to the graph).

For a reversible reaction process in electroanalysis, the current response is obtained from the cyclic voltammograms as shown in Figure 2.1 (**b**). The concentration of the electroactive species and the peak current relationship is given by the Randles-Sevcik equation at a temperature of 25 ^{0}C:

Randles-Sevcik Equation: $I_p = 2.69 \times 10^5 \, n^{3/2} \, A \, C \, D^{1/2} \, V^{1/2}$……2.1

- i_p = peak current in amps
- n = number of electrons transferred in the redox reaction
- A = electrode area in cm^2
- D = diffusion coefficient in $cm^2 \, s^{-1}$
- C = concentration in mol cm^{-3}
- ν = scan rate in V s^{-1}

Two conventions are commonly used to report CV data but seldom is a statement provided that describes the sign convention used for acquiring and plotting the data.

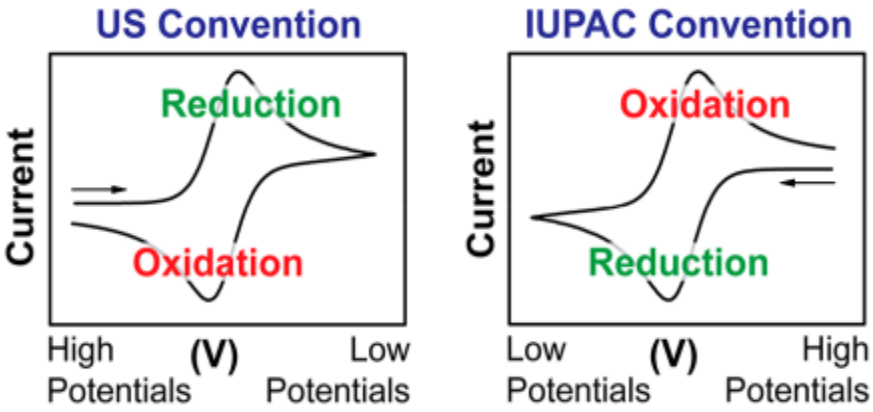

Figure 2.2: Two conventions are used to report CV data: the US convention and the IUPAC convention [122].

Each trace contains an arrow indicating the direction in which the potential was scanned to record the data. The arrow indicates the beginning and sweeps direction of the first segment (or "forward scan"), and the caption indicates the conditions of the experiment.

2.5.2 Differential Pulse Voltammetry

In differential pulse voltammetry (DPV), constant value pulses superimposed on a linear potential ramp are applied to the working electrode at a time just before the end of the drop. The current is sampled twice, just before the pulse application and again late in the pulsing life after ~40 minutes when the double layer charging current has decayed [121].

The first current is instrumentally subtracted from the second, and this current difference is plotted versus the applied potential. The resulting differential pulse voltammogram consists of current peaks, with heights that are directly proportional to the concentration of the corresponding analyte, while peak potential (E_p) can be used to identify the species, as it occurs near the polarographic half-wave potential:

$$E_p = \left[E_{1/2} - \frac{\Delta E}{2}\right] \quad \text{..... 2.1}$$

DPV is a useful technique for measuring trace levels of organic and inorganic species at concentrations as low as 10^{-8} M.

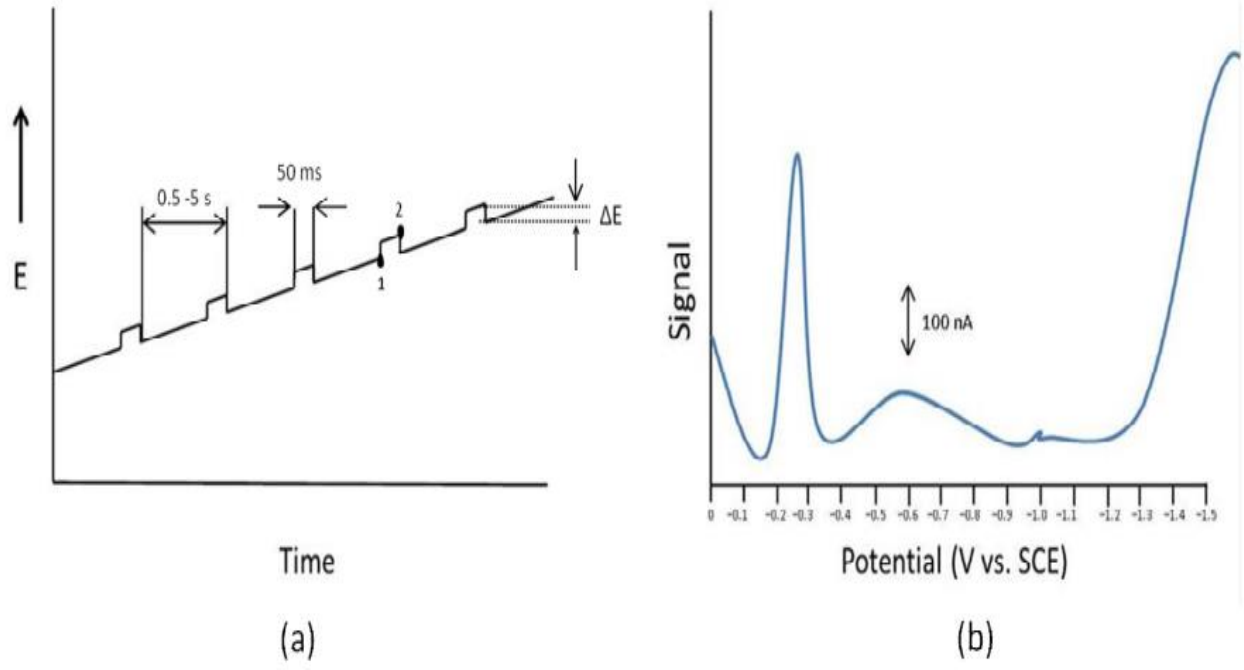

Figure 2.3: (a) Excitation signals for DPV. (b) Typical DP voltammograms [121].

2.6 Electrochemical cell and type of electrodes

2.6.1 Electrolytic cell

An electrolytic cell is an electrochemical tool wherein electric power is transformed into chemical energy. A typical cell consists of three electrodes held apart from each other and in contact with an electrolyte solution called a supporting electrolyte, usually a dissolved ionic compound(s). Three electrode cells are commonly used in controlled potential experiments.

In a three-electrode system, the potentiostat supplies the voltage between the working electrode and the reference electrode and current only passes between the working electrode and the counter electrode. As a result, the observed voltammograms provide a direct measurement of redox phenomena occurring only at the working electrode.

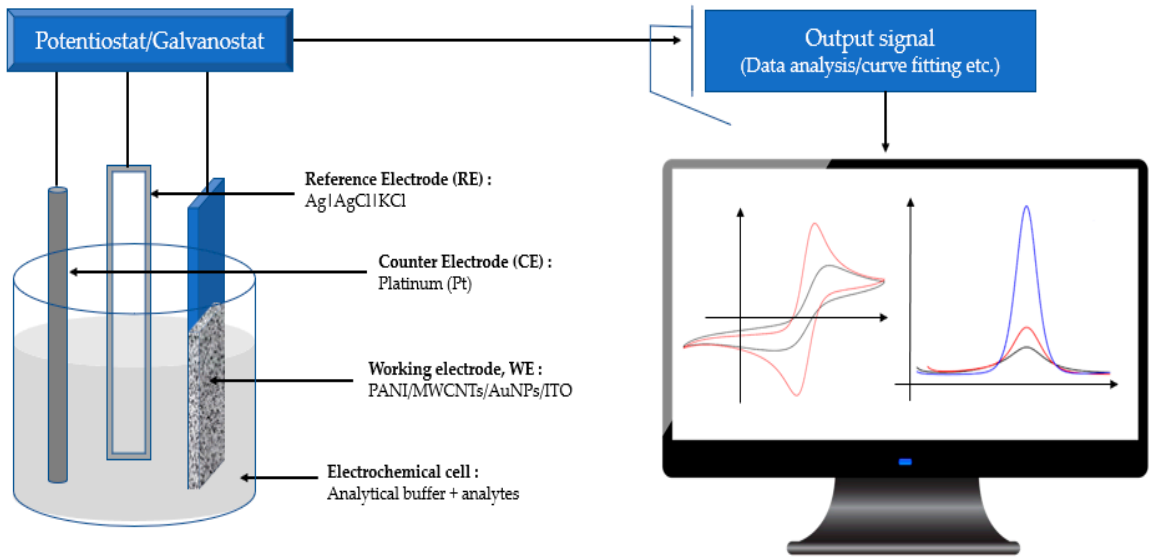

Figure 2.4: Three electrode system, potentiostat, data analysis (Output signal) [123].

The current of the working electrode is recorded as a function of its potential measured against the reference electrode, as the voltage is applied between them and the reference electrode potential is constant. Figure 2.4 displays the three-electrode arrangement system. When an analyte is oxidized at the working electrode, a current passes through the external electric circuit to the counter electrode. This current then flows from the counter electrode to the working electrode. The reverse

process takes place when an analyte is reduced at the working electrode. This current resulting from redox reactions at the working and counter electrode is called faradic current.

2.6.1.1 **Working electrode**

A working electrode is an important tool in an electrochemical device, as the reaction of interest takes place on the surface of the working electrode. Examples of this type of electrode include; metal electrodes (MEs), glassy carbon electrodes, and carbon-based electrodes (CEs). Working electrodes should provide high signal-to-noise characteristics, as well as a reproducible response for analysis [119].

An ideal working electrode should possess the following characteristics for it to qualify as a suitable candidate for electrochemical analysis. These include technical stability, chemical inertness, low background current over a wide potential window, high rate of reproducibility, non-toxic, low-cost maintenance, the capability of chemical modification for a specific analyte under investigation, and also appropriate surface [122].

A glassy carbon electrode is used in the electrochemical analysis. It is very famous due to its super mechanical and electric properties, huge potential window, chemical inertness (solvent resistance), and comparatively reproducible performance [114], [119]. The structure of glassy carbon consists of thin, tangled ribbons of cross-linked graphite-like sheets. Because of its excessive density and small pore size, no impregnating procedure is needed. However, surfaces require a pre-treatment before being employed to create active and reproducible glassy carbon electrodes and to enhance their analytical performance [113].

2.6.1.2 **Reference electrode**

A reference electrode (RE) is an electrode for which the electrode potential is known and constant. This electrode potential has to be stable (with time and temperature) and independent of the properties of the solution. There are three common REs used i.e. standard hydrogen electrode, silver-silver chloride (Ag/AgCl), and saturated calomel electrode (SCE) [124].

2.6.1.3 **Counter electrode**

The counter electrode (CE) or (auxiliary electrode) is used to complete the circuit carrying the current flowing through the cell. The CE is of opposite polarity to the WE and typically has a larger surface area than the WE to ensure that the rate of redox reaction at the WE determines the current. The commonly used counter electrodes are a platinum plate, platinum coil, and a short length of platinum wire [122].

2.6.1.4 **Supporting electrolyte**

An electrolyte is a salt introduced in extra to the analyte solution. Most commonly, it is an alkali metal salt that does not react at the working electrode at the potential being used and has ionic conductivity. The supporting electrolyte can also be an acid, base, buffer solution, or complex. The ions exhibit a discharge potential far from that of the reduction or oxidation of the substance (analyte) being analyzed. The solution resistance is minimized at the interfacial region by the addition of supporting electrolytes. The supporting electrolyte and its concentration should be chosen so that the transport numbers of the electroactive species are practically zero [125].

Electrolyte solution should be purged with inert gases. For example, nitrogen purging for oxygen removal is necessary before taking the measurements to minimize interfering oxygen potential to that of the analyte. The supporting electrolyte should be prepared from highly purified reagents, and should not be easily oxidized or reduced hence minimizing potential contamination or background contributions. The usual electrolyte concentration range for a supporting electrolyte is 0.1 – 1.0 M, that is, in a large excess of the concentration of all electroactive species. Significantly lower levels can be employed in connection with ultramicroscale working electrodes [126].

References

1. Liu, X, Liu, J. (2021). Biosensors and sensors for dopamine detection. *View*; *2*, 1-16.

2. Renedo, O. D., Alonso-Lomillo, M. A., & Martinez, M. A. (2007). Recent developments in the field of screen-printed electrodes and their related applications. *Talanta*, *73*, 202-219.

3. Saei, A. A., Dolatabadi, J. E. N., Najafi-Marandi, P., Abhari, A., & de la Guardia, M. (2013). Electrochemical biosensors for glucose based on metal nanoparticles. *TrAC Trends in Analytical Chemistry*, *42*, 216-227.

4. Sajid, M., Nazal, M. K., Mansha, M., Alsharaa, A., Jillani, S. M. S., & Basheer, C. (2016). Chemically modified electrodes for electrochemical detection of dopamine in the presence of uric acid and ascorbic acid: a review. *TrAC Trends in Analytical Chemistry*, *76*, 15-29.

5. Beitollahi, H., Safaei, M., & Tajik, S. (2019). Different electrochemical sensors for determination of dopamine as neurotransmitter in mixed and clinical samples: A review. *Analytical and Bioanalytical Chemistry Research*, *6*, 81-96.

6. Alwarappan, S., Liu, G., & Li, C. Z. (2010). Simultaneous detection of dopamine, ascorbic acid, and uric acid at electrochemically pretreated carbon nanotube biosensors. *Nanomedicine: Nanotechnology, Biology and Medicine*, *6*, 52-57.

7. Pumera, M., Ambrosi, A., Bonanni, A., Chng, E. L. K., & Poh, H. L. (2010). Graphene for electrochemical sensing and biosensing. *TrAC Trends in Analytical Chemistry*, *29*, 954-965.

8. Yu, J., & Kim, T. H. (2017). A facile electrochemical fabrication of reduced graphene oxide-modified glassy carbon electrode for simultaneous detection of dopamine, ascorbic acid, and uric acid. *Journal of Electrochemical Science and Technology*, *8*, 274-281.

9. Wang, Y., & Bi, C. (2013). Simultaneous electrochemical determination of ascorbic acid, dopamine and uric acid using poly (tyrosine)/functionalized multi-walled carbon nanotubes composite film modified electrode. *Journal of Molecular Liquids*, *177*, 26-31.

10. Zheng, X., Zhou, X., Ji, X., Lin, R., & Lin, W. (2013). Simultaneous determination of ascorbic acid, dopamine and uric acid using poly (4-aminobutyric acid) modified glassy carbon electrode. *Sensors and Actuators B: Chemical*, *178*, 359-365.

11. Liu, X., Zhang, L., Wei, S., Chen, S., Ou, X., & Lu, Q. (2014). Overoxidized polyimidazole/graphene oxide copolymer modified electrode for the simultaneous determination of ascorbic acid, dopamine, uric acid, guanine and adenine. *Biosensors and Bioelectronics*, *57*, 232-238.

12. Ulubay, Ş., & Dursun, Z. (2010). Cu nanoparticles incorporated polypyrrole modified GCE for sensitive simultaneous determination of dopamine and uric acid. *Talanta*, *80*, 1461-1466.

13. Yao, H., Sun, Y., Lin, X., Tang, Y., & Huang, L. (2007). Electrochemical characterization of poly (eriochrome black T) modified glassy carbon electrode and its application to simultaneous determination of dopamine, ascorbic acid and uric acid. *Electrochimica Acta*, *52*, 6165-6171.

14. Du, J., Yue, R., Ren, F., Yao, Z., Jiang, F., Yang, P., & Du, Y. (2013). Simultaneous determination of uric acid and dopamine using a carbon fiber electrode modified by layer-by-layer assembly of graphene and gold nanoparticles. *Gold Bulletin*, *46*, 137-144.

15. Palanisamy, S. (2014). Simultaneous electrochemical detection of dopamine and uric acid over ceria supported three dimensional gold nanoclusters. *Materials Research Express*, *1*, 045020.

16. Sun, C. L., Lee, H. H., Yang, J. M., & Wu, C. C. (2011). The simultaneous electrochemical detection of ascorbic acid, dopamine, and uric acid using graphene/size-selected Pt nanocomposites. *Biosensors and Bioelectronics*, *26*, 3450-3455.

17. Liu, Y., Zhu, W., Wu, D., & Wei, Q. (2015). Electrochemical determination of dopamine in the presence of uric acid using palladium-loaded mesoporous Fe3O4 nanoparticles. *Measurement*, *60*, 1-5.

18. Sun, D., Zhao, Q., Tan, F., Wang, X., & Gao, J. (2012). Simultaneous detection of dopamine, uric acid, and ascorbic acid using SnO 2 nanoparticles/multi-walled carbon nanotubes/carbon paste electrode. *Analytical Methods*, *4*, 3283-3289.

19. Pillarisetti, S., Uthaman, S., Huh, K. M., Koh, Y. S., Lee, S., & Park, I. K. (2019). Multimodal composite iron oxide nanoparticles for biomedical applications. *Tissue Engineering and Regenerative Medicine*, *16*, 451-465.

20. Alim, S., Vejayan, J., Yusoff, M. M., & Kafi, A. K. M. (2018). Recent uses of carbon nanotubes & gold nanoparticles in electrochemistry with application in biosensing: A review. *Biosensors and Bioelectronics*, *121*, 125-136.

21. Adekunle, A. S., Agboola, B. O., Pillay, J., & Ozoemena, K. I. (2010). Electrocatalytic detection of dopamine at single-walled carbon nanotubes–iron (III) oxide nanoparticles platform. *Sensors and Actuators B: Chemical*, *148*, 93-102.

22. Mani, V., Chen, T. W., & Selvaraj, S. (2017). MWCNTs/MoS2 decorated cobalt oxide polyhedrons composite film modified electrode for electrochemical determination of dopamine in rat brain and human blood serum samples. *Int. J. Electrochem. Sci*, *12*, 7435-7445.

23. Hsu, C. Y., Vasantha, V. S., Chen, P. Y., & Ho, K. C. (2009). A new stable Fe (CN) 63−/4−-immobilized poly (butyl viologen)-modified electrode for dopamine determination. *Sensors and Actuators B: Chemical*, *137*, 313-319.

24. Xu, C. X., Huang, K. J., Fan, Y., Wu, Z. W., Li, J., & Gan, T. (2012). Simultaneous electrochemical determination of dopamine and tryptophan using a TiO2-graphene/poly (4-aminobenzenesulfonic acid) composite film based platform. *Materials Science and Engineering: C*, *32*, 969-974.

25. Dakshayini, B. S., Reddy, K. R., Mishra, A., Shetti, N. P., Malode, S. J., Basu, S., ... & Raghu, A. V. (2019). Role of conducting polymer and metal oxide-based hybrids for applications in ampereometric sensors and biosensors. *Microchemical Journal*, *147*, 7-24.

26. Shrivastava, S., Jadon, N., & Jain, R. (2016). Next-generation polymer nanocomposite-based electrochemical sensors and biosensors: A review. *TrAC Trends in Analytical Chemistry*, *82*, 55-67.

27. Kondratiev, V. V., Malev, V. V., & Eliseeva, S. N. (2016). Composite electrode materials based on conducting polymers loaded with metal nanostructures. *Russian Chemical Reviews*, *85*, 14-37.

28. Huong, V. T., Shimanouchi, T., Quan, D. P., Umakoshi, H., Viet, P. H., & Kuboi, R. (2009). Polymethylthiophene/Nafion-modified glassy carbon electrode for selective detection of dopamine in the presence of ascorbic acid. *Journal of Applied Electrochemistry*, *39*, 2035-2042.

29. Xu, G., Li, B., Cui, X. T., Ling, L., & Luo, X. (2013). Electrodeposited conducting polymer PEDOT doped with pure carbon nanotubes for the detection of dopamine in the presence of ascorbic acid. *Sensors and Actuators B: Chemical*, *188*, 405-410.

30. Mathiyarasu, J., & Nyholm, L. (2010). Voltammetric Determination of L-Dopa on Poly (3, 4-ethylenedioxythiophene) -Single-Walled Carbon Nanotube Composite Modified Microelectrodes. *Electroanalysis: An International Journal Devoted to Fundamental and Practical Aspects of Electroanalysis*, *22*, 449-454.

31. Swamy, B. K., & Venton, B. J. (2007). Carbon nanotube-modified microelectrodes for simultaneous detection of dopamine and serotonin in vivo. *Analyst*, *132*, 876-884.

32. Kumar, S. S., Mathiyarasu, J., & Phani, K. L. (2005). Exploration of synergism between a polymer matrix and gold nanoparticles for selective determination of dopamine. *Journal of Electroanalytical Chemistry*, *578*, 95-103.

33. Zanardi, C., Terzi, F., & Seeber, R. (2010). Composite electrode coatings in amperometric sensors. Effects of differently encapsulated gold nanoparticles in poly (3, 4-ethylendioxythiophene) system. *Sensors and Actuators B: Chemical*, *148*, 277-282.

34. Atta, N. F., Galal, A., & Ekram, H. (2012). Gold nanoparticles-coated poly (3, 4-ethylene-dioxythiophene) for the selective determination of sub-nano concentrations of dopamine in presence of sodium dodecyl sulfate. *Electrochimica Acta*, *69*, 102-111.

35. Lupu, S., Balaure, P. C., Lete, C., Marin, M., & Totir, N. (2008). Voltammetric determination of dopamine at PEDOT-Prussian Blue composite modified electrodes. *Revue Roumaine de Chimie*, *53*, 931-939.

36. Lupu, S., del Campo, F. J., & Muñoz, F. X. (2010). Development of microelectrode arrays modified with inorganic–organic composite materials for dopamine electroanalysis. *Journal of Electroanalytical Chemistry*, *639*, 147-153.

37. Mashhadizadeh, M. H., Yousefi, T., & Golikand, A. N. (2012). A nickel hexacyanoferrate and poly (1-naphthol) hybrid film modified electrode used in the selective electroanalysis of dopamine. *Electrochimica Acta*, *59*, 321-328.

38. Atta, N. F., & El-Kady, M. F. (2010). Novel poly (3-methylthiophene)/Pd, Pt nanoparticle sensor: Synthesis, characterization and its application to the simultaneous analysis of dopamine and ascorbic acid in biological fluids. *Sensors and Actuators B: Chemical*, *145*, 299-310.

39. Stoyanova, A., & Tsakova, V. (2010). Copper-modified poly (3, 4-ethylenedioxythiophene) layers for selective determination of dopamine in the presence of ascorbic acid: II Role of the characteristics of the metal deposit. *Journal of Solid State Electrochemistry*, *14*, 1957-1965.

40. Liu, S., Xing, X., Yu, J., Lian, W., Li, J., Cui, M., & Huang, J. (2012). A novel label-free electrochemical aptasensor based on graphene–polyaniline composite film for dopamine determination. *Biosensors and Bioelectronics*, *36*, 186-191.

41. Xue, C., Han, Q., Wang, Y., Wu, J., Wen, T., Wang, R., ... & Jiang, H. (2013). Amperometric detection of dopamine in human serumby electrochemical sensor based on gold nanoparticles doped molecularly imprinted polymers. *Biosensors and Bioelectronics*, *49*, 199-203.

42. Choukairi, M., Bouchta, D., Bounab, L., Elkhamlichi, R., Chaouket, F., Raissouni, I., & Rodriguez, I. N. (2015). Electrochemical detection of uric acid and ascorbic acid: Application in serum. *Journal of Electroanalytical Chemistry*, *758*, 117-124.

43. Lakshmi, D., Whitcombe, M. J., Davis, F., Sharma, P. S., & Prasad, B. B. (2011). Electrochemical detection of uric acid in mixed and clinical samples: a review. *Electroanalysis*, *23*, 305-320.

44. Eryiğit, M., Urhan, B. K., Doğan, H. Ö., Özer, T. Ö., & Demir, Ü. (2022). ZnO nanosheets-decorated ERGO layers: An efficient electrochemical sensor for non-enzymatic uric acid detection. *IEEE Sensors Journal*, *22*, 5555-5561

45. Xue, Y., Zhao, H., Wu, Z., Li, X., He, Y., & Yuan, Z. (2011). The comparison of different gold nanoparticles/graphene nanosheets hybrid nanocomposites in electrochemical performance and the construction of a sensitive uric acid electrochemical sensor with novel hybrid nanocomposites. *Biosensors and Bioelectronics*, *29*, 102-108.

46. Suresh, R., Giribabu, K., Manigandan, R., Vijayaraj, A., Prabu, R., Stephen, A., & Narayanan, V. (2014). α-Fe_2O_3 nanoflowers: synthesis, characterization, electrochemical sensing and photocatalytic property. *Journal of the Iranian Chemical Society*, *11*, 645-652.

47. Ghanbari, K. H., & Hajian, A. (2017). Electrochemical characterization of Au/ZnO/PPy/RGO nanocomposite and its application for simultaneous determination of ascorbic acid, epinephrine, and uric acid. *Journal of Electroanalytical Chemistry*, *801*, 466-479.

48. Reddy, Y. V. M., Sravani, B., Agarwal, S., Gupta, V. K., & Madhavi, G. (2018). Electrochemical sensor for detection of uric acid in the presence of ascorbic acid and dopamine using the poly (DPA)/SiO_2@ Fe_3O_4 modified carbon paste electrode. *Journal of Electroanalytical Chemistry*, *820*, 168-175.

49. Dai, H., Wang, N., Wang, D., Zhang, X., Ma, H., & Lin, M. (2016). Voltammetric uric acid sensor based on a glassy carbon electrode modified with a nanocomposite consisting of polytetraphenylporphyrin, polypyrrole, and graphene oxide. *Microchimica Acta*, *183*, 3053-3059.

50. Arora, K., Choudhary, M., & Malhotra, B. D. (2014). Enhancing performance of uricase using multiwalled carbon nanotube doped polyaniline. *Applied Biochemistry and Biotechnology*, *174*, 1174-1187.

51. Bai, Z., Zhou, C., Xu, H., Wang, G., Pang, H., & Ma, H. (2017). Polyoxometalates-doped Au nanoparticles and reduced graphene oxide: a new material for the detection of uric acid in urine. *Sensors and Actuators B: Chemical*, *243*, 361-371.

52. Ulubay, Ş., & Dursun, Z. (2010). Cu nanoparticles incorporated polypyrrole modified GCE for sensitive simultaneous determination of dopamine and uric acid. *Talanta*, *80*, 1461-1466.

53. Wang, C., Yuan, R., Chai, Y., Zhang, Y., Hu, F., & Zhang, M. (2011). Au-nanoclusters incorporated 3-amino-5-mercapto-1, 2, 4-triazole film modified electrode for the simultaneous determination of ascorbic acid, dopamine, uric acid, and nitrite. *Biosensors and Bioelectronics*, *30*, 315-319.

54. X. Liu, L. Zhang, S. Wei, S. Chen, X. Ou, Q. Lu, (2014). Overoxidized polyimidazole/graphene oxide copolymer modified electrode for the simultaneous determination of ascorbic acid, dopamine, uric acid, guanine, and adenine., *Biosens. Bioelectron*.57, 232–8.

55. Tang, J., Jiang, S., Liu, Y., Zheng, S., Bai, L., Guo, J., & Wang, J. (2018). Electrochemical determination of dopamine and uric acid using a glassy carbon electrode modified with a composite consisting of a Co (II)-based metalorganic framework (ZIF-67) and graphene oxide. *Microchimica Acta*, *185*, 1-11.

56. Ensafi, A. A., Taei, M., Khayamian, T., & Arabzadeh, A. (2010). Highly selective determination of ascorbic acid, dopamine, and uric acid by differential pulse voltammetry using poly (sulfonazo III) modified glassy carbon electrode. *Sensors and Actuators B: Chemical*, *147*, 213-221.

57. Zhang, R., Jin, G. D., Chen, D., & Hu, X. Y. (2009). Simultaneous electrochemical determination of dopamine, ascorbic acid and uric acid using poly (acid chrome blue K) modified glassy carbon electrode. *Sensors and Actuators B: Chemical*, *138*, 174-181.

58. Lin, K. C., Tsai, T. H., & Chen, S. M. (2010). Performing enzyme-free H_2O_2 biosensor and simultaneous determination for AA, DA, and UA by MWCNT–PEDOT film. *Biosensors and Bioelectronics*, *26*, 608-614.

59. Jeyalakshmi, S. R., Kumar, S. S., Mathiyarasu, J., Phani, K. L. N., & Yegnaraman, V. (2007). Simultaneous determination of ascorbic acid, dopamine and uric acid using PEDOT polymer modified electrodes. *Indian Journal of Chemistry-Section A*, *46*, 957-961

60. Manjunatha, R., Suresh, G. S., Melo, J. S., D'Souza, S. F., & Venkatesha, T. V. (2010). Simultaneous determination of ascorbic acid, dopamine and uric acid using polystyrene sulfonate wrapped multiwalled carbon nanotubes bound to graphite electrode through layer-by-layer technique. *Sensors and Actuators B: Chemical*, *145*, 643-650.

61. Mathiyarasu, J., Senthilkumar, S., Phani, K. L. N., & Yegnaraman, V. (2008). PEDOT-Au nanocomposite film for electrochemical sensing. *Materials Letters*, *62*, 571-573.

62. Harish, S., Mathiyarasu, J., Phani, K. L. N., & Yegnaraman, V. (2008). PEDOT/Palladium composite material: synthesis, characterization and application to simultaneous determination of dopamine and uric acid. *Journal of Applied Electrochemistry*, *38*, 1583-1588.

63. Yu, S., Luo, C., Wang, L., Peng, H., & Zhu, Z. (2013). Poly (3, 4-ethylenedioxythiophene)-modified Ni/silicon microchannel plate electrode for the simultaneous determination of ascorbic acid, dopamine and uric acid. *Analyst*, *138*, 1149-1155.

64. Wang, C., Yuan, R., Chai, Y., Chen, S., Zhang, Y., Hu, F., & Zhang, M. (2012). Non-covalent iron (III)-porphyrin functionalized multi-walled carbon nanotubes for the simultaneous determination of ascorbic acid, dopamine, uric acid and nitrite. *Electrochimica Acta*, *62*, 109-115.

65. Xu, T. Q., Zhang, Q. L., Zheng, J. N., Lv, Z. Y., Wei, J., Wang, A. J., & Feng, J. J. (2014). Simultaneous determination of dopamine and uric acid in the presence of ascorbic acid using Pt nanoparticles supported on reduced graphene oxide. *Electrochimica Acta*, *115*, 109-115.

66. Sun, C. L., Lee, H. H., Yang, J. M., & Wu, C. C. (2011). The simultaneous electrochemical detection of ascorbic acid, dopamine, and uric acid using graphene/size-selected Pt nanocomposites. *Biosensors and Bioelectronics*, *26*(8), 3450-3455.

67. Wan, X., Yang, S., Cai, Z., He, Q., Ye, Y., Xia, Y., ... & Liu, J. (2019). Facile synthesis of MnO2 nanoflowers/N-doped reduced graphene oxide composite and its application for simultaneous determination of dopamine and uric acid. *Nanomaterials*, *9*, 847.

68. Cao, X., Shi, Y., Shi, W., Lu, G., Huang, X., Yan, Q., ... & Zhang, H. (2011). Preparation of novel 3D graphene networks for supercapacitor applications. *Small*, *7*, 3163-3168.

69. Cao, X., Yin, Z., & Zhang, H. (2014). Three-dimensional graphene materials: preparation, structures, and application in supercapacitors. *Energy & Environmental Science*, *7*, 1850-1865.

70. Abdulhakeem, B., Farshad, B., Damilola, M., Fatemeh, T., Mopeli, F., Julien, D., & Ncholu, M. (2014). Morphological characterization and impedance spectroscopy study of porous 3D carbons based on graphene foam-PVA/phenol-formaldehyde resin composite as an electrode material for supercapacitors. *RSC Advances*, *4*, 39066-39072.

71. Geim, A. K., & Novoselov, K. S. (2007). The rise of graphene. *Nature Materials*, *6*, 183-191.

72. Novoselov, K. S., Geim, A. K., Morozov, S. V., Jiang, D. E., Zhang, Y., Dubonos, S. V., ... & Firsov, A. A. (2004). Electric field effect in atomically thin carbon films. *Science*, *306*, 666-669.

73. Li, H., Sun, M., Zhang, T., Fang, Y., & Wang, G. (2014). Improving the performance of PEDOT-PSS coated sulfur@ activated porous graphene composite cathodes for lithium–sulfur batteries. *Journal of Materials Chemistry A*, *2*, 18345-18352.

74. Wang, X., & Shi, G. (2011). On the gelation of graphene oxide. *The Journal of Physical Chemistry C, 115*, 5545-5551.

75. Xu, Y., Sheng, K., Li, C., & Shi, G. (2010). Self-assembled graphene hydrogel via a one-step hydrothermal process. *ACS Nano, 4*, 4324-4330.

76. Wu, Z. S., Winter, A., Chen, L., Sun, Y., Turchanin, A., Feng, X., & Müllen, K. (2012). Three-dimensional nitrogen and boron co-doped graphene for high-performance all-solid-state supercapacitors. *Advanced Materials, 24*, 5130-5135.

77. Li, X., Cai, W., An, J., Kim, S., Nah, J., Yang, D., & Ruoff, R. S. (2009). Large-area synthesis of high-quality and uniform graphene films on copper foils. *Science, 324*, 1312-1314.

78. Reina, A., Jia, X., Ho, J., Nezich, D., Son, H., Bulovic, V., ... & Kong, J. (2009). Large area, few-layer graphene films on arbitrary substrates by chemical vapor deposition. *Nano Letters, 9*, 30-35.

79. Tynan, M. K., Johnson, D. W., Dobson, B. P., & Coleman, K. S. (2016). Formation of 3D graphene foams on soft templated metal monoliths. *Nanoscale, 8*, 13303-13310.

80. Wang, H. G., Wang, Y., Li, Y., Wan, Y., & Duan, Q. (2015). Exceptional electrochemical performance of nitrogen-doped porous carbon for lithium storage. *Carbon, 82*, 116-123.

81. Xie, Q., Qu, S., Zhang, Y., & Zhao, P. (2021). Nitrogen-enriched graphene-like carbon architecture with tunable porosity derived from coffee ground as high performance anodes for lithium ion batteries. *Applied Surface Science, 537*, 148092.

82. Trinsoutrot, P., Vergnes, H., & Caussat, B. (2014). Three dimensional graphene synthesis on nickel foam by chemical vapor deposition from ethylene. *Materials Science and*

Engineering: B, *179*, 12-16.

83. Kim, K. S., Zhao, Y., Jang, H., Lee, S. Y., Kim, J. M., Kim, K. S., ... & Hong, B. H. (2009). Large-scale pattern growth of graphene films for stretchable transparent electrodes. *Nature*, *457*, 706-710.

84. Dong, X., Ma, Y., Zhu, G., Huang, Y., Wang, J., Chan-Park, M. B., ... & Chen, P. (2012). Synthesis of graphene–carbon nanotube hybrid foam and its use as a novel three-dimensional electrode for electrochemical sensing. *Journal of Materials Chemistry*, *22*, 17044-17048.

85. Dong, X., Wang, X., Wang, L., Song, H., Zhang, H., Huang, W., & Chen, P. (2012). 3D graphene foam as a monolithic and macroporous carbon electrode for electrochemical sensing. *ACS Applied Materials & Interfaces*, *4*, 3129-3133.

86. Huang, S., Song, S., Yue, H., Gao, X., Wang, B., & Guo, E. (2018). ZnO nanosheet balls anchored onto graphene foam for electrochemical determination of dopamine in the presence of uric acid. *Sensors and Actuators B: Chemical*, *277*, 381-387.

87. Yu, B., Kuang, D., Liu, S., Liu, C., & Zhang, T. (2014). Template-assisted self-assembly method to prepare three-dimensional reduced graphene oxide for dopamine sensing. *Sensors and Actuators B: Chemical*, *205*, 120-126.

88. Jiang, J., Wang, J., Wang, P., Lin, X., & Diao, G. (2023). Three-dimensional graphene foams with two hierarchical pore structures for metal-free electrochemical assays of dopamine and uric acid from high concentration of ascorbic acid. *Journal of Electroanalytical Chemistry*, *928*, 117056.

89. Li, H., Wang, Y., Ye, D., Luo, J., Su, B., Zhang, S., & Kong, J. (2014). An electrochemical sensor for simultaneous determination of ascorbic acid, dopamine, uric acid and tryptophan based on MWNTs bridged mesocellular graphene foam nanocomposite. *Talanta*, *127*, 255-261.

90. Wang, Z., Yue, H. Y., Yu, Z. M., Huang, S., Gao, X., Wang, B., ... & Zhang, H. J. (2019). Synthesis of the 3D graphene foam by chemical vapor deposition using nickel powders and

application for simultaneous electrochemical detection of dopamine and uric acid. *Ionics*, *25*, 1813-1823.

91. Shen, L., Qiao, Y., Guo, Y., Meng, S., Yang, G., Wu, M., & Zhao, J. (2014). Facile co-precipitation synthesis of shape-controlled magnetite nanoparticles. *Ceramics International*, *40*, 1519-1524.

92. Xie, W., Guo, Z., Gao, F., Gao, Q., Wang, D., Liaw, B. S., ... & Zhao, L. (2018). Shape-, size-and structure-controlled synthesis and biocompatibility of iron oxide nanoparticles for magnetic theranostics. *Theranostics*, *8*, 3284.

93. Kim, I., Yang, H. M., Park, C. W., Yoon, I. H., & Sihn, Y. Environmental applications of magnetic nanoparticles. In *Magnetic Nanoparticle-Based Hybrid Materials* (529-545). 1st Edition. June 23, 2021.

94. Teja, A. S., & Koh, P. Y. (2009). Synthesis, properties, and applications of magnetic iron oxide nanoparticles. *Progress in Crystal Growth and Characterization of Materials*, *55*, 22-45.

95. Yang, M., Yang, Y., Liu, Y., Shen, G., & Yu, R. (2006). Platinum nanoparticles-doped sol–gel/carbon nanotubes composite electrochemical sensors and biosensors. *Biosensors and Bioelectronics*, *21*, 1125-1131.

96. Rickerby, D. G., & Morrison, M. (2007). Nanotechnology and the environment: A European perspective. *Science and Technology of Advanced Materials*, *8*, 19-24.

97. Katz, E., & Willner, I. (2005). Switching of directions of bioelectrocatalytic currents and photocurrents at electrode surfaces by using hydrophobic magnetic nanoparticles. *Angewandte Chemie*, *117*, 4869-4872.

98. Yu, S., & Chow, G. M. (2004). Carboxyl group (–CO 2 H) functionalized ferrimagnetic iron oxide nanoparticles for potential bio-applications. *Journal of Materials Chemistry*, *14*, 2781-

2786.

99. Wan, J., Cai, W., Feng, J., Meng, X., & Liu, E. (2007). In situ decoration of carbon nanotubes with nearly monodisperse magnetite nanoparticles in liquid polyols. *Journal of Materials Chemistry*, *17*, 1188-1192.

100. Ognjanović, M., Stanković, D. M., Jaćimović, Ž. K., Kosović-Perutović, M., Dojčinović, B., & Antić, B. (2021). The effect of surface-modifier of magnetite nanoparticles on electrochemical detection of dopamine and heating efficiency in magnetic hyperthermia. *Journal of Alloys and Compounds*, *884*, 161075.

101. Kulpa-Koterwa, A., Ossowski, T., & Niedziałkowski, P. (2021). Functionalized Fe3O4 Nanoparticles as Glassy Carbon Electrode Modifiers for Heavy Metal Ions Detection—A Mini Review. *Materials*, *14*, 7725.

102. Shashanka, R., Jayaprakash, G. K., BG, P., Kumar, M., & Kumara Swamy, B. E. (2022). Electrocatalytic determination of ascorbic acid using a green synthesised magnetite nano-flake modified carbon paste electrode by cyclic voltammetric method. *Materials Research Innovations*, *26*, 229-239.

103. Canevari, T. C., Cincotto, F. H., Gomes, D., Landers, R., & Toma, H. E. (2017). Magnetite nanoparticles bonded carbon quantum dots magnetically confined onto screen printed carbon electrodes and their performance as electrochemical sensor for NADH. *Electroanalysis*, *29*, 1968-1975.

104. Thu, N. T. A., Duc, H. V., Hai Phong, N., Cuong, N. D., Hoan, N. T. V., & Quang Khieu, D. (2018). Electrochemical determination of paracetamol using Fe_3O_4/reduced graphene-oxide-based electrode. *Journal of Nanomaterials*, *2018*, 1-15.

105. Nanditha, A., Manokaran, J., & Balasubramanian, N. (2014). Fabrication of Lys-PVA-Fe3O4 modified electrode for the electrochemical determination of uric acid. *Research Journal of Chemistry and Environment*, *18*, 54-61.

106. Tang, T., Zhou, M., Lv, J., Cheng, H., Wang, H., Qin, D., ... & Liu, X. (2022). Sensitive and selective electrochemical determination of uric acid in urine based on ultrasmall iron oxide nanoparticles decorated urchin-like nitrogen-doped carbon. *Colloids and Surfaces B: Biointerfaces*, *216*, 112538.

107. Heidarinejad, Z., Dehghani, M. H., Heidari, M., Javedan, G., Ali, I., & Sillanpää, M. (2020). Methods for preparation and activation of activated carbon: a review. *Environmental Chemistry Letters*, *18*, 393-415.

108. Sinha, P., Banerjee, S., & Kar, K. K. (2020). Characteristics of activated carbon. Handbook of Nanocomposite Supercapacitor Materials I*: Characteristics, 300*, 125-154.

109. Wannasri, N., Uppachai, P., Butwong, N., Jantrasee, S., Isa, I. M., Loiha, S., ... & Mukdasai, S. (2022). A facile nonenzymatic electrochemical sensor based on copper oxide nanoparticles deposited on activated carbon for the highly sensitive detection of methyl parathion. *Journal of Applied Electrochemistry*, *52*, 595-606.

110. Hayat, A., Rhouati, A., Mishra, R. K., Alonso, G. A., Nasir, M., Istamboulie, G., & Marty, J. L. (2016). An electrochemical sensor based on TiO_2/activated carbon nanocomposite modified screen printed electrode and its performance for phenolic compounds detection in water samples. *International Journal of Environmental Analytical Chemistry*, *96*, 237-246.

111. Lamiel, C., Lee, Y. R., Cho, M. H., Tuma, D., & Shim, J. J. (2017). Enhanced electrochemical performance of nickel-cobalt-oxide@ reduced graphene oxide/activated carbon asymmetric supercapacitors by the addition of a redox-active electrolyte. *Journal of*

Colloid and Interface Science, *507*, 300-309.

112. Veerakumar, P., Veeramani, V., Chen, S. M., Madhu, R., & Liu, S. B. (2016). Palladium nanoparticle incorporated porous activated carbon: electrochemical detection of toxic metal ions. *ACS Applied Materials & Interfaces*, *8*, 1319-1326.

113. M. Lyons. (2014). "Electro-analytical Chemistry".

114. Garrido, E. M., Delerue-Matos, C., Lima, J. L. F. C., & Brett, A. O. (2004). Electrochemical methods in pesticides control. *Analytical Letters*, *37*, 1755.

115. Minta, D., Moyseowicz, A., Gryglewicz, S., & Gryglewicz, G. (2020). A promising electrochemical platform for dopamine and uric acid detection based on a polyaniline/iron oxide-tin oxide/reduced graphene oxide ternary composite. *Molecules*, *25*, 5869.

116. Bobade, R. S. (2011). Polythiophene composites: a review of selected applications. *Journal of Polymer Engineering*, *31*, 209-215.

117. Mathew, M. R., & Kumar, K. G. (2020). Poly (amino hydroxy naphthalene sulphonic acid) modified glassy carbon electrode; an effective sensing platform for the simultaneous determination of xanthine and hypoxanthine. *Journal of the Electrochemical Society*, *167*, 047519.

118. Li, Y., Xie, Y., & Qin, Y. (2014). Polymeric membrane sensors with boronic acid functionalized boron dipyrromethene for selective measurement of dopamine. *Sensors and Actuators B: Chemical*, *191*, 227.

119. Gary A. Mabbott (2020) Electroanalytical Chemistry: Principles, Best Practices, and Case Studies. 1st Ed.Wiley.

120. Xie, W., Guo, Z., Gao, F., Gao, Q., Wang, D., Liaw, B. S., & Zhao, L. (2018). Shape-, size-and structure-controlled synthesis and biocompatibility of iron oxide nanoparticles for magnetic theranostics. *Theranostics*, *8*, 3284.

121. Wang, Joseph. (2000). Analytical Electrochemistry, *2nd Edition.* vol. 3. JOHN WILEY & SONS, New York.

122. Elgrishi, N., Rountree, K. J., McCarthy, B. D., Rountree, E. S., Eisenhart, T. T., & Dempsey, J. L. (2018). A practical beginner's guide to cyclic voltammetry. *Journal of Chemical Education*, *95*, 197.

123. Bohari, N. A., Siddiquee, S., Saallah, S., Misson, M., & Arshad, S. E. (2020). Optimization and analytical behavior of electrochemical sensors based on the modification of indium tin oxide (ITO) using PANI/MWCNTs/AuNPs for mercury detection. *Sensors*, *20*, 6502.

124. 124 Sophocleous, M., & Atkinson, J. K. (2017). A review of screen-printed silver/silver chloride (Ag/AgCl) reference electrodes potentially suitable for environmental potentiometric sensors. *Sensors and Actuators A: Physical*, *267*, 106-120.

125. 125 Dickinson, E. J., Limon-Petersen, J. G., Rees, N. V., & Compton, R. G. (2009). How much supporting electrolyte is required to make a cyclic voltammetry experiment quantitatively "diffusional"? A theoretical and experimental investigation. *The Journal of Physical Chemistry C*, *113*, 11157-11171.

126. 126 Szamocki, R., Velichko, A., Holzapfel, C., Mücklich, F., Ravaine, S., Garrigue, P., ... & Kuhn, A. (2007). Macroporous ultramicroelectrodes for improved electroanalytical measurements. *Analytical Chemistry*, *79*, 533-539.

Chapter 3
Methodology

3.1 Research design

The research design involves:

1. Preparation of graphene foam, and iron oxide
2. Surface morphology and elemental composition experiments of the synthesized materials using FT-IR, SEM, EDS, XRD, and interpretation of the results.
3. Preparation of electrochemical sensor composites based on "Activated carbon-iron oxide/graphene foam" (AC-Fe_3O_4/GF).
4. Electrode modification (AC-Fe_3O_4/GF/GCE) and electrochemical interrogation in a 5 mM potassium ferrocyanide solution.
5. Use cyclic voltammetry (CV) and differential pulse voltammetry (DPV) as electrochemical techniques to obtain electrochemical measurement data.
6. Estimation of the electroactive surface area of the unmodified and modified GCE.
7. Electrochemical analysis of uric acid and dopamine at a bare glassy carbon electrode (GCE)
8. Comparison of the cyclic voltammograms of unmodified and modified GCE responses for uric acid and dopamine.
9. Optimization of experimental parameters such as pH.
10. Explore the linear range and impact of interferences.
11. Electrochemical measurements on real sample analysis.

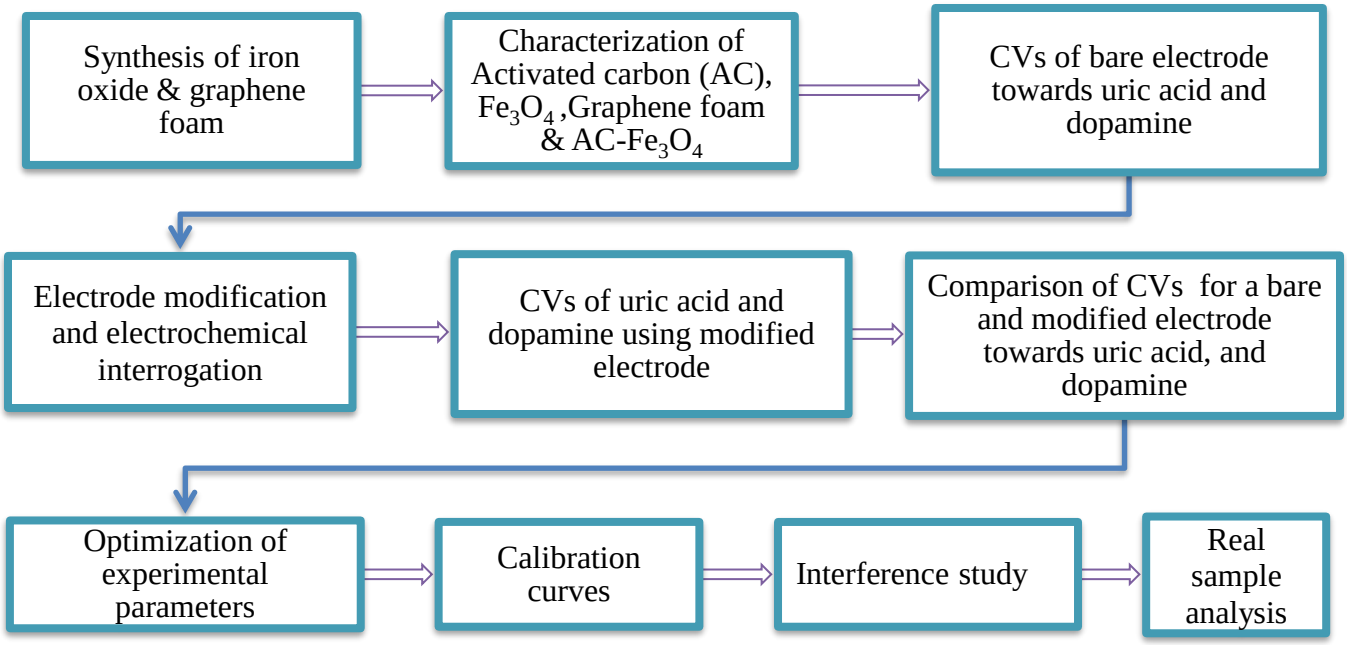

Scheme 3.1: Flow chart of the research design.

3.2 Experimental

3.2.1 Materials and Reagents

All reagents used for the investigations were of analytical grade. Deionized water was used for preparing all aqueous solutions. The aqueous solutions were prepared using ultra-purified water of resistivity 18.3 MΩ cm, obtained from ELGA PURELAB Option-Q (UK) water purification system. Nitrogen gas was used to purge solutions to eliminate dissolved oxygen and prevent any form of interfering electrochemical reactions. Dopamine hydrochloride, uric acid, activated carbon (charcoal), ethanol (98%), ammonium hydroxide (25%), ferric chloride hexahydrate ($FeCl_3.6H_2O$), ferrous chloride tetrahydrate ($FeCl_2.4H_2O$), sodium dihydrogen phosphate, and disodium hydrogen phosphate were purchased from Sigma-Aldrich. Hydrochloric acid and sodium hydroxide were used to adjust the pH of the supporting electrolyte. Alumina micro powder (1.0, 0.3, and 0.05 µm) was used to polish the glassy carbon electrode on the micro-cloth polishing pad. Silver-silver chloride (Ag|AgCl, 3.0 M), reference electrode, and platinum wire as a counter electrode were used for the electrochemical cell.

3.2.2 Instrumentation

An electrochemical analyzer (BAS 100B Bioanalytical system, U.S.A), interfaced with a PC was used for electrochemical characterization and analysis. HANNA HI 8314 pH meter was utilized for pH measurement. For surface morphology characterization and analysis, Scanning electron microscope (JEOL JSM – 7800F), Energy dispersive x-ray spectroscopy (EDS), X-ray diffraction (Rigaku Smartlab XRD, with Cu Kα radiation) and Fourier transform infrared spectra (Perkin Elmer FTIR, 100 spectrometer Frontier) were used.

3.2.3 Synthesis of iron-oxide (Magnetite)

Iron oxide (Fe_3O_4) was prepared according to the method outlined in the literature [1]. Briefly, ferric chloride hexahydrate ($FeCl_3.6H_2O$) and ferrous chloride tetrahydrate ($FeCl_2.4H_2O$) were dissolved in deionized water under vigorous stirring (concentration ratio Fe^{3+} : Fe^{2+} = 2: 1), 25% ammonium hydroxide was added drop-wise until the pH was 12.

Vigorous mechanical stirring is applied to achieve good mixing of the reactants and to prevent a possible agglomeration of the formed particles. Then followed by the addition of 3.0 M sulphuric acid until the pH was 7, and the stirring continued for at least 30 min. The temperature of the mixture was increased to 90 ℃, for 24 hours under magnetic stirring. The product was washed with deionized water and finally with ethanol and dried at 60 ℃.

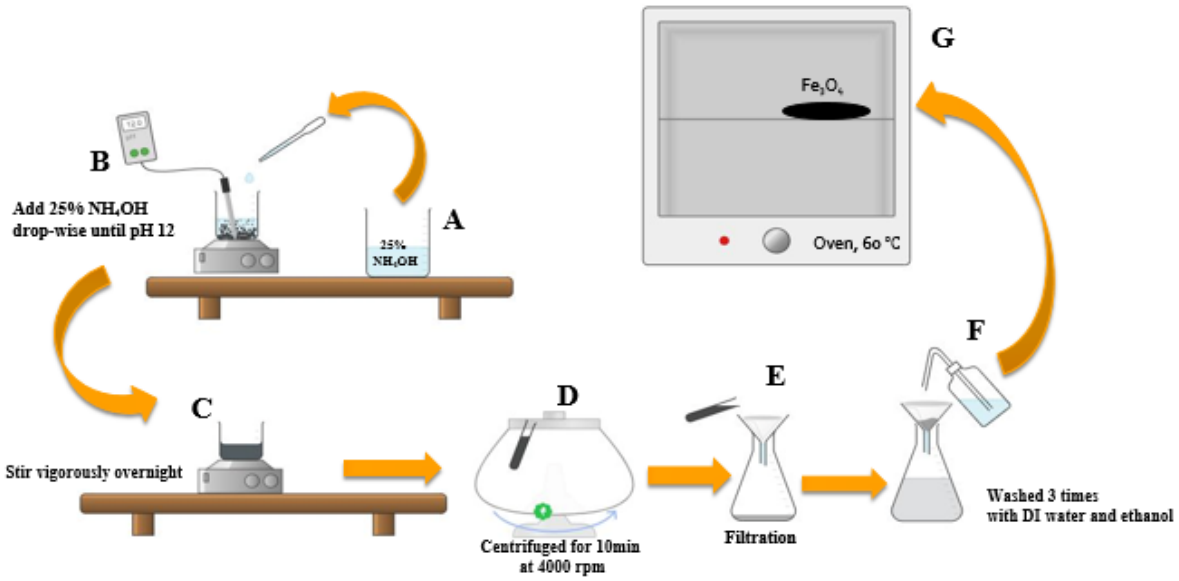

Scheme 3.2: Synthesis of iron oxide (magnetite-Fe_3O_4).

A: 25% NH_4OH, **B:** Measuring the pH of the solution, **C:** Vigorous stirring for 24 hours, **D:** Centrifugation of the product, **E:** Filtration process, **F:** Residue washed with distilled water, **G:** Sample drying in an oven at 60 ^oC.

3.2.4 Synthesis of graphene foam

Graphene foam was received as a donation from the University of Pretoria and was prepared under the reported procedure [2]. The chemical vapor deposition method was employed where nickel foam as a template was subjected to 1000 ℃ temperature as a substrate. Hydrogen and argon gases were allowed to pass through the quartz tube for 1 h to eliminate possible impurities and create an inert environment. Methane gas was then introduced into the quartz tube for 10 minutes after which the furnace was allowed to cool to room temperature. The sample was then soaked in 3.0 M hydrochloric acid at 80 ℃ to completely remove nickel from the sample. Thereafter, ultra-purified water was used to wash the sample severally and dried for 12 h at 70 ^oC, yielding the final graphene foam.

Scheme 3.3: Synthesis of graphene foam (GF) via chemical vapor deposition method.

3.2.5 Electrode Modification

The glassy carbon electrode was polished with (0.05, 0.3, and 1.0 µm in diameter) to a mirror finish with water-alumina slurry on a micro cloth polishing pad, and cleaned consecutively and thoroughly with ultra-pure water and sonicate in the ethanol-water mixture. When polishing in a circular motion, the cleaning may become uneven and the surface can be slanted. Whereas in figure-eight motions all the angles can be thoroughly cleaned.

Drop-casting method was used to modify the electrode. Graphene foam material was assembled into a thin circular paper-like sheet and adsorbed on the cleaned surface of the electrode [3]. About 1 mg of each iron oxide (magnetite) and activated carbon were suspended in 1 mL ethanol. The suspension was dispersed by ultrasonic vibration for 30 minutes, and a 5 µL aliquot was dropped onto the graphene foam thin film circular sheet and left at room temperature to allow air to dry to obtain the desired modified electrode.

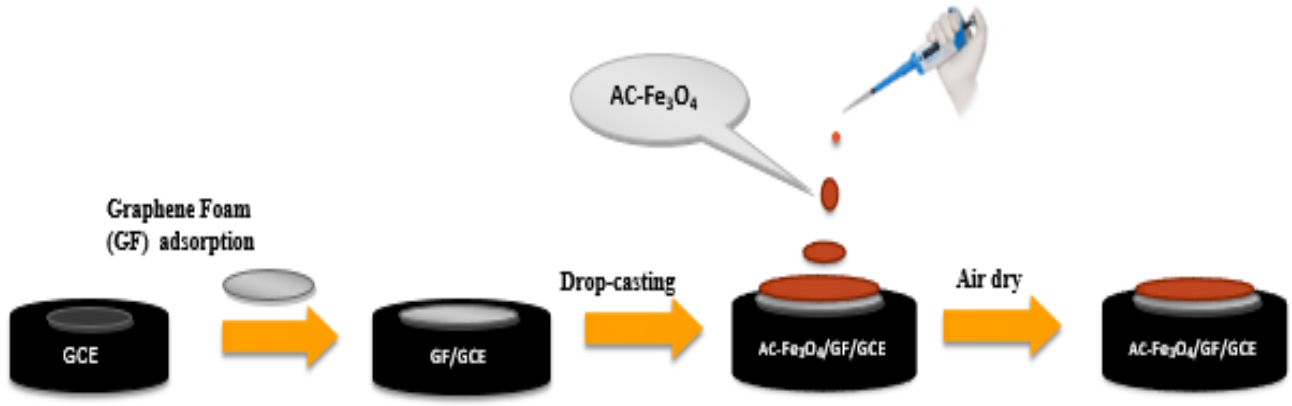

Scheme 3.4: Electrode modification process.

3.2.6 Characterization

3.2.6.1 Structure and Morphology

The elemental composition and morphologies of the prepared material were observed with field emission Scanning electrochemical microscopy (SECM) (JEOL JSM – 7800F) coupled with a Thermo Scientific Ultradry EDS detector. XRD spectra were recorded on a Rigaku Smartlab X-ray diffractometer with Cu Kα radiation. FT-IR patterns were recorded on a Perkin Elmer FTIR spectrometer Frontier (spectrometer 100) with the KBr pellets procedure. The measurements were carried out at UNISA chemistry laboratories.

3.2.6.2 Electrochemical characterization

The electrochemical interrogations were performed in 2.5 mM potassium ferrocyanide solution using a three-electrode configuration, on an electrochemical analyzer (BAS 100B Bioanalytical system, U.S.A), interfaced with a PC. Fabricated glassy carbon electrode (GCE), platinum wire, and silver/silver chloride (Ag/AgCl, 3.0 M) were used as working, counter, and reference electrodes, respectively. The cyclic voltammetry measurements were recorded at a scan rate of 50 mV s^{-1} in the potential range of – 0.2 to 0.6 V.

Electrochemical experiments were performed to establish both the modification of the electrode and the study of the electrochemical behavior of bare and modified GCE. Cyclic voltammetry was employed mainly to characterize the properties of the electrodes.

3.2.7 The surface area of bare and modified GCE

A solution of 5 mM potassium ferrocyanide was prepared in 0.1 M potassium chloride, and a cyclic voltammetry technique was employed for surface area determination in the potential range of – 0.2 to 0.6 V at different scan rates (20 – 250 mV s^{-1}). The diffusion coefficient of potassium ferrocyanide, (6.70 x 10^{-6} cm^2 s^{-1}), was used to determine the surface area of both bare and modified GCE [4]. The plots of peak current versus the square root of the scan rate were made.

The surface areas of the unmodified and modified GCE were determined from the slope of the linear plots obtained.

3.2.8 Electrocatalytic oxidation and reduction of uric acid and dopamine

3.2.8.1 Uric acid

Electrochemical characterization of 5 mM uric acid was investigated using cyclic voltammetry (CV) in a 0.1 M phosphate buffer solution of pH 6. The experiments were performed in the potential window; 0.22 to 0.55 V at 50 mV s^{-1} scan rate. The oxidation processes of uric acid (5 mM) at bare and modified GCE was investigated. The diffusion coefficient of uric acid (0.291 mM) using the calculated electroactive surface area of the modified electrode was determined.

3.2.8.2 Dopamine

The electrocatalytic oxidation behavior of dopamine was investigated under cyclic voltammetry (CV) in 0.1 M phosphate buffer solution as a supporting electrolyte. CV experiments were conducted in the potential range of 0.05 to 0.45 V at a 50 mV s^{-1} scan rate. Redox processes of dopamine (185 µM) at bare and modified GCE were also investigated. The diffusion coefficient of dopamine (1 mM) using the calculated electroactive surface area of the modified electrode was determined.

3.2.9 Calibration curve and detection limits

3.2.9.1 Uric acid

From the prepared stock solution of uric acid in 0.1 M phosphate buffer solution, a series of solutions (5 µM to 1360 mM) of uric acid were prepared. The anodic peak current responses for varying uric acid concentrations were examined using differential pulse voltammetry at the AC-Fe_3O_4/GF/GCE modified electrode.

3.2.9.2 **Dopamine**

About 4.798 mM stock solution of dopamine was prepared in 0.1 M phosphate buffer solution, and a series of solutions of 5 µM to 400 µM were prepared from the stock solution. Electroanalysis was performed on the different dopamine concentrations using differential pulse voltammetry at AC-Fe_3O_4/GF/GCE.

3.2.9.3 **Uric acid and dopamine**

Differential pulse voltammetry measurements for different concentrations of dopamine in the presence of constant 60 µM uric acid concentration using AC-Fe_3O_4/GF modified GCE, at the scan rate of 50 mVs^{-1} were conducted. The concentrations of dopamine range from 5.0 to 400 µM.

Differential pulse voltammetry measurements with increasing concentrations of uric acid ranging from 2.5 µM to 450 µM in the presence of a constant 60 µM uric dopamine were carried out. The peak current increases linearly in the potential window from 0 to 0.5 V with increasing concentration. The peak currents versus different concentrations were plotted to obtain their relationship.

3.2.10 Study of foreign compounds

3.2.10.1 **Uric acid**

Eighty microliters (80 µM) solutions of suspected interfering species were prepared and each was spiked to 10 mL of 60 µM uric acid, to assess their impact on the electroanalysis of uric acid. Ascorbic acid, glutamic acid, glucose, tartaric acid, L-lysine, and cysteine were selected as potential interfering species. The investigation was carried out using differential pulse voltammetry in the potential range of 0.2 to 0.55 V, at 50 mV s^{-1} scan rate.

3.2.10.2 **Dopamine**

Eighty microliters (80 µM) solutions of suspected interfering compounds were prepared and each was spiked to 10 mL of 60 µM dopamine prepared in 0.1 M PBS of pH 7, to assess their impact on the electroanalysis of dopamine. Glucose, ascorbic acid, glutamic acid, cysteine, L-lysine, and tartaric acid were selected as potential interfering species. The investigation was carried out using differential pulse voltammetry in the potential range of 0 to 0.4 V, at 50 mV s^{-1} scan rate.

3.2.10.3 **Uric acid and dopamine mixture**

Eighty microliters (80 µM) concentrations of the possible interfering species were prepared and 10 mL of 60 µM of the mixture of uric acid and dopamine were each spiked into the solutions to assess their impact for simultaneous determination. The following are some of the chosen interferences; glucose, glutamic acid, L-lysine, cysteine, ascorbic acid, and tartaric acid. The analysis was carried out using differential pulse voltammetry (DPV) in the potential window of 0.05 to 0.55 V.

3.2.11 Determination of dopamine and uric acid in real sample

Real sample analyses were conducted to confirm the practical application of the developed electrochemical sensor toward uric acid and dopamine. The urine sample was used without further purification and three replicates were performed for each electrochemical determination using the standard addition method. Differential pulse voltammetry was employed for the analysis.

3.2.11.1 **Uric acid**

A stock solution of 5.6 x 10^{-3} g of uric acid was dissolved in 0.1 M phosphate buffer solution, from which 10, 20, and 30 µM uric acid were prepared and each was spiked to 10 mL of the prepared human urine sample solution. Before measurements, 15 mL of urine was filtered and then 10 mL aliquot of the sample was diluted 100-fold with 0.1 M PBS pH 6. The analysis was carried out in replicates in the electrochemical cell without any pretreatment process.

3.2.11.2 **Dopamine**

A stock solution of 5.6 x 10^{-3} g of dopamine was prepared in 0.1 M PBS, from which 10, 20, and 30 µM dopamine solutions were prepared and each was spiked to 10 mL prepared urine sample solution. The urine sample was filtered, and a 10 mL aliquot of the sample was diluted 100-fold with 0.1 M PBS pH 7. The analysis was carried out in replicates in the electrochemical cell without any pretreatment process.

3.2.11.3 **Dopamine and uric acid**

A mixture of dopamine and uric acid prepared in 0.1 M PBS of pH 6.5 was used to prepare 10, 20, and 30 µM dopamine and uric acid solutions and each was spiked to 10 mL prepared urine sample solution. The urine sample was filtered, and a 10 mL aliquot of the sample was diluted 10-fold with 0.1 M PBS pH 6.5. The analysis was carried out in replicates in the electrochemical cell without any pretreatment process.

References

1. Petcharoen, K., & Sirivat, A. J. (2012). Synthesis and characterization of magnetite nanoparticles via the chemical co-precipitation method. *Materials Science and Engineering*: *B*, *177*, 421-427.

2. Banciu, C. A., Nastase, F., Istrate, A. I., & Veca, L. M. (2022). 3D Graphene Foam by Chemical Vapor Deposition: Synthesis, Properties, and Energy-Related Applications. *Molecules*, *27*, 3634 (1-33).

3. Elgrishi, N., Rountree, K. J., McCarthy, B. D., Rountree, E. S., Eisenhart, T. T., & Dempsey, J. L. (2018). A practical beginner's guide to cyclic voltammetry. *Journal of Chemical Education*, *95*, 197-206.

4. Nayak, P., Kurra, N., Xia, C., & Alshareef, H. N. (2016). Highly efficient laser-scribed graphene electrodes for on-chip electrochemical sensing applications. *Advanced Electronic Materials*, *2*, 1600185 (1-11).

Chapter 4
Results and Discussions

4.1 Spectroscopic and microscopic characterization

The XRD, FT-IR, SEM, and EDS were used to investigate the prepared materials' structural morphologies and chemical integrity.

4.1.1 X-Ray Diffraction Spectroscopy (XRD)

Figure 4.1 depicts the X-ray diffraction pattern of (**a**) Iron oxide (Magnetite – Fe_3O_4), (**b**) activated carbon (AC), (**c**) Iron oxide-activated carbon composite (Fe_3O_4-AC or AC-Fe_3O_4), (**d**) graphene foam (GF). To confirm the formation and crystallinity or amorphous structure of the synthesized materials, an X-ray diffraction analysis was conducted. Three peaks are observed at $2\theta = 35.4°$, $2\theta = 56.2°$, and $2\theta = 62.6°$ for iron oxide (Fe_3O_4), which correspond to (311), (511), and (440) crystalline planes of magnetite structure [1]. These sharp peaks confirm the regular arrangement of the atoms of the compound and diffract the X-ray at one particular angle. The most common form of iron oxide is a face-centered cubic spinel structure. High-intensity peak is observed at $2\theta = 35.4°$, this shows the high periodicity of the compound, and therefore iron oxide possesses crystallinity in nature.

The XRD spectrum of activated carbon is shown in Figure 4.1 (**b**) and broad peaks at $2\theta = 24.9°$, and $2\theta = 44.1°$ were observed. The peak at $2\theta = 24.9°$ is of high intensity relative to that at $2\theta = 44.1°$, this depicts that there are more atoms diffracting X-rays at $2\theta = 24.9°$ than that at $2\theta = 44.1°$. The wide peaks show that atoms in this compound diffract X-rays at different patterns hence there are broad peaks. The absence of a sharp peak reveals that activated carbon is a predominantly amorphous structure [2].

The XRD spectrum of the developed composite (Fe_3O_4-AC) shown in Figure 4.1 (**c**) gives rise to sharp peaks at $2\theta = 30.2°$, $2\theta = 35.4°$ $2\theta = 56.2°$, and $2\theta = 62.6°$. Magnetite (Fe_3O_4) retains its properties from the composite material as the material gives rise to diffraction peaks observed for iron oxide only in the previous XRD spectrum. It is also observed that amorphous activated carbon has now taken the crystallinity properties when combined with the iron oxide in this composite. Therefore the composite is said to be a crystalline solid material that diffracts X-rays. The last

XRD spectrum is for graphene foam (GF) which is depicted in Figure 4.1 (**d**). Extremely high and narrow intensity peak is observed at $2\theta = 26.4°$ corresponds to the (002) plane of graphite, and a weak peak intensity at $2\theta = 54.7°$ to the (004) plane [3]. This material has atoms arranged in an orderly manner as it gives narrow peaks, and that means there is high periodicity which shows high-intensity diffraction X-rays. Only peaks of carbon-based graphene were detected, indicating a pure and clean graphene foam without any residues from the Ni template [4].

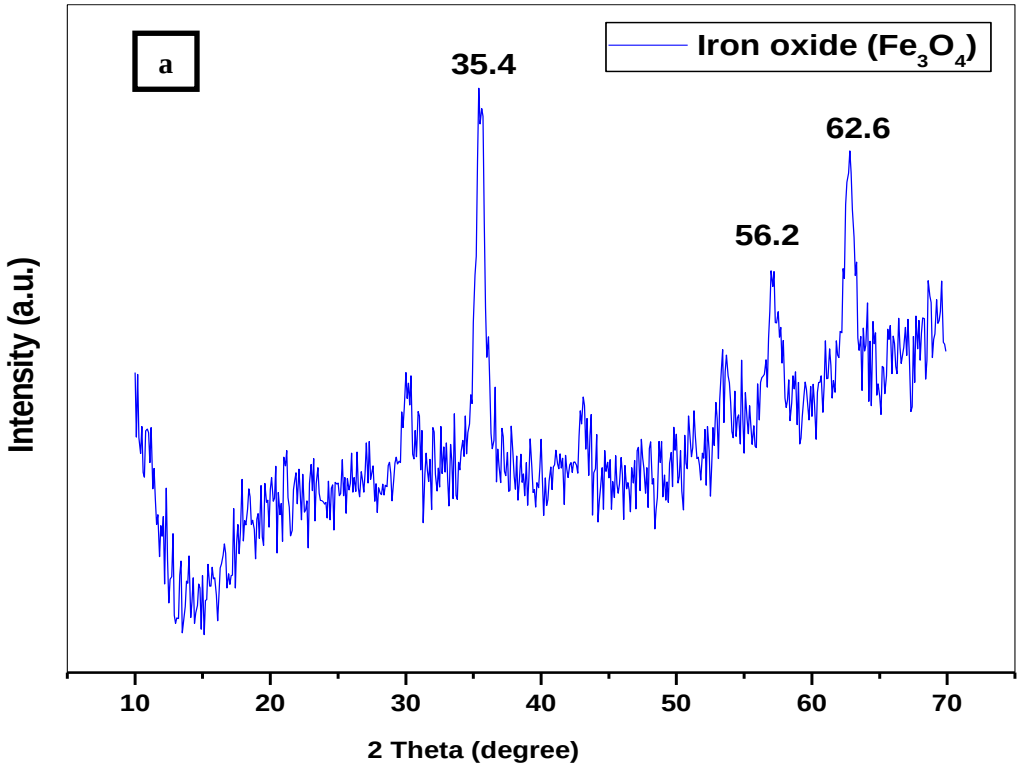
a
Iron oxide (Fe_3O_4)
35.4
62.6
56.2
Intensity (a.u.)
10
20
30
40
50
60
70
2 Theta (degree)

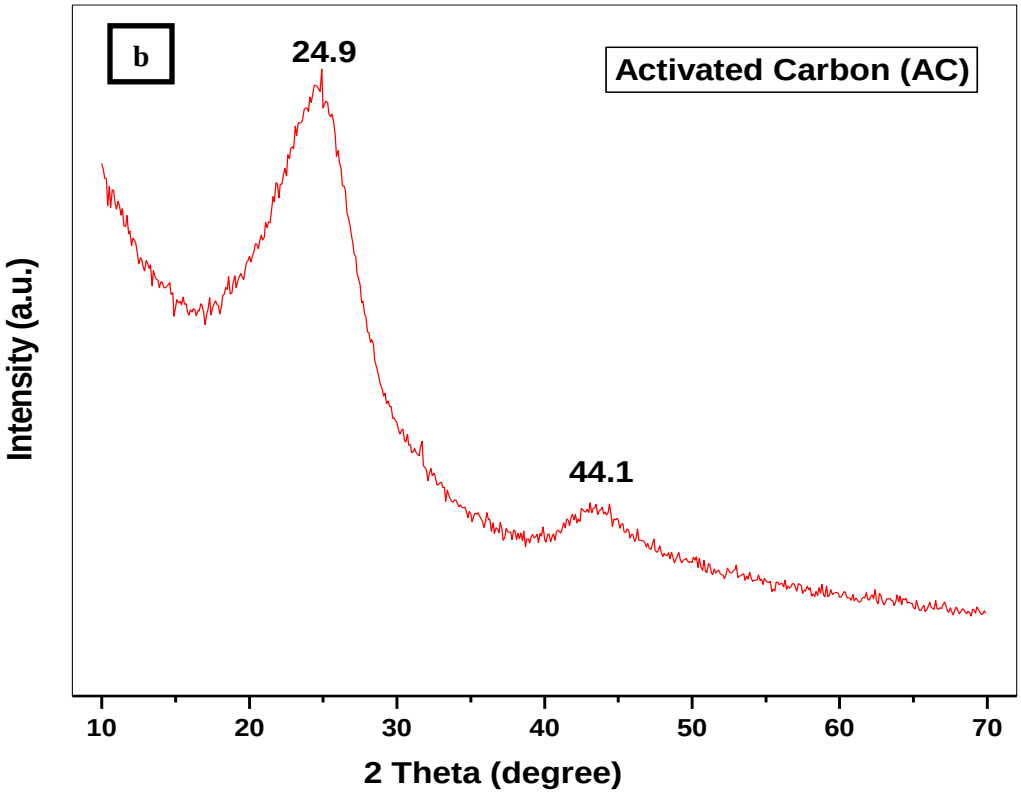
b
24.9
Activated Carbon (AC)
44.1
Intensity (a.u.)
10
20
30
40
50
60
70
2 Theta (degree)

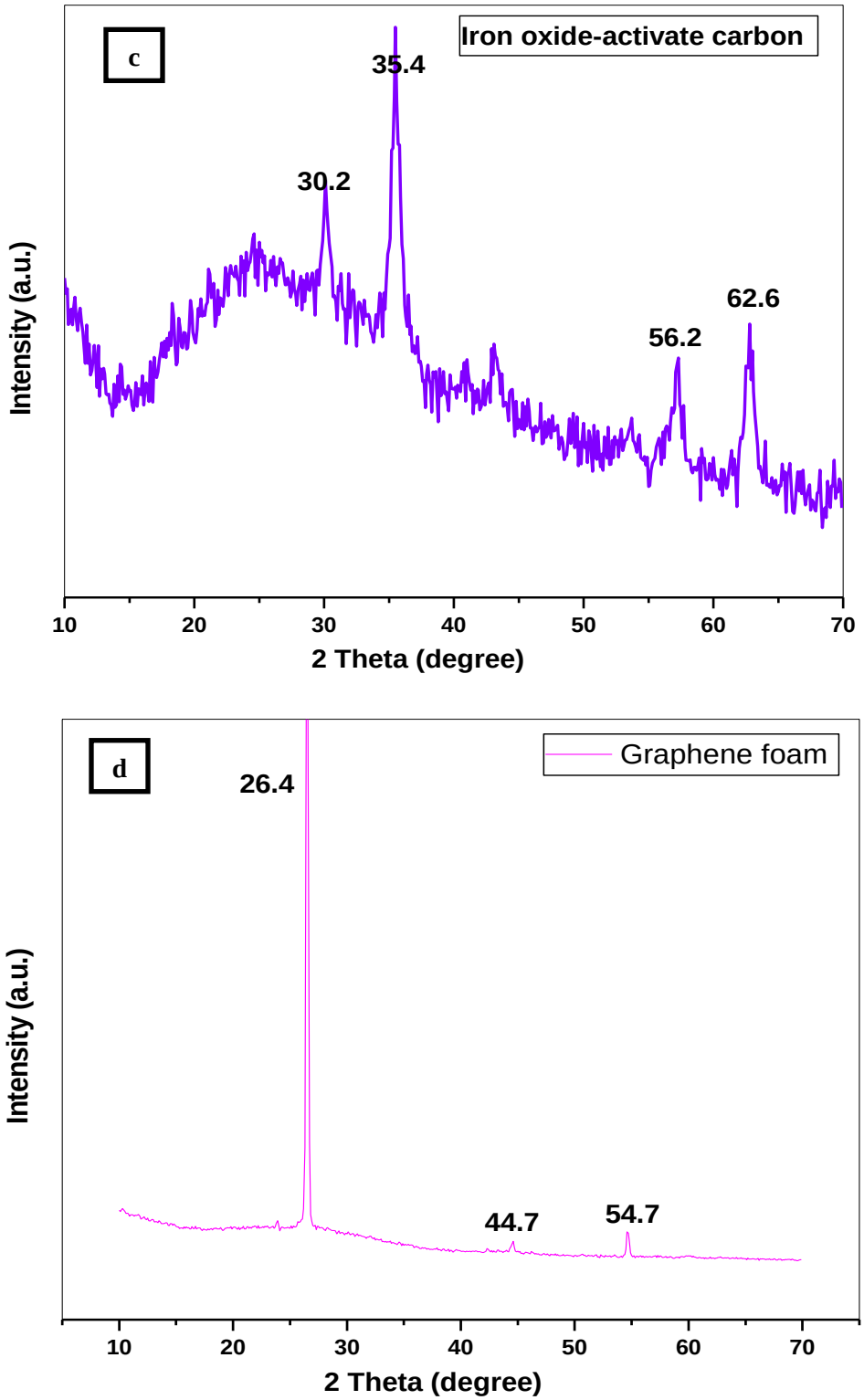

Figure 4.1: XRD spectra of **(a)** Iron oxide (Magnetite – Fe_3O_4), **(b)** activated carbon (AC), **(c)** activated carbon -iron oxide (AC-Fe_3O_4), **(d)** graphene foam (GF).

4.1.2 Fourier transform- Infrared Spectroscopy (FT-IR)

Figure 4.2 shows some comparative FT-IR spectra of activated carbon (AC), Iron oxide (Magnetite – Fe_3O_4), Iron oxide-activated carbon composite (AC-Fe_3O_4 or Fe_3O_4-AC), and graphene foam (GF) respectively.

From the Iron oxide (Fe_3O_4) spectrum; the bands observed at 570 cm^{-1} correspond to the Fe-O stretching mode of the tetrahedral and octahedral side of the magnetite complex. The peaks at 3425 cm^{-1} and 1620 cm^{-1} can be assigned to the stretching and vibration of the O-H groups that may be adsorbed on the surface of the compound [5]. FT-IR spectrum for activated carbon shows bands at 3429 and 1080 cm^{-1} are assigned to O-H bonds and C-OH stretching of phenolic groups, respectively. Based on the literature, the bands observed in the range; 1700 cm^{-1} and 1490 cm^{-1} are attributed to C=C symmetrical stretching of pyrone groups and C=O of carboxylic groups [6].

Fe_3O_4-AC composite gives rise to the bands at 3450 cm^{-1} and around 1650 cm^{-1}, which can be attributed due to the external adsorption of the hydroxyl group(s). the stretching of symmetrical C=C in the range 1700 cm^{-1} and 1490 cm^{-1} and that of Fe-O at 570 cm^{-1} are observed. This reveals that each compound retains its functional groups present in its pure forms.

Further, Figure 4.2 illustrates the FTIR spectrum of the 3D graphene foam. It can be seen that there are strong absorption peaks at 1650, 1400, and 2320 cm^{-1} [7]. The peaks at 1650, and 1400 cm^{-1} are due to C=C stretching bands for the aromatic rings, and C−OH stretching respectively. Moreover, the peaks at 2320 cm^{-1} and around 3450 cm^{-1} are assigned to the external environment as a consequence of carbon dioxide and hydroxyl groups.

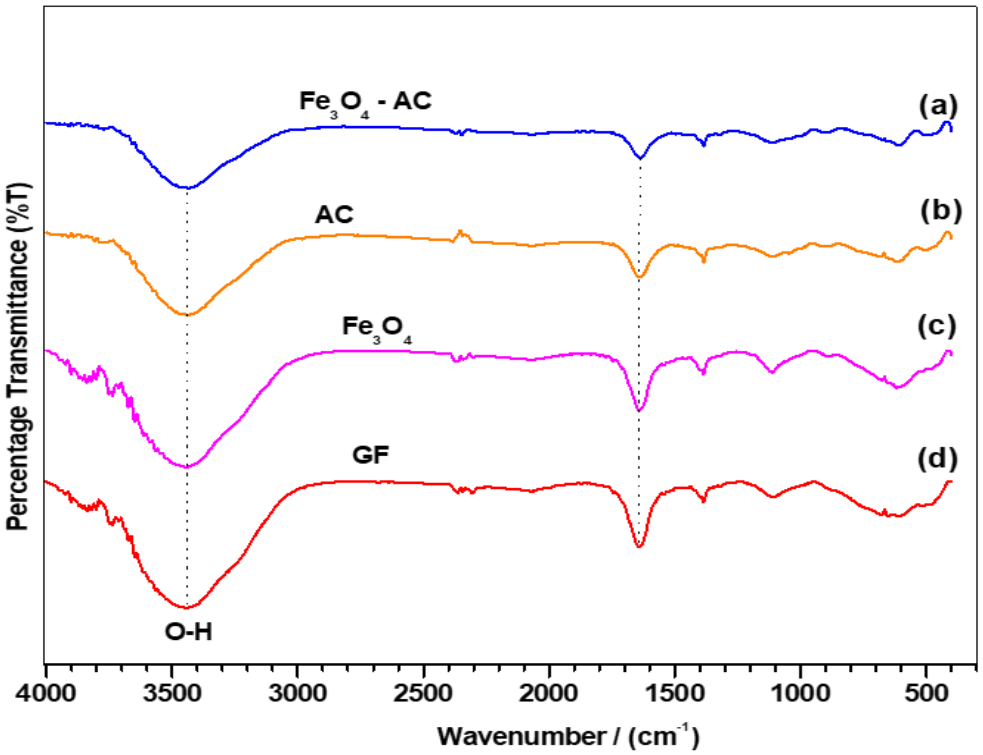

Figure 4.2: FT-IR spectra of; **(a)** Iron oxide-activated carbon composite (Fe_3O_4-AC), **(b)** activated carbon (AC), **(c)** Iron oxide (Magnetite – Fe_3O_4), **(d)** graphene foam (GF) respectively.

4.1.3 Energy dispersive X-ray spectroscopy (EDS)

Figure 4.3 shows the energy dispersive X-ray (EDS) spectra of (**a**) activated carbon (AC), (**b**) Iron oxide (Magnetite – Fe_3O_4), (**c**) Iron oxide-activated carbon composite (Fe_3O_4-AC), (**d**) graphene foam (GF). To confirm the formation of the composite, graphene foam, and the elemental composition of the materials, an EDS analysis was performed. During the measurements, different areas were focused, and the corresponding peaks were shown.

Figure 4.3 (**a**), the EDS spectra of activated carbon show that, carbon and oxygen were mostly present. The elemental composition of carbon-C (%wt = 79.7) in the activated carbon sample, has a greater ratio than that of oxygen (%wt = 18.6) [8]. The spectra also depict the presence of other elements, such as sodium (%wt = 1.0) and phosphorus (%wt = 0.7).

Figure 4.3 (**b**) shows the iron oxide spectrum with a high-intensity peak at 0.5 KeV for oxygen (O), lower peaks at 0.7 KeV for iron (III), and 5.4 KeV for iron (II). To distinguish the oxidations

of the iron in the magnetite, the peak ratios of oxygen and iron were calculated. That is, the atomic ratio of oxygen and iron is approximately 3:4, which is roughly the correct composition of magnetite [9]. The analysis shows a purely synthesized form of magnetite with a percentage weight of 49.2% Fe, 33.3% O, and 17.5% C which could be due to the adsorption of impurities of carbon in which the source could be the material used to set the sample for EDS analysis.

Figure 4.3 (**c**) depicts the EDS spectrum for iron oxide-activated carbon composite that shows the peaks corresponding to the elemental composition of both magnetite and activated carbon. Carbon, oxygen, and iron are present with a small peak due to the presence of sulfur. The composite seemed to be rich with carbon with high peak intensity and different oxidation states of iron are also present as in the iron oxide spectrum. Therefore the EDS confirms the elemental composition of the desired material as expected.

In spectrum 4, Figure 4.3 (**d**) below; graphene foam shows only one carbon peak at 0.4 KeV with high uniformity with no impurities detected (100.0 wt% C), and no Ni peaks observed, indicating that the removal of the original Ni template was successful during the acid leaching process [3]. This result implies that the synthesized graphene foam was purely formed and contained almost 100% carbon atoms.

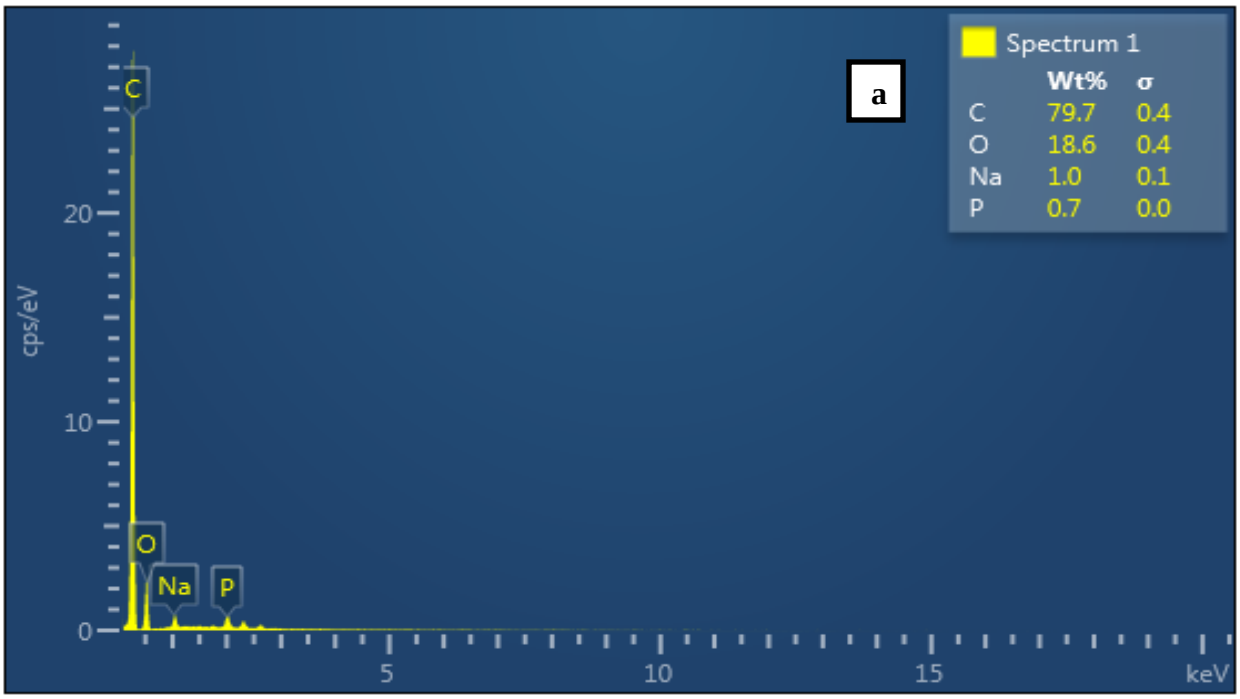
a
Spectrum 1
Wt% σ
C 79.7 0.4
O 18.6 0.4
Na 1.0 0.1
P 0.7 0.0
cps/eV
20
10
0
C
O
Na
P
5
10
15
keV

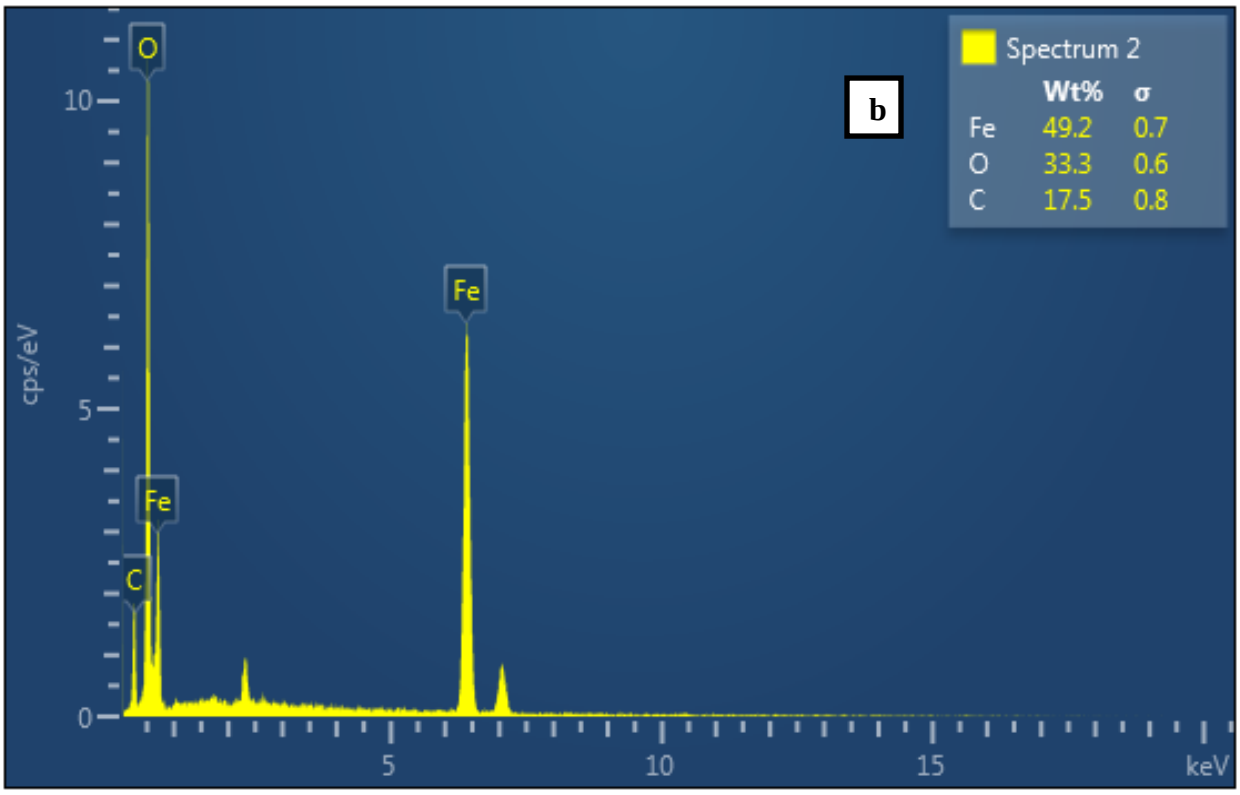
b
Spectrum 2
Wt% σ
Fe 49.2 0.7
O 33.3 0.6
C 17.5 0.8
cps/eV
10
5
0
O
Fe
Fe
C
5
10
15
keV

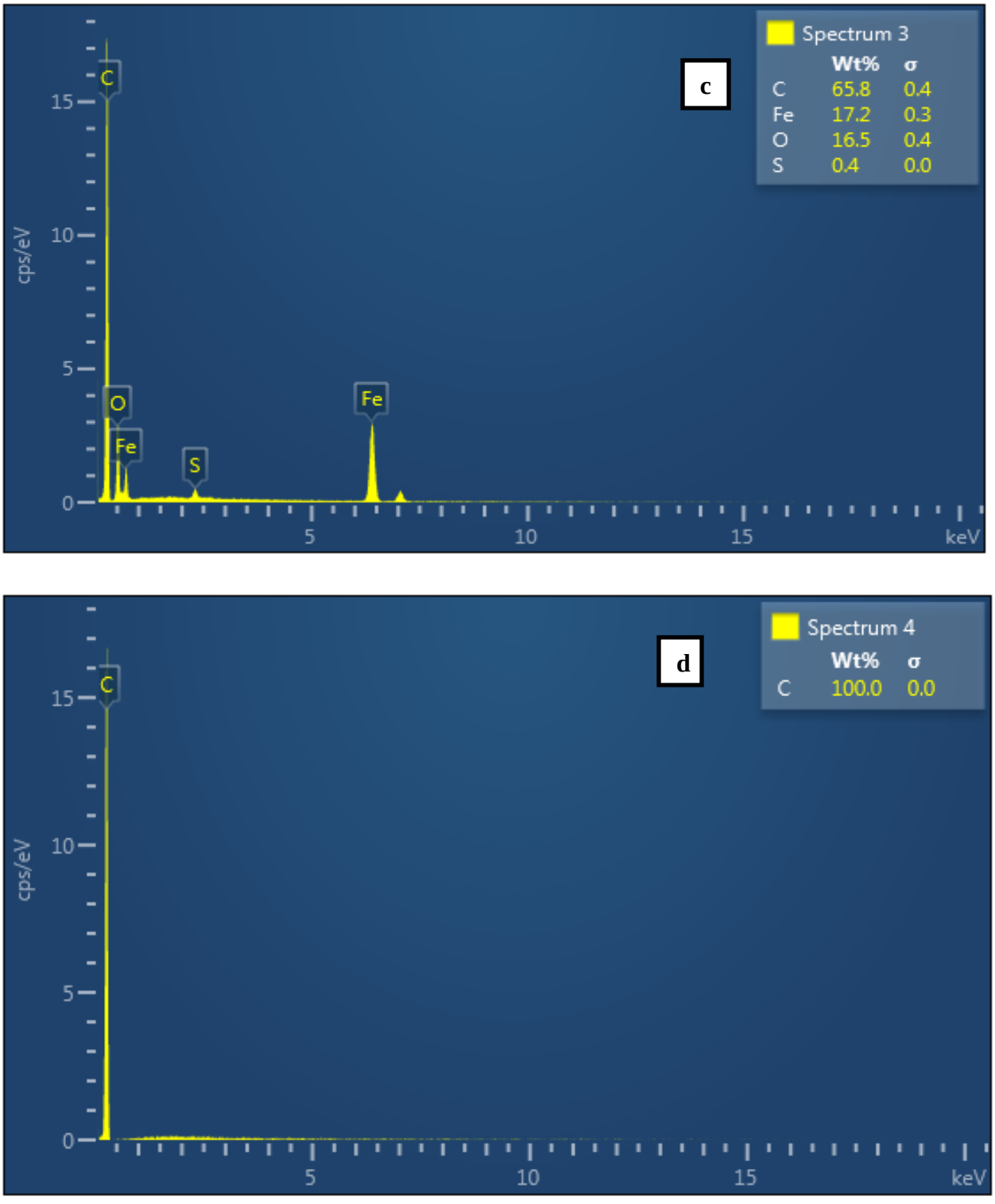

Figure 4.3: EDS spectra of **a)** activated carbon-spectrum 1 (AC), **b)** Iron oxide (Magnetite – Fe_3O_4) spectrum 2, **c)** Iron oxide-activated carbon composite (Fe_3O_4-AC) spectrum 3, **d)** graphene foam (GF) spectrum 4.

4.1.4 Scanning electrochemical microscopy (SECM)

The scanning electrochemical microscopy (SECM) micrograph for synthesized magnetite nanoparticles is shown in Figure 4.4 (a). The particles have a narrow size distribution with angular shape on the surface, and there are no existing pores on the magnetite surface observed. Therefore the magnetite nanoparticles were successfully synthesized using the co-precipitation method.

The micrograph shown in Figure 4.4 (b) depicts the rough surface morphology of activated carbon, which exhibits irregular shapes. The SECM image for composite (c), activated carbon-iron oxide; showed some crystalline structure and fine irregular surface structures, which show that both iron oxide and activated carbon morphologies.

Thin-film sheet of graphene foam (d) observed under (SECM), reveals that the graphene foam was synthesized using the chemical vapor deposition (CVD) method, and has a thin-film structure. This means that atoms in the structure of graphene foam are arranged in a regular pattern based on EDS and XRD data. Thin-film structural material possesses a high surface area.

a)

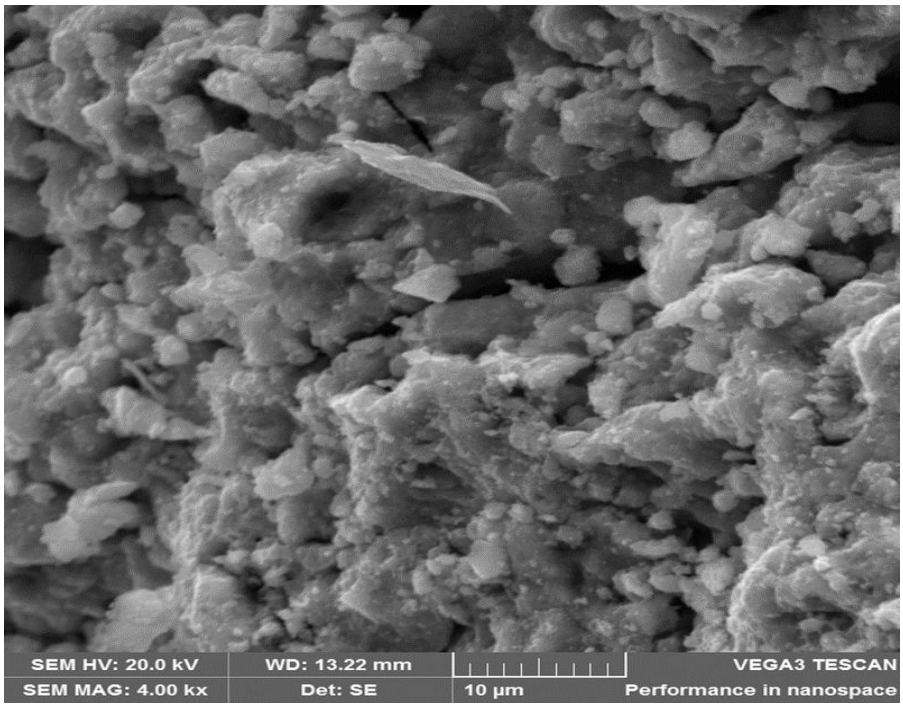

b)

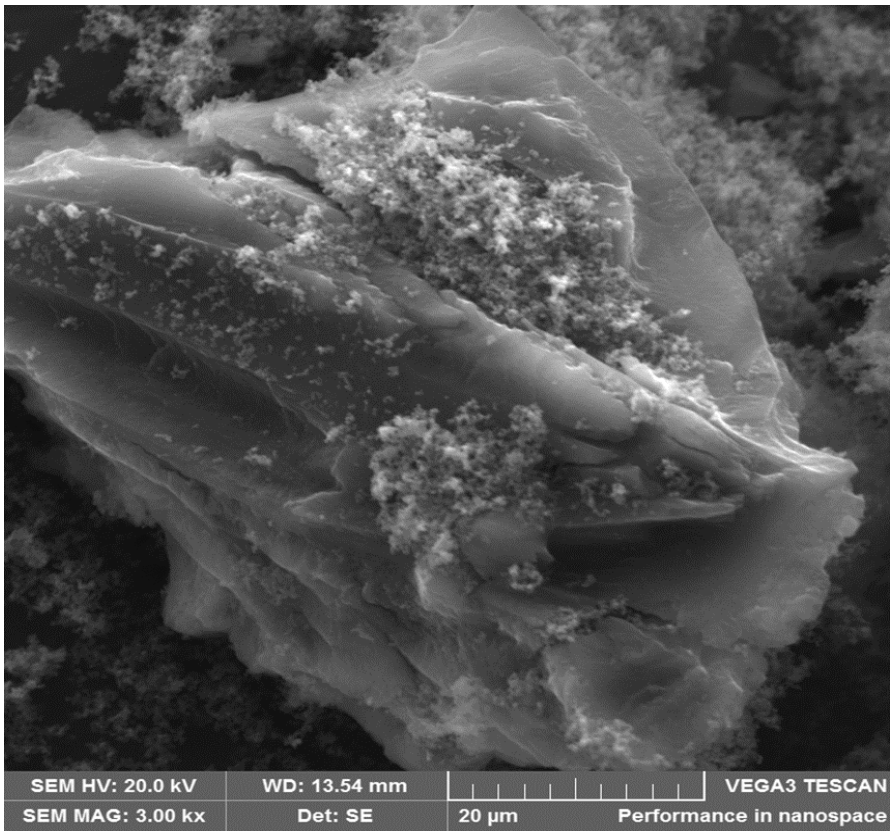
SEM HV: 20.0 kV
WD: 13.54 mm
VEGA3 TESCAN
SEM MAG: 3.00 kx
Det: SE
20 µm
Performance in nanospace

c)

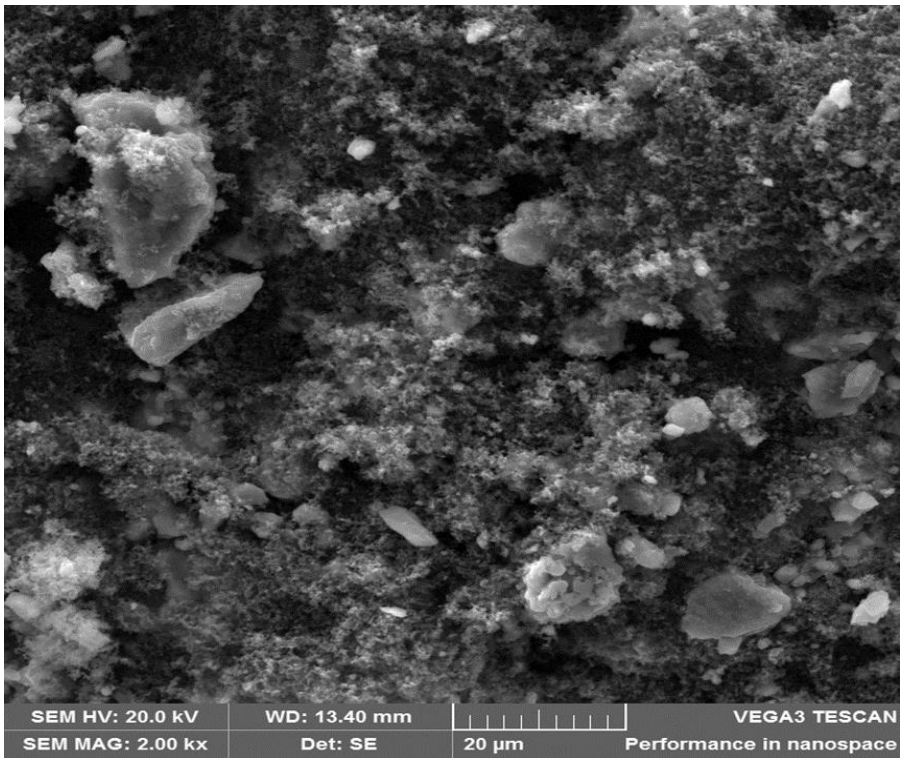
SEM HV: 20.0 kV
WD: 13.40 mm
VEGA3 TESCAN
SEM MAG: 2.00 kx
Det: SE
20 µm
Performance in nanospace

d)

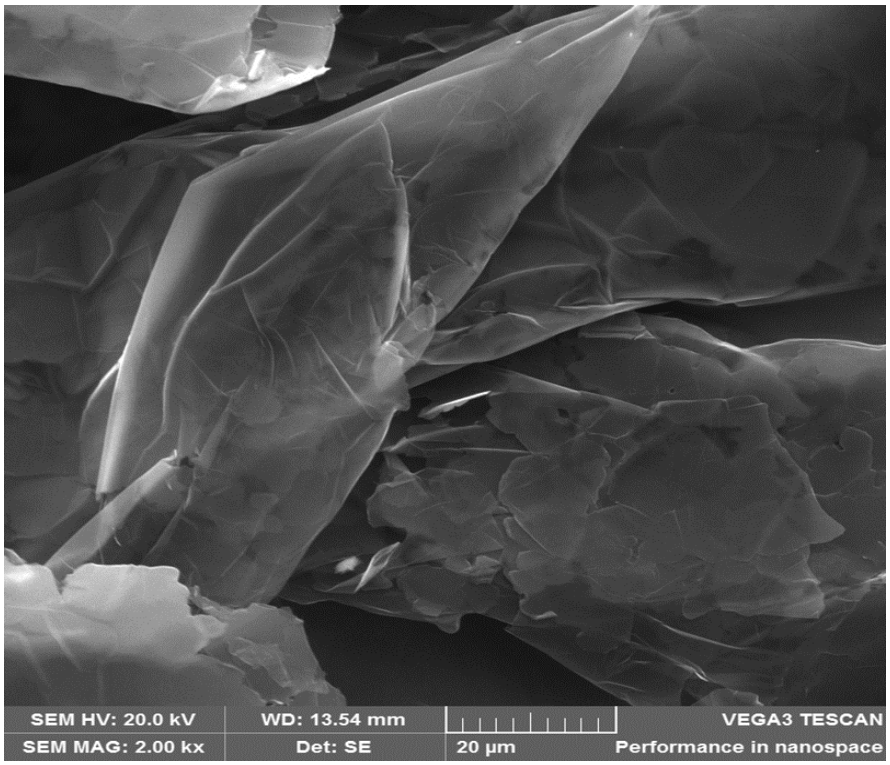

Figure 4.4: Scanning electrochemical microscopic images of **a)** Iron oxide (Magnetite – Fe_3O_4), **b)** activated carbon (AC), **c)** Iron oxide-activated carbon composite (Fe_3O_4-AC), **d)** graphene foam (GF).

4.2 Electrochemical characterization

4.2.1 The electroactive surface area of the unmodified electrode

The effective electroactive surface area of the bare glassy carbon electrode was calculated using the Randles-Sevcik equation at 25^{o}C and from the linear plot of the square root of the scan rate versus the peak current. The cyclic voltammograms at different scan rates are shown in Figure 4.5.

Randles-Sevcik Equation: $I_p = 2.69 \times 10^5 \, n^{3/2} \, A \, C \, D^{1/2} \, V^{1/2}$……4.1

where $\mathbf{I_p}$ (A) is the peak current, **n** is the number of electrons transferred in the redox reaction, **A** cm^2) is the electroactive surface area, D ($cm^2 \, s^{-1}$) is the diffusion coefficient (that is 6.70×10^{-6}

$cm^2\ s^{-1}$ for $[Fe(CN)_6]^{4-}$ [10], **C** (mol cm^{-3}) is the concentration of the species (5 x 10^{-6} mol cm^{-3} for $[Fe(CN)_6]^{4-}$) and **v** (V s^{-1}) is the scan rate.

A three-electrode electrochemical cell was employed for the estimation of the surface area of a bare and modified GCE. Ag/AgCl (3.0 M KCl) as the reference electrode, platinum (Pt) wire as the counter electrode, and bare or modified GCE as a working electrode. An electrolyte solution of 5 mM $K_4[Fe(CN)_6]$ was prepared in 0.1 M KCl solution. The cyclic voltammograms were run for scan rates from 20 – 250 mV s^{-1} in the potential window of -200 to 600 mV.

This reaction is controlled by the diffusion of ferrocyanide ions and has good reversibility on the GCE surface. Therefore, the peak current is proportional to the electroactive surface area of the working electrode and can be expressed by the Randles-Sevcik equation [11]. Figure 4.5 (a) shows a typical current-potential plot for the oxidation and reduction of potassium ferrocyanide at various scan rates at a bare GCE. A plot of anodic peak current versus the square root of scan rates shown in Figure 4.5 (b), displayed a very good linear relationship indicating that the process is diffusion-controlled.

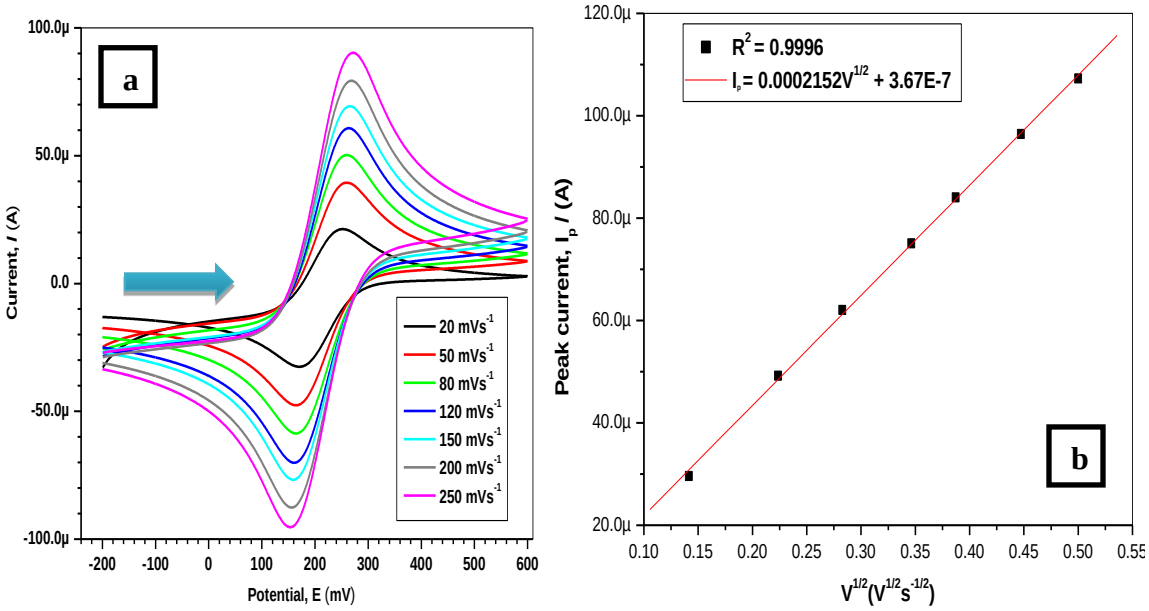

Figure 4.5: (a) Cyclic voltammograms of 5 mM $K_4[Fe(CN)_6]$ prepared in 0.1 M KCl solution at different scan rates using a bare GCE. **(b)** A linear plot of peak current as a function of the square root of the scan rate.

From the slope of this plot, the effective surface area of the bare GCE was calculated to be 0.0596 cm^2.

4.2.2 The surface area of the modified electrode

The same experimental procedure was conducted for a modified GCE labeled (AC-Fe_3O_4/GF/GCE). Figure 4.6 depicts (**a**) cyclic voltammograms of 5 mM $K_4[Fe(CN)_6]$ prepared in 0.1 M KCl solution at different scan rates (20 – 250 mV s^{-1}) using an AC-Fe_3O_4/GF/GCE. (**b**). The plot of anodic peak currents versus the square root of the scan rate gave a linear relationship.

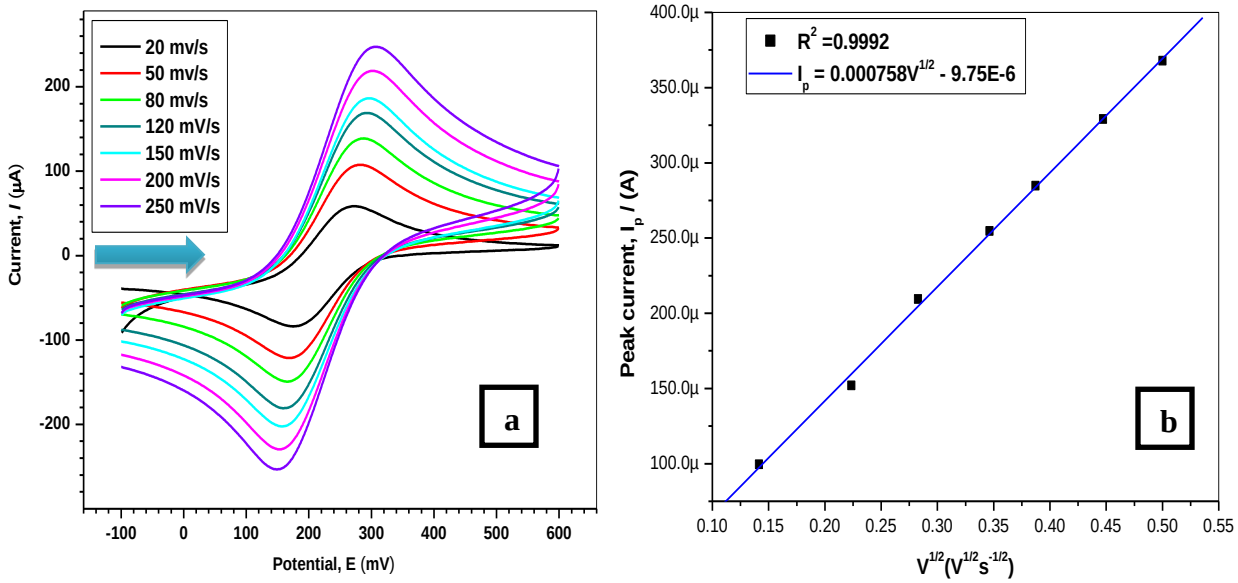

Figure 4.6: (a) Cyclic voltammograms of 5 mM $K_4[Fe(CN)_6]$ prepared in 0.1 M KCl solution at different scan rates using a modified electrode, AC-Fe_3O_4/GF/GCE. **(b)** The plot of peak current as a function of the square root of the scan rate.

From the slope of the linear plot of Figure 4.6 (b) the electroactive surface area of the modified GCE was then calculated to be 0.210 cm^2, and the ratio of the surface area of the modified GCE to the unmodified GCE was determined to be 3.5. This implies that the surface area of the electrode was enhanced by a factor of 3.5, which is about a 350% surface increase. Moreover, the peak current intensity was increased as expected relative to that of bare GCE. The effective electroactive surface area signifies the superior electrochemical reactivity of AC-Fe_3O_4/GF/GCE.

There was a slight shift in both anodic and cathodic peak currents as the scan rate was increased from 20 – 250 mV s^{-1}. This observation suggests the stability of the developed electrochemical sensor. A major shift in the peak potential was not observed which indicates that the leaching of the modifier did not occur. A plot of anodic peak currents as a function of the square root of scan rates displayed a good linear relationship as shown in Figure 4.6 (b). The linear regression equation obtained for the scan rate was $I_p(\mu A) = 7.58 \times 10^{-4} V^{1/2} - 9.75 \times 10^{-6}$, with a correlation coefficient of $R^2 = 0.9992$.

The redox peak current response increases and the peak potentials of the anodic and cathodic were also increasing. Moreover, peak separation was observed in all cyclic scan rates. All these findings cement the fact that the redox reaction is diffusion-controlled.

4.2.3 Cyclic voltammetric measurements at different modifiers

The electrochemical characterizations of glassy carbon electrodes with various modifications were examined by cyclic voltammetry using potassium ferrocyanide in a 0.1 M potassium chloride redox probe at a scan rate of 50 mV s^{-1}. The bare glassy carbon electrode (bare-GCE) has quasi-reversible redox features for 2.5 mM $[Fe(CN)_6]^{4-}$ probe with a peak-to-peak separation (ΔE_p) of 116 mV [12]. The composite, activated carbon-iron oxide/glassy carbon electrode (AC-Fe_3O_4/GCE) also shows reversible redox peaks and peak separation of 130 mV, while iron oxide/graphene foam/ glassy carbon electrode (Fe_3O_4/GF/GCE) depicts a higher quasi-reversible redox peaks with peak to peak separation of 223 mV.

Figure 4.7 also exhibited a peak separation of 114 mV for graphene foam/glassy carbon electrode (GF/GCE). Furthermore, the combination of activated carbon/graphene foam/glassy carbon electrode (AC/GF/GCE) exhibits a good pair of redox peaks through oxidation and reduction contributions at 1.02×10^{-4} A and -1.07×10^{-4} A (vs. Ag|AgCl, 3.0 M), respectively. However, an activated carbon-iron oxide/graphene foam electrochemical sensor on a glassy carbon electrode (AC-Fe_3O_4/GF/GCE) shows well-defined redox peaks with a peak separation of 146 mV. In addition, the redox peak current ratio ($I_{pa}/I_{pc} \approx 1$), describes the quasi-reversible electrochemical process with one electron transfer cycle. From the cyclic voltammograms, it can be observed that bare GCE, AC-Fe_3O_4/GCE, Fe_3O_4/GF/GCE, /GF/GCE, and AC/GF/GCE exhibit lower peak

currents whilst AC-Fe_3O_4/GF/GCE displays a much higher redox peak currents with less peak separation compared to Fe_3O_4/GF/GCE and AC/GF/GCE.

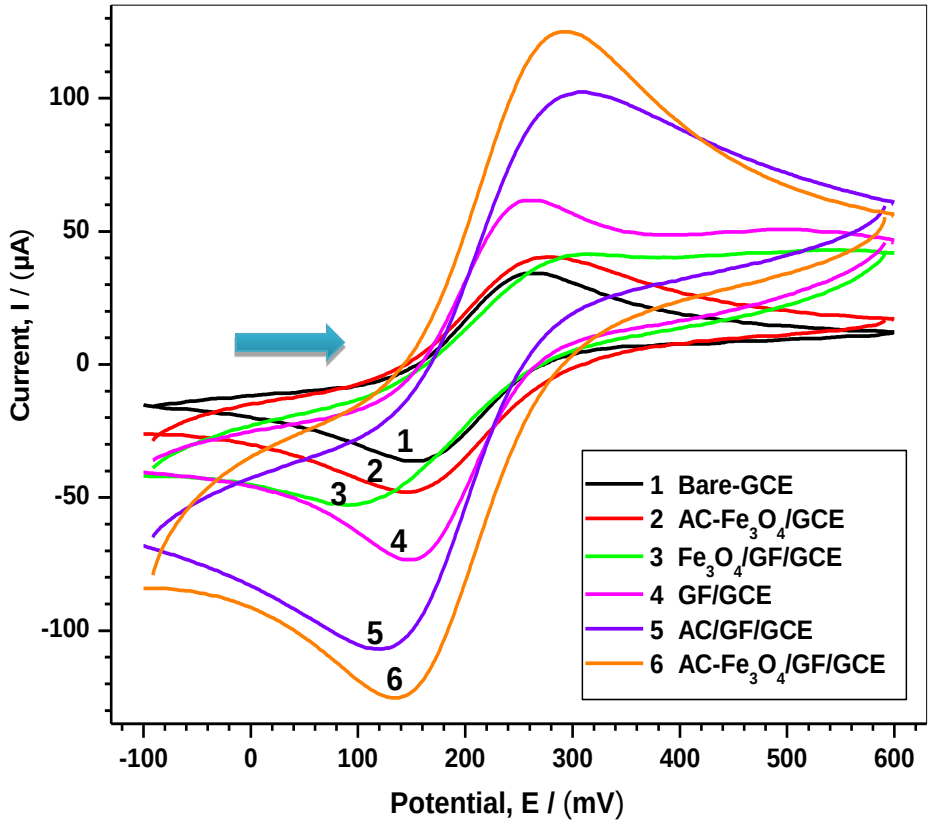

Figure 4.7: Cyclic voltammograms of unmodified and modified electrodes in 2.5 mM $K_4[Fe(CN)_6]$ prepared in 0.1 M KCl electrolyte system, at the scan rate of 50 mVs^{-1}.

Table 4.1 summarizes the electrochemical data that were obtained using the unmodified and modified electrodes in 2.5 mM $K_4[Fe_3(CN)_6]$ prepared in a 0.1M KCl solution. The ratio of anodic and cathodic peak currents (I_{pa}/I_{pc}), and the peak-to-peak separation (ΔEp/V) values are shown. The peak separation values were lowest for GF/GCE (114 mV) and highest for Fe_3O_4/GF/GCE (233 mV). It must be noted that AC-Fe_3O_4/GF/GCE (146 mV) gave rise to the highest peak current signals (anodic peak current I_{pa} = 125 µA and cathodic peak current I_{pc} = 125µA), greater than that of unmodified and other modified electrodes. Based on the peak-to-peak potential difference, the order of reversibility can be given as GF/GCE ≈ Bare-GCE > AC-Fe_3O_4/GCE > AC-Fe_3O_4/GF/GCE > AC/GF/GCE > Fe_3O_4/GF/GCE. On the other hand, the rate of the electron

transfer on the basis of the current responses can be assigned as AC-Fe_3O_4/GF/GCE > AC/GF/GCE ≈ bare GCE, > GF/GCE ≈ AC-Fe_3O_4/GCE > Fe_3O_4/GF/GCE. This order clearly shows that the AC-Fe_3O_4/GF/GCE electrode exhibits the highest catalytic activity towards the oxidation and reduction of ferrocyanide/ ferricyanide redox couple.

Table 4.1: Summary of cyclic voltammetric data obtained for unmodified and modified electrodes in 2.5 mM $[Fe(CN)_6]^{4-}$ prepared in 0.1 M KCl solution.

Electrode	I_{pa} /µA	I_{pc} /µA	I_{pa}/I_{pc}	E_{pa} /mV	E_{pc} /mV	ΔE_p
1. Bare-GCE	3.42E-05	3.62E-05	0.95	269	153	116
2. AC-Fe_3O_4/GCE	4.04E-05	4.79E-05	0.84	278	148	130
3. Fe_3O_4/GF/GCE	4.14E-05	5.28E-05	0.78	324	91	233
4. GF/GCE	6.16E-05	7.34E-05	0.84	262	148	114
5. AC/GF/GCE	1.02E-04	1.07E-04	0.95	309	121	188
6. AC-Fe_3O_4/GF/GCE	1.25E-04	1.25E-04	1.0	289	143	146

4.3 Electrocatalytic oxidation of uric acid

4.3.1 Electrocatalytic oxidation and reduction of uric acid

As shown above, the modified electrode AC-Fe_3O_4/GF/GCE has demonstrated a superior current response for the potassium ferrocyanide solution. Thus, this electrode was used for the subsequent electrochemical investigations of uric acid. Figure 4.8 represents the cyclic voltammetry response of 5 mM uric acid in 0.1 M phosphate buffer solution (PBS) of pH 6 at bare and modified GCE at 50 mV s^{-1} scan rate.

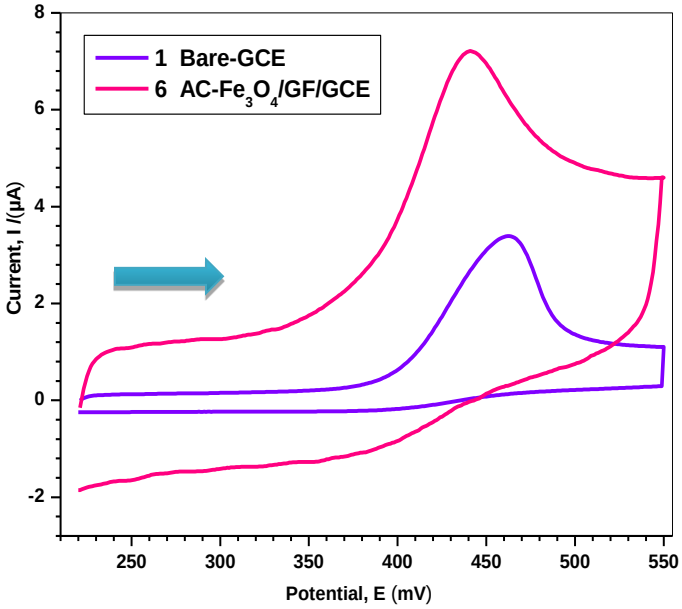

Figure 4.8: Cyclic voltammograms of 5 mM Uric acid in 0.1 M Phosphate buffer pH 6, on bare GCE (**1**) and modified GCE, AC-Fe_3O_4/GF/GCE **(6)** at a scan rate of 50 mV s^{-1}.

Bare-GCE evinces less anodic oxidation peak current intensity along the peak potential at 451 mV (check the potential) against the Ag|AgCl electrode, revealing the insignificant electrocatalytic characteristics towards uric acid. On the reverse scan (reduction); no peak current was observed, this suggests that the oxidation of uric acid is an irreversible reaction on bare GCE. The AC-Fe_3O_4/GF modified GCE indicates a rapid peak current response with an oxidation peak potential at 433 mV against the Ag|AgCl electrode and the oxidation response is at least 3-fold higher than that of the bare GCE. These results correlate with the fact that the electroactive surface area of the GCE had increased as depicted in Figure 4.6. On the reverse scan, the cyclic voltammogram exhibited a smaller peak at the modified electrode. The absence of a reduction peak could be due to a fast chemical reaction following the oxidation of uric acid. This means the product formed during the oxidation process might have been chemically 'removed' from the surface of the electrode (EC mechanism). The background current of AC-Fe_3O_4/GF/GCE was greater than the bare GCE which shows the existence of nanoparticles and carbon materials used as an electrochemical sensor on the surface of the electrode [13]. The high background current is attributed to the high double-layer current.

4.3.2 Effect of scan rate on uric acid oxidation

Figure 4.9 shows the influence of scan rate in the range of (20 – 350 mV s^{-1}), for the oxidation of 5 mM uric acid which was investigated by cyclic voltammetry in 0.1 M phosphate buffer solution, pH 6 at the modified electrode AC-Fe_3O_4/GF/GCE. Figure 4.9 (**a**) depicts the cyclic voltammograms obtained in the potential window of 0.35 to 0.65 V, and it was noticed that the oxidation peak current of uric acid increased with increasing scan rate. As can be seen from the voltammograms, the peak potentials shift towards more positive values with increasing scan rates, indicating that the electron transfer processes become irreversible with increasing scan rates.

Figure 4.9 (**b**) demonstrates the plot of anodic peak current (I_{pa}) versus the square root of the scan rate ($U^{1/2}$). A linear equation, $I_p = -9.5 \times 10^{-6} V^{1/2} + 6.94 \times 10^{-5}$ with a correlation coefficient of $R^2 = 0.989$ was obtained. Based on the observation of the high current response for the electrochemical oxidation of uric acid at AC-Fe_3O_4/GF/GCE, it is believed that a surface-confined process with relatively fast electron transfer is taking place with a synergic effect of the materials used for electrode modification.

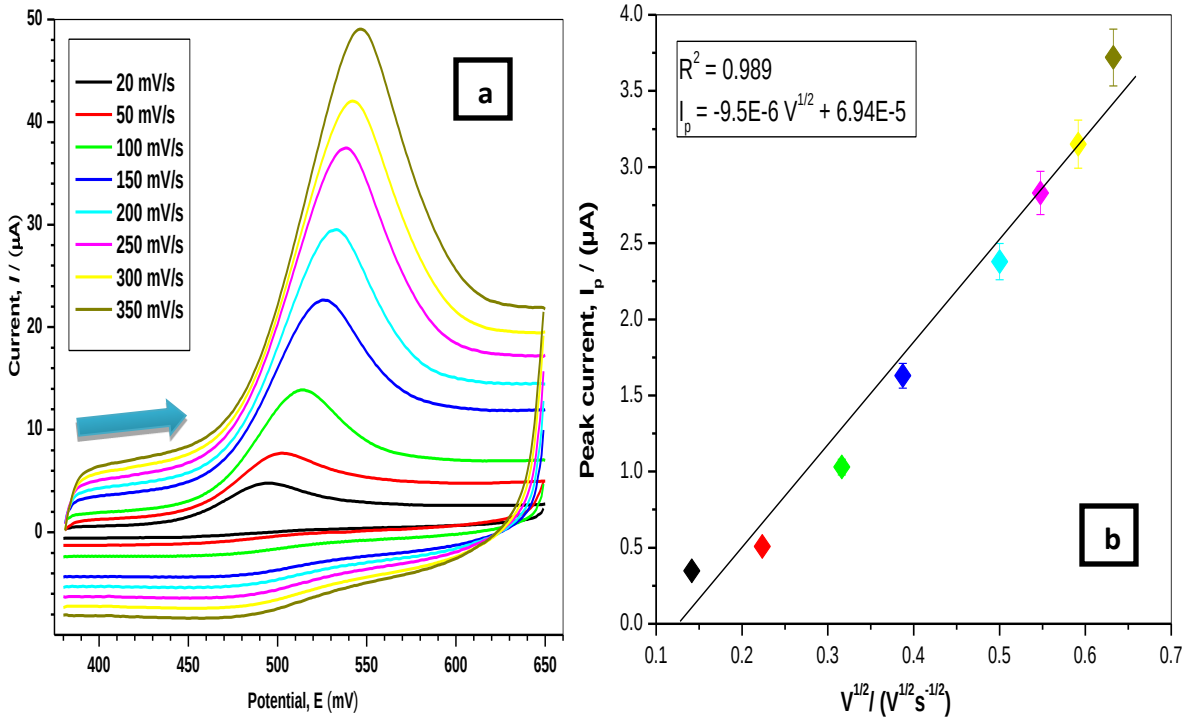

Figure 4.9: (**a**) Cyclic voltammograms of 5 mM uric acid in 0.1M Phosphate buffer pH 4, on AC-Fe_3O_4/GF/GCE at different scan rates, and (**b**) Linear dependence of anodic peak current as a function of the square root of the scan rate.

4.3.3 Estimation of the diffusion coefficient of uric acid using the modified electrode

The electroactive surface area of the modified electrode was calculated as shown in Section 4.2.1 Therefore, with the known surface area of the modified electrode, the same procedure was conducted as in Figure 4.6 using 0.1 M phosphate buffer solution containing 0.291 mM uric acid in a range of 20 – 250 mV s^{-1} scan rates. First, the optimum pH value of the supporting electrolyte system was optimized under cyclic voltammetry as depicted in Figure 4.10 ranging from pH 3 to 7.

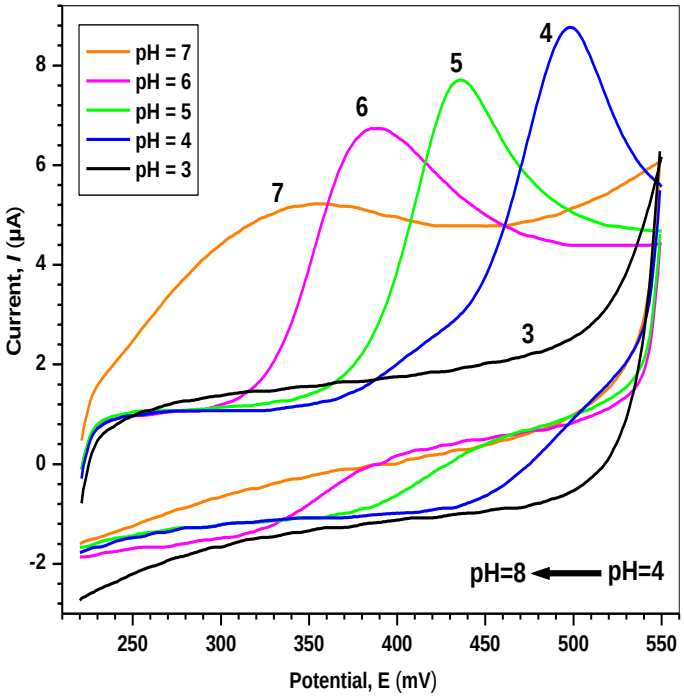

Figure 4.10: Cyclic voltammograms at modified GCE at different pH of 0.291 mM uric acid in a 0.1M Phosphate buffer solution, at the scan rate of 50 mV s^{-1}.

It was observed that the highest anodic peak current for the oxidation process of uric acid was obtained at pH 4. This pH value was chosen as the optimum pH under cyclic voltammetry to determine the diffusion coefficient of uric acid.

The electrochemical behavior of uric acid was examined under the scan rate of (20 – 250 mV s^{-1}) as depicted in Figure 4.11 under this pH.

The plot of the anodic peak current of uric acid versus the square root of the scan rate gives a straight line as shown in Figure 4.11 (**b**) following the Randles-Sevcik equation and the slope from the linear plot ($I_p = 1.66 \times 10^{-4} V^{1/2} - 8.4 \times 10^{-6}$), was used to calculate the diffusion coefficient (D) of uric acid. The diffusion coefficient was calculated to be 12.8 x 10^{-6} cm^2 s^{-1}. This value is comparable with the reported diffusion coefficient of 0.5 mM uric acid at chemically assembled carboxylated single-walled carbon nanotubes netlike electrode, which was calculated to be 7.5 x 10^{-6} cm^2 s^{-1} [14]. In another study, it was found to be 5.91 x 10^{-6} cm^2 s^{-1} using a carbon paste electrode modified with Lewatit FO36 nano resin [15].

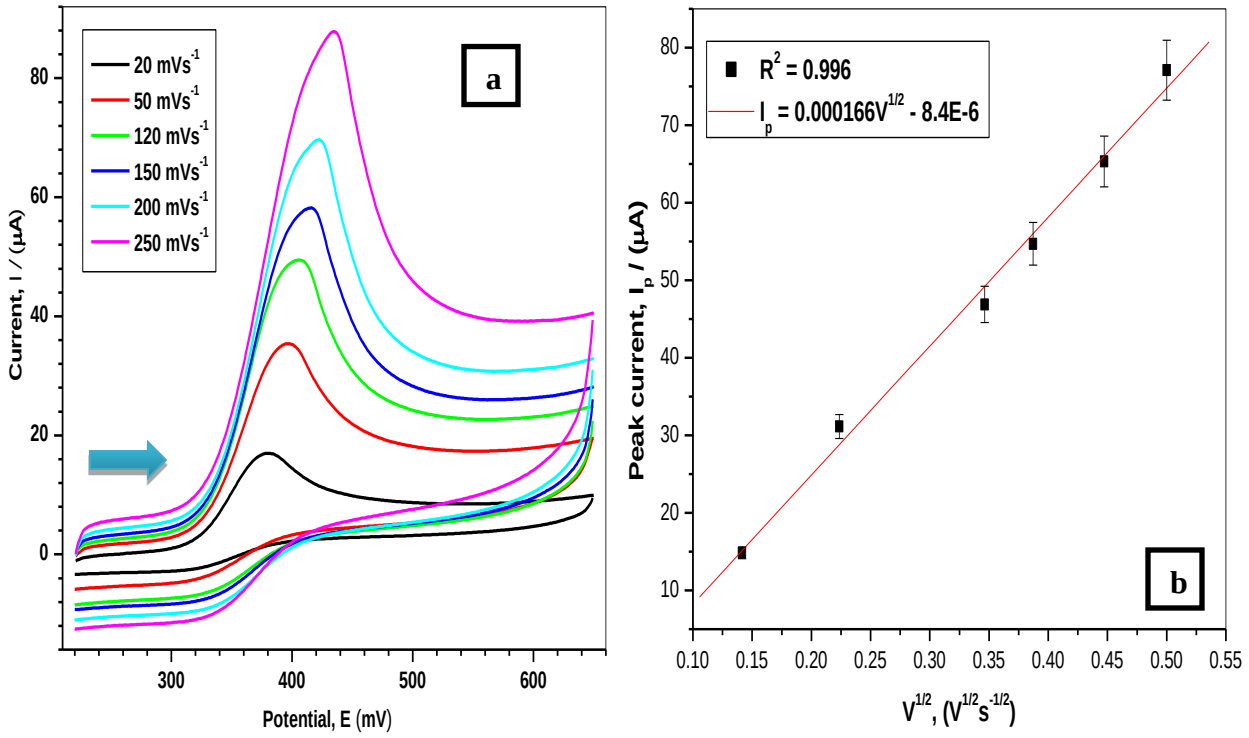

Figure 4.11: (**a**) Cyclic voltammograms of 0.291 mM uric acid in 0.1 M Phosphate buffer pH 4, on AC-Fe_3O_4/GF/GCE at different scan rates, and (**b**) Linear dependence of anodic peak current as a function of the square root of the scan rate.

4.3.4 Optimized instrumental parameters for uric acid detection

For the differential pulse voltammetric measurements, the instrumental parameters such as pulse scan rate 0.05 V s^{-1}, pulse width 0.05 s, pulse amplitude 0.05 V, sample width 0.017 s, potential window 0.2 to 0.55 V, pulse period 0.2 s, and quite time 2 s were optimized for catalytic oxidation of uric acid.

4.3.5 Influence of pH on the electrochemical oxidation of Uric acid under DPV

To obtain the best optimum pH value for the determination of uric acid (UA), 0.1 M (PBS) containing 0.5 mM UA was investigated at different pH levels. NaOH and HCl aqueous solutions were used to adjust the pH of the buffer solutions. Since the differential pulse voltammetry (DPV) technique has a major influence on the elimination of the double-layer charging current as compared to cyclic voltammetric (CV), it offers a highly sensitive faradic current. Hence DPV was

chosen as a better technique to investigate the effect of the pH of the electrolyte system on the electrochemical properties of uric acid and to obtain good sensitivity [16]. Figure 4.12 (**a**) shows the plot of differential pulse voltammograms at different pH for 0.5 mM uric acid in 0.1 M phosphate buffer solutions.

Figure 4.12 (**a**) shows that with the increase of pH from 4 to 8, the oxidation peak current increases from pH 4 to 6. A maximum peak current is observed at pH 6. Thereafter, the anodic peak current decreases for pH 7 and 8. The current response for uric acid was obtained to be the best at pH 6, as shown in Figure 4.12 (**b**), which is closer to the biological activity medium. Therefore, pH 6 was selected as the optimum pH for further analyses of uric acid. Three differential pulse runs were performed for each pH buffer system and reproducible voltammograms were obtained.

Figure 4.12 (a) further shows that the voltammograms shift in the negative potential direction with increasing pH. Fig. 4.12(c) is a plot of uric acid oxidation potential as a function of pH. The plot shows a linearly decreasing potential as a function of pH. The shift in the oxidative peak potential to the negative direction indicates that the electrode process is influenced by protonation reactions. The linear fitting equation for the plot was found to be: $E_P = - 0.058\ pH + 0.697$ ($R^2 = 0.998$). The corresponding slope of 58 mV pH^{-1} is close to the theoretical value of the slope of the Nernst equation of 59 mV pH^{-1} [17]. This result indicates that the number of protons and electrons transferred is the same during the oxidation process of uric acid in which the oxidation of uric acid involves the loss of two electrons and two protons, respectively as shown by Scheme 4.1 for the oxidation reaction of uric acid [15].

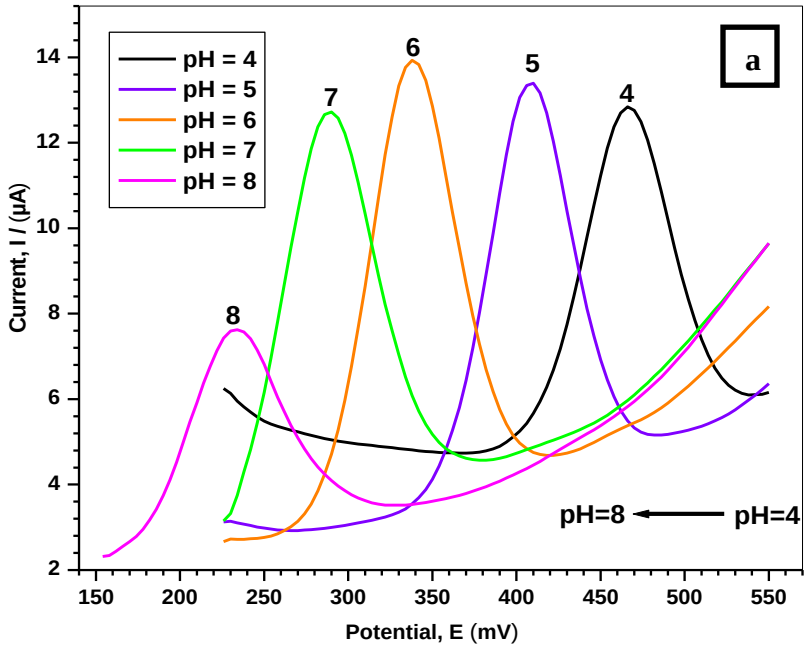
a
pH = 4
pH = 5
pH = 6
pH = 7
pH = 8
8
7
6
5
4
pH=8
pH=4
Current, I / (μA)
Potential, E (mV)

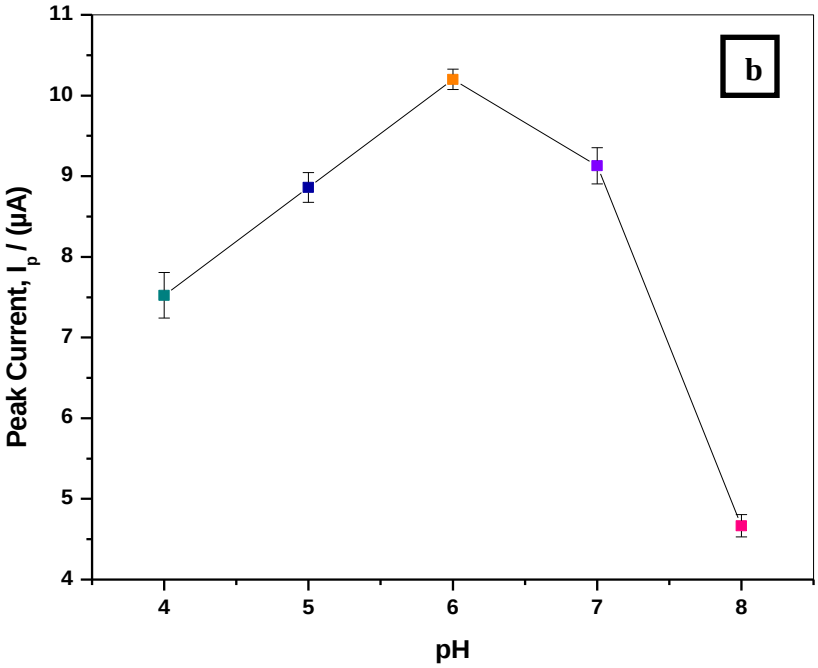
b
Peak Current, I_p / (μA)
pH

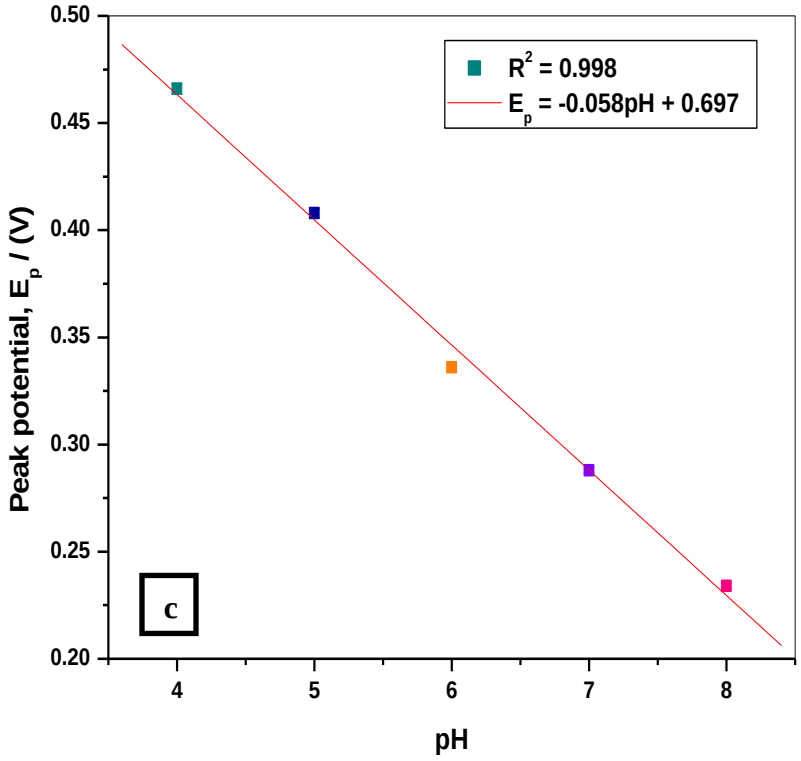

Figure 4.12: (**a**) Differential pulse voltammograms of AC-Fe_3O_4/GF/GCE in 0.5 mM uric acid prepared in a 0.1 M phosphate buffer solution at different pH. (**b**)The plot of oxidation peak current as a function of pH. (**c**) The linear plot for oxidation peak potentials of uric acid against pH.

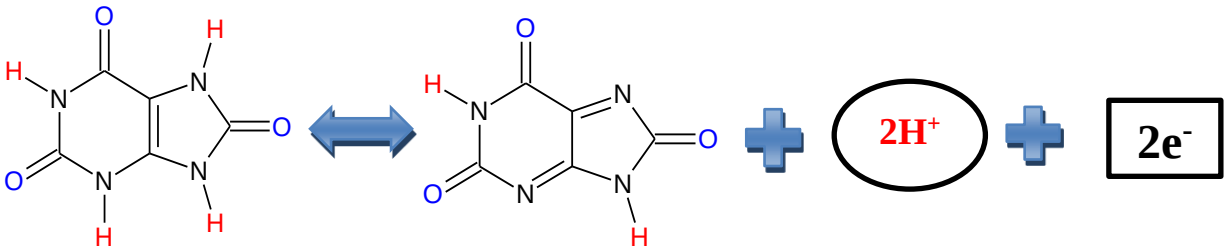

Scheme 4.1: Proposed reaction mechanism of uric acid oxidation.

4.3.6 Calibration curve and detection limit of uric acid

To obtain calibration curves for the electrode and determine the relationship between the anodic peak current and uric acid concentration, differential pulse voltammograms were measured under the optimized parameters in pH 6 PBS aqueous buffer solution.

Table 4.2 summarizes the experimental optimized parameters for the calibration curve and detection limit of uric acid. Figure 4.13 (a) and (b) show typical differential pulse voltammograms of UA at the AC-Fe_3O_4/GF/GCE in the concentration range of 5 to 1630 µM of uric acid. Under these optimized parameters, to achieve the working range of the developed electrochemical sensor, the differential pulse voltammograms of UA were performed with 3 replicates for each concentration.

Table 4.2: Optimized differential pulse voltammetric (DPV) experimental parameters.

Optimized parameters	Values
Supporting electrolyte (0.1M Phosphate Buffer Aqueous Solution)	pH 6.0
Scan Rate	0.05 V s^{-1}
Pulse width	0.05 s
Pulse amplitude	0.05 V
Sample width	0.017 s
Potential window	(0.2 to 0.55) V
Pulse Period	0.2 s
Quite time	2 s

As shown in the Figure, the peak currents increased with increasing uric acid concentrations, and a linear calibration plot was obtained with a calibration equation. It can be observed that the concentration increase of UA leads to the enhancement of uric acid oxidation peak current. It can also be observed that the developed electrochemical sensor possesses a wide linear range. Figure 4.13 (b) magnifies the voltammograms with very low concentrations which are hidden when merged in a single plot as shown in Figure 4.13 (a).

The relationship between the peak current versus the concentration of uric acid shows the linear dependence with an equation I_p (μA) = 0.129 [UA] (μM) + 1.05 x 10^{-6} from 5 to 1630 μM with a limit of detection of 2.55 μM and limit of quantification of 7.703 μM (according to the equations: 3.3 (**S**/**m**) and 10 (**S**/**m**) [18]. Where **S** is the relative standard deviation of the intercept of the y-coordinate from the linear fit plot and **m** is the slope of the same line. The summarized data from this linear range are depicted in Table 4.3**.**

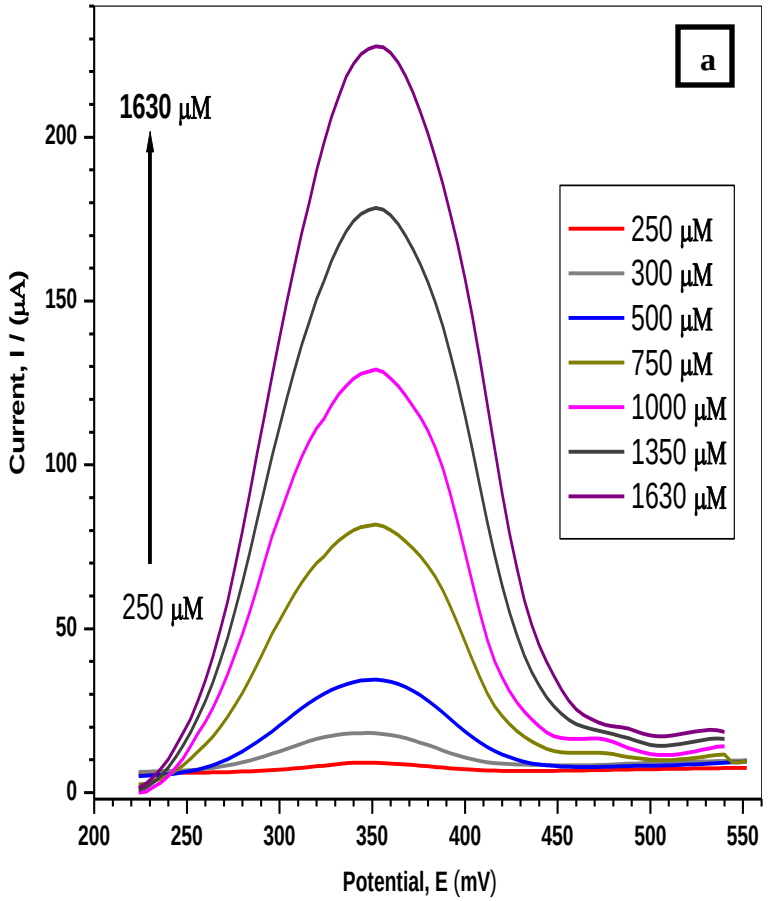

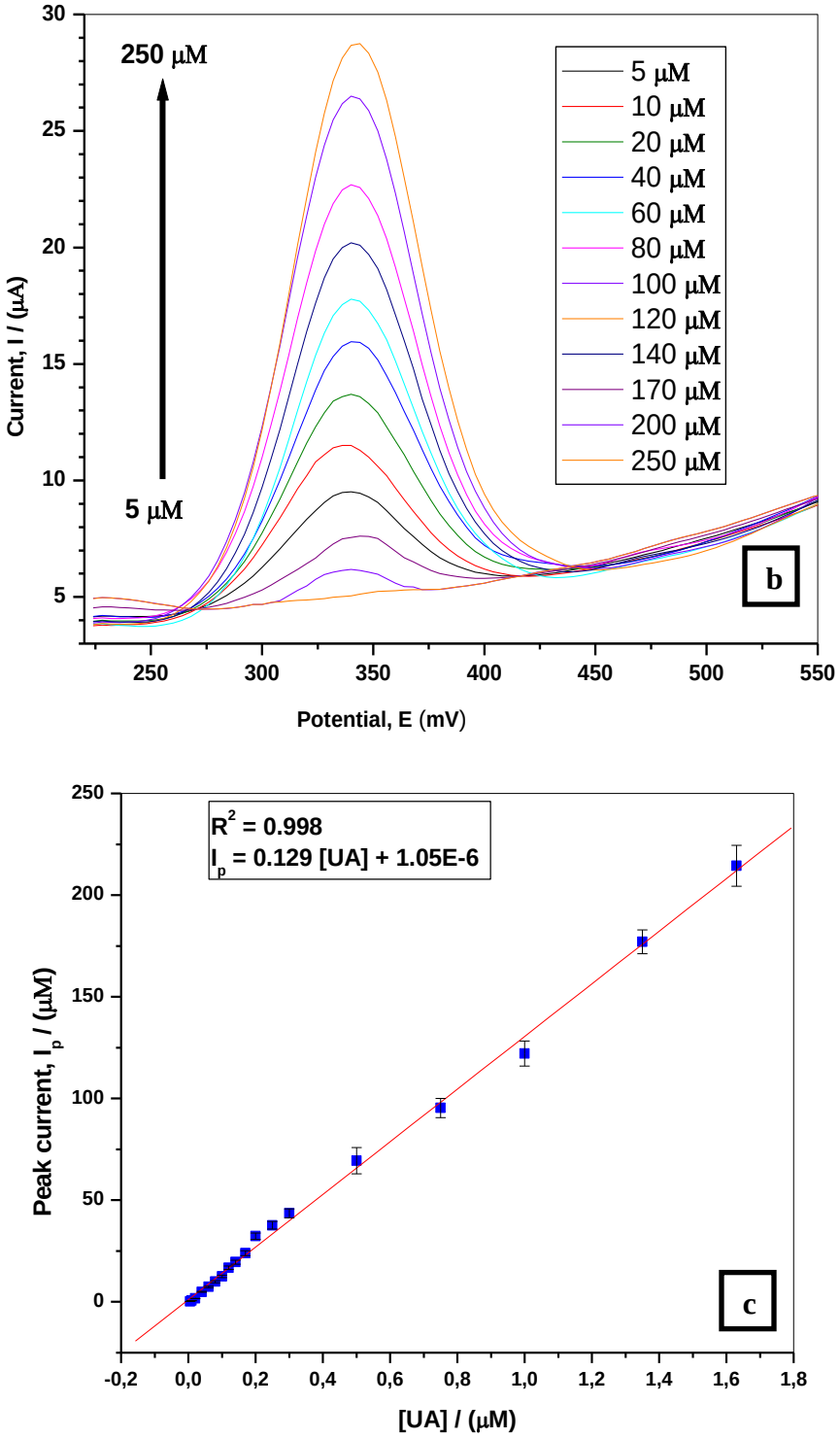

Figure 4.13: (a), (b) Differential pulse voltammograms of AC-Fe_3O_4/GF/GCE modified electrode in 5.0 - 1630.0 µM uric acid prepared in a 0.1 M PBS of pH 6. (**c**) The plot of peak current response against uric acid concentrations.

Table 4.3: Calibration curve parameters.

Differential pulse voltammetry (DPV)	
Concentration range / (mol. L^{-1})	1.63×10^{-3} - 5×10^{-6}
Slope	0.129
Intercept	1.046×10^{-6}
Correlation coefficient (R^2)	0.998
LoD / (mol. L^{-1})	2.55×10^{-6}
LoQ / (mol. L^{-1})	7.703×10^{-6}

Table 4.4 compares the characteristics response of the AC-Fe_3O_4/GF/GCE with other modified electrodes that have been reported for uric acid determination. As shown in the Table, the developed electrode exhibits more appropriate analytical properties, for instance, the pH of the supporting electrolyte system. The limit of detection (LoD) was comparable to that of [21] and lower than that reported by [12], [19], [20], and [22]. The wide linear dynamic range was observed for AC-Fe_3O_4/GF modified electrode for electrochemical determination of UA (5.0 to 1630 µM). This range was quite higher than the reported ranges in references[12], [19], [20], [21], and [22]. Most of the reported work did not show the correlation between the electroactive surface area of the modified electrode and the diffusion coefficient of the analyte of interest. The electroactive surface area of reference [20] was higher than that of AC-Fe_3O_4/GF/GCE, on the contrary; the latter had a higher surface area as compared to reference [19]. This indicates that the higher the electroactive surface area of the modified electrode increases the active sites of the modified electrode and the electrode system is governed by the surface adsorption-controlled electrochemical process which agrees reasonably with other previous reports. To cement that, the diffusion coefficient of uric acid using AC-Fe_3O_4/GF/GCE was calculated to be 12.8×10^{-6} cm^2 s^{-1}, this value was higher than the reported diffusion coefficient [12] and [22].

In addition, the modified electrode can be employed for biological and pharmaceutical analysis of uric acid which can detect a concentration lower than the reported abnormal level (1.49 – 4.46 mM).

Table 4.4: Comparison of the analytical performance of AC-Fe_3O_4/GF/GCE with other reported sensors for uric acid determination.

Sensor	Surface Area /cm^2	pH	Diffusion coefficient (D) / $cm^2\ s^{-1}$	Linear range / (µM)	LOD / (µM)	Ref.
Fe_3O_4@SiO_2/GO/GCE	-	7	3.15×10^{-6}	0.5 - 250	0.07	[12]
MC-GO-Fe_3O_4/GCE	0.163	7	-	0.5 -140	0.17	[19]
H-Fe_3O_4@C/GNs/GCE	0.283	6	-	1.0 - 100	0.41	[20]
3D-GFs/GCE	-	7	-	5 - 500	1.27	[21]
Fe_3O_4@SiO_2/MWCNTS/CPE	-	6	3.70×10^{-6}	0.6 - 100	0.13	[22]
AC-Fe_3O_4/GF/GCE	0.210	7	12.8×10^{-6}	5.0 – 1630	2.55	This work

Abbreviations: CPE-carbon paste electrode**,** GCE-Glassy carbon electrode, MWCNT - multi-wall carbon nanotubes, AC-activated carbon, GF-graphene foam, SiO_2- silicon dioxide, CPE-carbon paste electrode, Fe_3O_4- iron oxide, H-Fe_3O_4 – Hollow iron oxide, GNS – graphene oxide nanosheet, PEDOT - Poly(3,4-ethylene-dioxythiophene), MC - methylcellulose, GO - graphene oxide.

4.3.7 Interference study

The impact of foreign substances was carried out to assess the selectivity of the developed electrochemical sensor AC-Fe_3O_4/GF/GCE. A differential pulse voltammetry technique was performed during these analyses on the selected interfering species based on the fact that they are most likely to be present in human biological samples. The compounds include; glucose, ascorbic acid, lysine, glutamic acid, tartaric acid, and cysteine. Eighty micromolar of the interfering compound was prepared using 0.1 M PSB buffer solution of pH 6. Then 100 µL of the compound was spiked into the buffer solution containing 10 mL uric acid of concentration 60 µM. Tartaric

acid and lysine showed a slightly increased peak current by 5.24% relative to the oxidative peak current of uric acid. While the other foreign interfering compounds; namely glucose, glutamic acid, ascorbic acid, and cysteine showed an average drop of 3.94% in the oxidation peak current of uric acid.

The results shown in Figure 4.14 reveal that no significant changes in the current responses of uric acid in the presence of these species were observed. The results indicated that the Fe_3O_4- AC/GF electrochemical sensor was selective for uric acid determination in the presence of the interfering compounds.

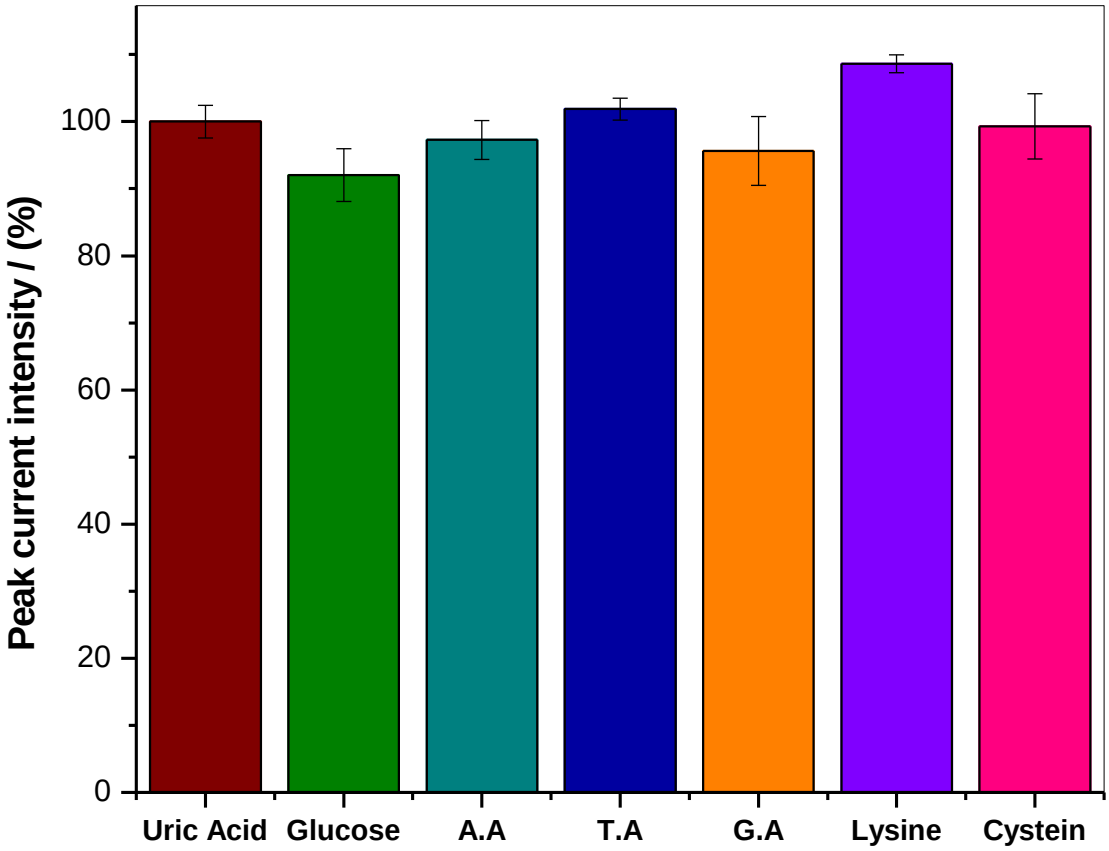

Figure 4.14: The variation of oxidation peak current intensity for interfering compounds concerning uric acid as a percentage by DPV at AC-Fe_3O_4/GF/GCE modified electrode in 0.1 M PBS at a scan rate of 50 mV s^{-1}.

4.3.8 Determination of Uric acid from the urine sample

Abnormal concentration of uric acid in human fluids influences parts of the body systems. This could cause diseases such as gout, obesity, diabetes, and pneumonia. The electrochemical determination of UA in urine as a real sample is one of the most crucial factors for the diagnosis of such diseases and health control. The differential pulse voltammetry technique was performed under optimized conditions for the determination of UA in urine samples. The human urine sample was collected from the local hospital and stored in the refrigerator. For experimental determination of uric acid from human urine, 15 mL of urine sample was first filtered using filter paper. Ten milliliters of the filtrate urine sample was diluted 100-fold with a 0.1 M phosphate buffer solution of pH 6.

The standard addition method was employed for uric acid determination in a human urine sample. Prepared concentrations of 25, 45, 65, and 85 µM uric acid were each spiked into the sample, and the current was measured. The peak current responses were observed to increase with the addition of known concentrations. The linear plot of peak currents against concentration was obtained. From the extrapolated plot, the equation of the straight line was used to calculate the concentration of uric acid in a sample and estimated to be 13.7 µM. This value falls within the range of the level of uric acid in a healthy human [23]. Therefore, the results demonstrate the applicability of the prepared modified electrode in real sample analysis.

The recovery tests were conducted on the urine sample spiked with different concentrations ranging from 10 to 30 µM uric acid, to evaluate the feasibility of the modified electrode.

A hundred microliter of each prepared concentration was spiked into the prepared urine sample. Three determinations for each run were conducted, and the peak current responses were recorded. From the linear plot of peak current as a function of concentration, satisfactory recoveries were obtained as summarized in Table 4.5 (102.2% - 104.3%). An average current response of 4.8% increase was observed, which could indicate that the urine sample might have already had uric acid. This indicates the potential application of AC-Fe_3O_4/GF/GCE for the detection of uric acid in human urine samples.

Table 4.5: Determination of uric acid in human urine sample by differential pulse voltammetry.

Sample	Spiked / (µM)	Found [a] / (µM)	Recovery / (%)	R.S.D. (%) (n = 3)
Urine	10.0	10.36	103.6	0.15
	20.0	20.43	102.2	1.53
	30.0	31.3	104.3	0.3

[a] Average value of three determinations.

4.3.9 Conclusion

A simple, effective, and reproducible method for uric acid determination using a glassy carbon electrode modified with activated carbon-iron oxide/ graphene foam using differential pulse voltammetry has been presented. The optimized instrumental and experimental parameters allowed for consistent and reproducible results. The use of AC-Fe_3O_4/GF/GCE showed a superior electrocatalytic activity compared to bare GCE toward oxidation of uric acid. The modified electrode exhibited a wide linear range and had a detection limit lower than the allowed concentration range of uric acid in a healthy human urine sample, demonstrating its analytical significance. The applicability of the proposed electrochemical sensor was highlighted by its application in a real human urine sample.

4.4 Electrocatalytic studies of dopamine hydrochloride

4.4.1 Electrocatalytic oxidation-reduction of dopamine

As shown in Section 4.2.1, the modified electrode AC-Fe_3O_4/GF/GCE had superior electrocatalytic activity and demonstrated the highest current response in the ferrocyanide redox probe. Hence the labeled electrode was utilized for the subsequent electrochemical experiments of dopamine. Figure 4.15 depicts the cyclic voltammetry responses of 185 µM dopamine in 0.1 M phosphate buffer solution of pH 6 at bare GCE and modified electrode, AC-Fe_3O_4/GF/GCE at the scan rate of 50 mV s^{-1}. The CV technique was performed in the potential window 0.05 – 0.45 V. The black arrow shows the forward scan (oxidation) from 0.05 V to 0.45 V, and the red arrow for the reverse scan (reduction) from 0.45V to 0.05V. Bare GCE manifests less redox peak current intensities with the anodic peak potential (E_{pa}) of 0.281 V and the cathodic peak potential (E_{pc}) of 0.212 V. The voltammograms show the oxidation-reduction process for dopamine 0.069 V ΔE_p.

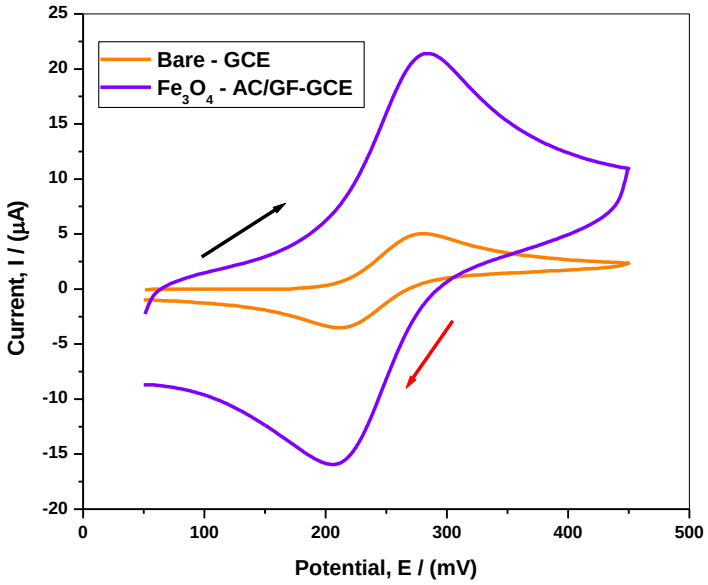

Figure 4.15: Cyclic voltammograms of 185 µM Uric acid in 0.1M Phosphate buffer solution of pH 6, on bare GCE (orange color) and modified GCE, AC- Fe_3O_4/GF/GCE (purple color) at a scan rate of 50 mV s^{-1}.

The modified GCE, AC- Fe_3O_4/GF/GCE demonstrates a rapid current response with the anodic and cathodic peak currents of 5.04 µA and 0.149 µA respectively. These peak currents were 4 times higher than that of bare GCE. The results therefore imply that the surface area of the electrode has increased as shown in section 4.2.1. The fact that the AC-Fe_3O_4/GF/GCE background current was greater than that of bare GCE, indicates the presence of these carbon-based materials and iron oxide used for the development of electrochemical sensors.

Well-defined redox peaks of DA are observed and the peak currents significantly increased at the AC-Fe_3O_4/GF/GCE with the anodic peak potential shifting negatively to 0.278 V and the corresponding cathodic peak potential is 0.211 V. The separation peak potential (ΔE_p) is 0.067 V, indicating that the sensor shows a fast electron transfer process. The high double-layer charging current is responsible for the high background current.

4.4.2 Estimation of the diffusion coefficient of dopamine using modified electrode

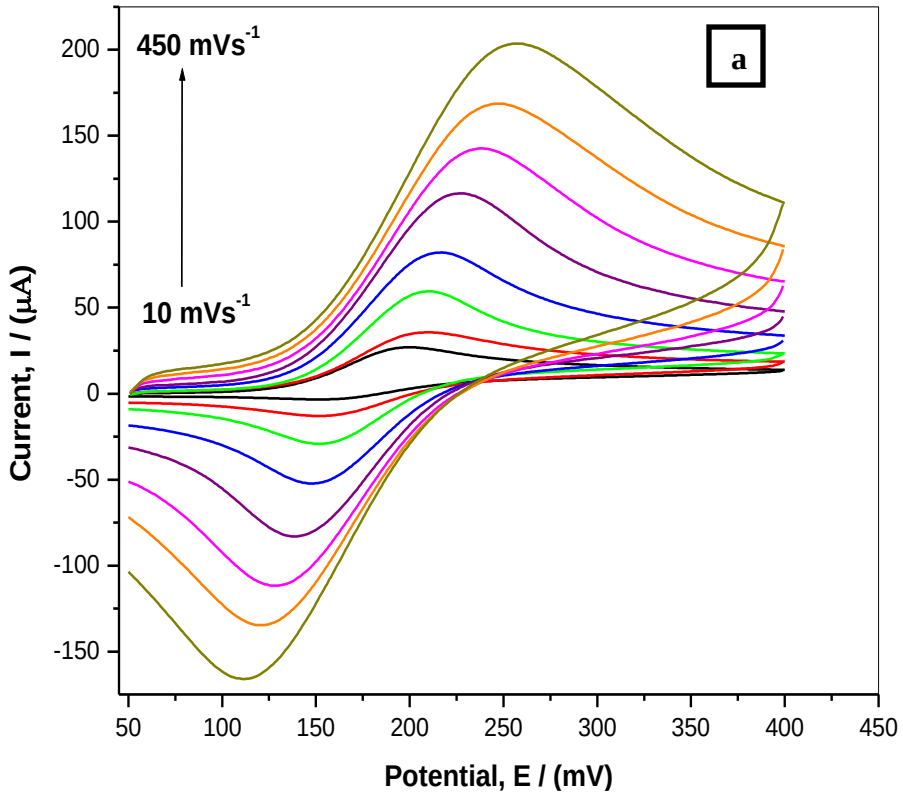

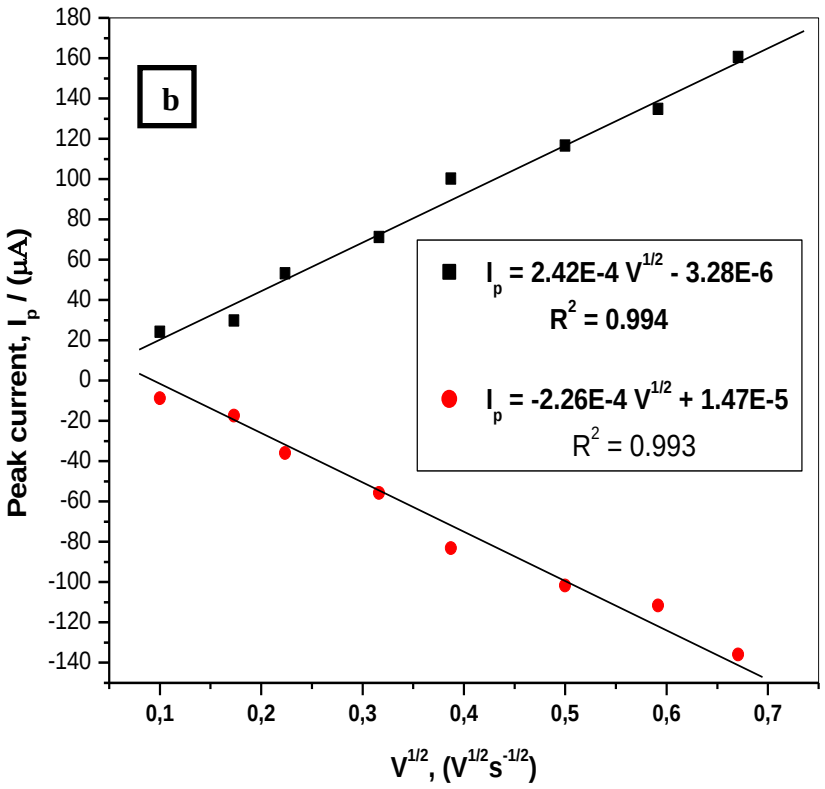

Figure 4.16: (**a**) Cyclic voltammograms of 1 mM dopamines in a 0.1 M phosphate buffer of pH 7, on AC-Fe_3O_4/GF/GCE at different scan rates. (**b**) The plots of the anodic and cathodic peak currents as a function of the square root of the scan rate.

With the calculated electroactive surface area of the modified electrode shown in Section 4.2.1, the diffusion coefficient of dopamine was estimated. Hence with this known surface area, the same experimental procedure was carried out as in Figure 4.6. The cyclic voltammograms of 1 mM dopamine in a 0.1 M phosphate buffer solution of pH 7 were recorded in the range of 10 – 450 mV s^{-1} scan rates as shown in Figure 4.16 (a).

It was observed that both the anodic and cathodic peak currents of dopamine linearly increased with the increasing scan rate. The plot of the anodic and cathodic peak currents as a function of the square root of the scan rate gives a linear response as shown in Figure 4.16 (b). This process consolidates the Rendles-Sevcik equation, which showed us the Mathematical relation that current is directly proportional to the square root of the scan rate.

Randles-Sevcik equation and the slope from the anodic linear plot: $I_p = 0.00242\ V^{1/2} - 3.28 \times 10^{-6}$, with correlation coefficient ($R^2 = 0.994$), were used to calculate the diffusion coefficient (D) of dopamine. The diffusion coefficient was then calculated to be D = 3.97 x 10^{-6} cm^2 s^{-1}. This value was comparable with the reported D values of dopamine at graphene oxide modified glassy carbon electrode, and carbon nanotube paste electrode of 2, 2 – [1, 2-ethanediylbis (nitriloethylidyne)]-bis-hydroquinone with the D = 2.26 (+/-0.01) x 10^{-6} cm^2 s^{-1} and 7.3 x 10^{-6} cm^2 s^{-1} respectively [24], [25]. This reveals that AC-Fe_3O_4/GF/GCE can be an applicable electrochemical sensor for the electrochemical determination of dopamine.

4.4.3 Optimized instrumental parameters toward dopamine detection

The instrumental parameters for differential pulse voltammetric measurements were optimized, these include the pulse width 0.05 s, pulse amplitude 0.05 V, scan rate 50 mV s^{-1}, sample width 0.017 s, potential window 0.0 to 0.4 V, quite time 2 s, and pulse period 0.2 s for catalytic oxidation of dopamine.

4.4.4 Influence of pH on the electrochemical oxidation-reduction of dopamine

The pH of a 0.1 M PBS containing 310 µM dopamine was adjusted with NaOH and HCl aqueous solutions to determine the best optimal pH value for dopamine determination. When compared to the cyclic voltammetric (CV) response, the differential pulse voltammetry technique offers a highly sensitive faradic current because it has a greater impact on the elimination of the double-layer charging current. As a result, DPV was chosen as a more effective technique to find out how the pH of the supporting electrolyte system affects the electrochemical oxidation-reduction of dopamine and achieves high sensitivity.

Figure 4.17 (**a**) shows the plot of differential pulse voltammograms at various pH levels for 310 µM dopamine in 0.1 m PBS. The voltammograms depict that with the increasing pH from 5 to 8, the oxidation peak current increases from pH 5 to 7. A maximum peak current is observed at pH 7. After that, for pH 7.5 and 8, the anodic peak current decreases. Figure 4.17 (b) shows that pH 7 produced the best current response for dopamine. As a result, pH 7 was chosen as the best optimum

pH for further dopamine electrochemical determination. Reproducible voltammograms were obtained for each pH buffer system under three differential pulse runs.

Figure 4.17 (a) further shows that the electro-oxidation peak potentials of dopamine shift in the negative potential direction (from high potential to lower potential), against the pH. This shift in the oxidative peak potential to the negative direction indicates that the electrode process is influenced by protonation reactions. The linear fitting equation for the oxidation peak potential of dopamine as a function of pH was found to be: E_P = - 0.065 pH + 0.659 (R^2 = 0.997). Figure 4.17 (c) is a plot of dopamine oxidation potential as a function of pH. The plot shows a linearly decreasing potential as a function of pH.

The corresponding slope of 65 mV pH^{-1} is close to the theoretical value of the slope of the Nernst equation of 59 mV pH^{-1} [17]. This experimental result indicates that the number of protons and electrons transferred during the electro-oxidation process of dopamine is the same [12]. It has been affirmed that two protons $2H^+$, and two electrons $2e^-$ participate in the redox reactions of DA at the electrode solution interface references [26], [27] as shown by Scheme 4.2.

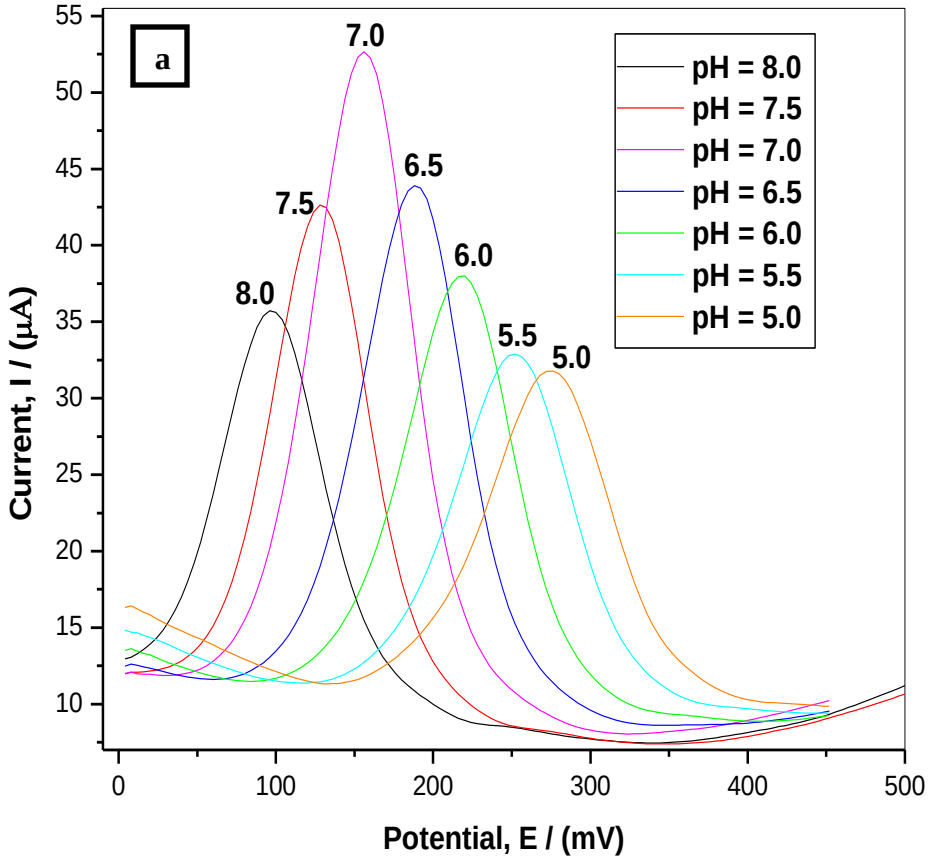
a
7.0
6.5
7.5
6.0
8.0
5.5
5.0
pH = 8.0
pH = 7.5
pH = 7.0
pH = 6.5
pH = 6.0
pH = 5.5
pH = 5.0
Current, I / (μA)
Potential, E / (mV)
55
50
45
40
35
30
25
20
15
10
0
100
200
300
400
500

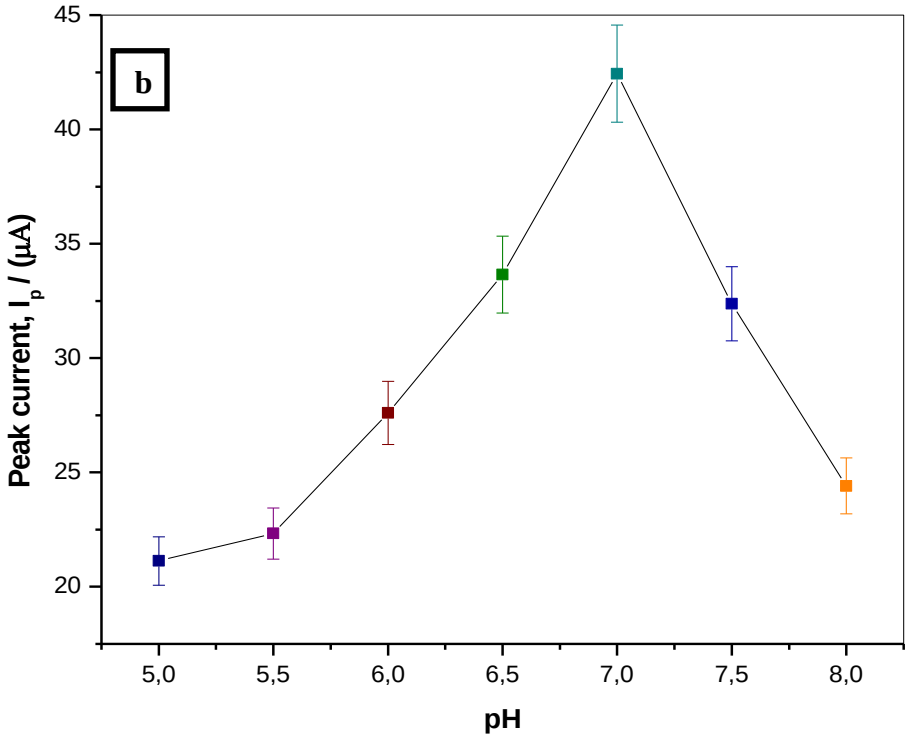
b
Peak current, I_p / (μA)
pH
45
40
35
30
25
20
5,0
5,5
6,0
6,5
7,0
7,5
8,0

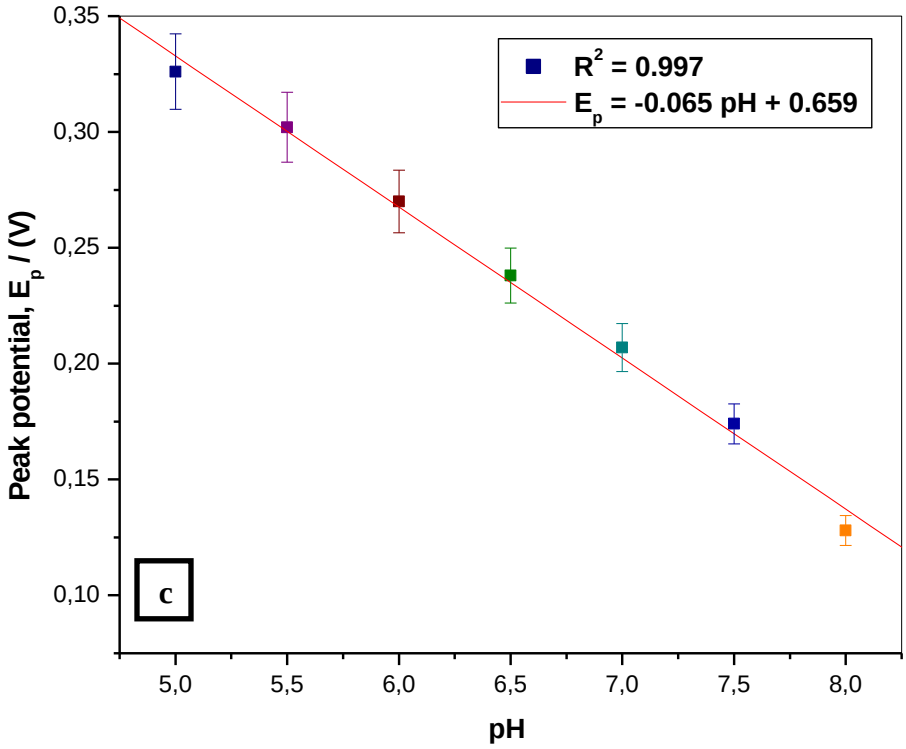

Figure 4.17: (**a**) Differential pulse voltammograms of AC-Fe_3O_4/GF/GCE in 0.1 M PBS containing 310.0 µM DA at different pH, at the scan rate of 50 mV s^{-1}. (**b**) The plot of the electro-oxidation peak current of dopamine as a function of pH. (**c**) The linear dependence of oxidation peak potentials of dopamine against the pH.

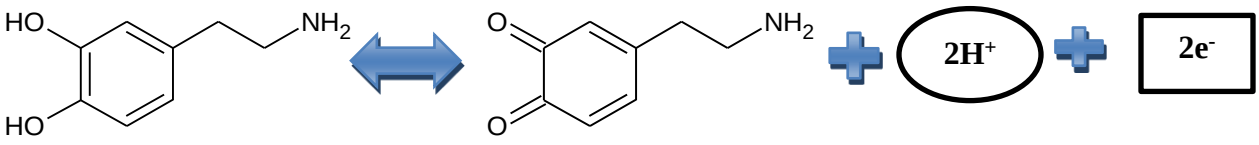

Scheme 4.2: Proposed electrochemical reaction mechanism of dopamine.

4.4.5 Calibration curve and detection limit of dopamine

Under optimal experimental conditions, the proposed sensor has been used to determine different concentrations of dopamine and to confirm the sensitivity of the modified electrode by differential pulse voltammetry (DPV). Table 4.6 summarises the experimental parameters for the calibration curve and detection limit of dopamine. As exhibited in Figure 4.18 (**a**), the differential pulse voltammograms of dopamine at AC-Fe_3O_4/GF/GCE are in the concentration range of 5 to 400 µM. The differential pulse voltammograms of dopamine were carried out in three replicates for each concentration under the optimized parameters to achieve the working range of the modified electrode.

Table 4.6: Optimized differential pulse voltammetric experimental parameters**.**

Optimized parameters	Value
Supporting electrolyte (0.1M Phosphate Buffer Solution)	pH 7.0
Scan Rate	50 mV s^{-1}
Pulse width	0.05 s
Pulse amplitude	0.05 V
Sample width	0.017 s
Potential window	(0.0 to 0.4)V
Pulse Period	0.2 s
Quite time	2 s

As shown in Figure 4.18 (a), the peak currents gradually increased with increasing dopamine concentrations, and the linear calibration plot was obtained as shown in Figure 4.18 (b).

For concentrations lower than 5 µM, oxidation peak current for DA was not observed, and thus 5 µM was noted as the lowest concentration. While concentrations of DA above 400 µM gave constant and/or comparable oxidation peak currents. This indicates that for concentrations above 400 µM, there was no existence of the diffusion process taking place and no concentration gradient.

It was therefore noted that the linear range of the electrode at AC-Fe_3O_4/GF/GCE is 5 to 400 µM. Figure 4.18 (b) further depicts a linear calibration plot of the peak current as a function of the concentration of dopamine. The corresponding linear equation was found to be: $I_p = 0.085$ [DA] + 2.49 x 10^{-6} and correlation coefficient ($R^2 = 0.997$), where I_p is the DPV peak current in µA. From the linear plot, the limit of detection (LoD) and the limit of quantification (LoQ) were determined to be 1.47 µM, and 4.91 µM respectively. These were calculated using the following equations: LoD = 3 (***s***/***m***) and LoQ = 10 (***s***/***m***). Where ***s*** is the relative standard deviation of the intercept of the y-coordinate from the linear fit plot and ***m*** is the slope of the same line.

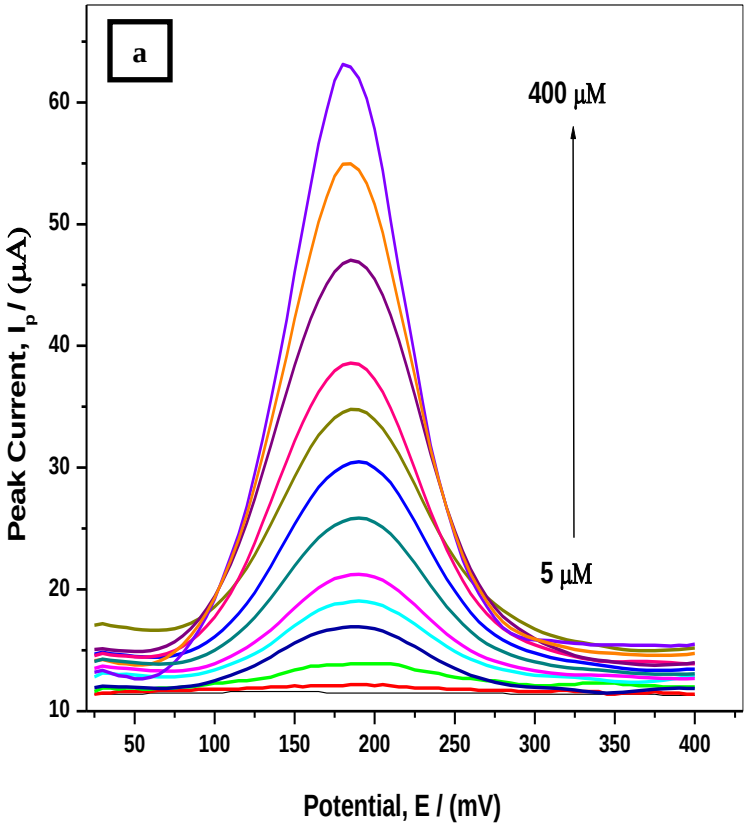

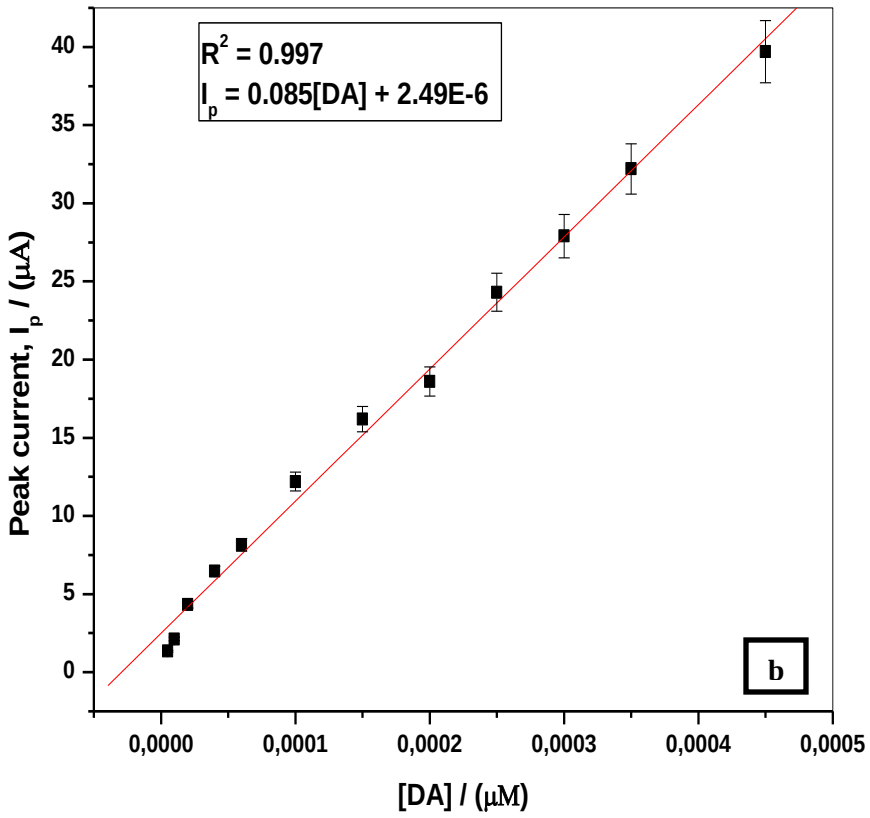

Figure 4.18: (a) Differential pulse voltammograms of the AC-Fe_3O_4/GF/GCE modified electrode in 5 - 450.0 µM of dopamine prepared in a 0.1 M PBS of pH 7. (**b**) The plot of pulse peak current as a function of dopamine concentrations.

The performance of the AC-Fe_3O_4/GF electrochemical sensor demonstrates superior electrocatalytic activity. This can be explained in terms of the large surface area calculated from Figure 4.6 with high catalytic sides, better crystallinity of activated carbon-iron oxide composite, and high conductivity graphene foam to facilitate ion diffusion and electron transfer easily.

Table 4.7 summarizes data from the electroanalysis of dopamine.

Table 4.7: Calibration curve parameters.

Differential pulse voltammetry	
Concentration range /(mol. L^{-1})	2.5×10^{-6} - 450×10^{-6}
Slope	0.0857
Intercept	1.87×10^{-6}
Correlation coefficient (r)	0.997
LoD (mol.L^{-1})	1.47×10^{-6}
LoQ (mol.L^{-1})	4.91×10^{-6}

The characteristic response of AC-Fe_3O_4/GF/GCE and other modified electrodes used for dopamine determination are compared in Table 4.8. The prepared sensor has more appropriate analytical properties, such as the pH of the supporting electrolyte, as shown in the Table.

The limit of detection and pH of the supporting electrolyte was comparable to that of reference [30] and [28], [32], [33] respectively. The pH values of 7.0 – 7.5, correlate to that of human blood medium, and therefore the developed electrode possesses good properties in terms of pH medium as the human blood. The wide linear range was obtained at AC-Fe_3O_4/GF/GCE for dopamine determination, which was comparable to that of reference [28] and higher than that of reference [29], [30], [31], and [32].

Again, the electroactive surface area was high as compared to reference [29], [30] and it was also observed that a high surface leads to a better diffusion coefficient of dopamine. A pencil graphite electrode modified with copper-oxide nanoparticles in 88 µM dopamine gave D = 3.29 x 10^{-6} cm^2 s^{-1} [30], and graphene oxide on GCE with D = 2.26 (+/-0.01) x 10^{-6} cm^2 s^{-1} [31].

Perhaps, this is associated with the excellent conductivity and enhanced surface area of the fabricated electrode material. Apart from this, the material synthesis involves a low-cost and rapid single-step synthesis strategy through which AC-Fe_3O_4 composite was obtained.

The data acquired is evident that the fabricated electrode material may be used for magnificent sensing abilities concerning better linear ranges, high electroactive surface area, and high diffusion coefficient of dopamine.

Table 4.8: Comparison of the analytical performance of AC- Fe_3O_4/GF/GCE with other reported sensors for dopamine determination.

Modifier	pH	Surface area /cm^2	Linear range / (µM)	LoD / (µM)	Diffusion	Ref.
MWCNTs/WO_3/GCE	7	-	20 – 500	0.018	5.43×10^{-8}	[28]
MnO_2/PEDOT/rGO/GCE	6.6	0.100	0.05 – 135	0.03	3.28×10^{-5}	[29]
Cu/Cu_xO NPs/PGE	5.8	0.08	0.3 - 53	1.06	3.29×10^{-6}	[30]
GO/GCE	5	-	1.0 - 15	0.27	2.26×10^{-6}	[31]
Graphene/GCE	7.4	-	4.0 - 100	2.64	-	[32]
Au-ZnONCAs/GF/ITO	7.5	-	0.0 - 80	0.04	-	[33]
AC-Fe_3O_4/GF/GCE	7	0.210	5 – 450	1.47	3.97×10^{-6}	This work

Abbreviations: MWCNT - multi-wall carbon nanotubes, GO - graphene oxide, rGO – reduced graphene oxide, AC-activated carbon, GF-graphene foam, tungsten oxide (WO_3), copper(x)-oxide nanoparticles, manganese-oxide (MnO_2), poly (3,4-ethylene dioxythiophene)-PEDOT, x-variable oxidation states of the cupper (Cu_x), Fe_3O_4- iron oxide, Au-ZnONCAs - gold nanoparticles-zinc oxide nanocone arrays, LoD – limit of detection.

4.4.6 Interference study on dopamine

The influence of some selected compounds was used as potential interferences capable of interrupting the voltammetric current response for dopamine at AC-Fe_3O_4/GF/GCE. The differential pulse voltammetry technique was used for the electrochemical oxidation of dopamine in the absence and presence of interfering compounds. The following are some foreign substances that were used namely ascorbic acid (A.A.), tartaric acid (T.A.), glutamic acid (G.A.), cysteine, lysine, and glucose. The selection of these species was based on the fact that they exist in the same medium as dopamine. Eighty micromolar of these compounds were prepared in a 0.1 M PBS of pH 7. The addition of 100 µL of each foreign compound into a 10 mL buffer solution containing 60 µM dopamine was examined using differential pulse voltammetry.

Figure 4.19 shows the variation of oxidation peak current intensities as a percentage for interfering compounds. The modified electrode had anti-interfering behavior towards the electro-oxidation of dopamine in the presence of interfering species with an average of only a 1.75% current drop on the peak current response. Hence, these results indicate that the proposed AC-Fe_3O_4/GF as an electrode modifier can be used to monitor real-time sample analysis for dopamine. Another predominant factor is that the results did not exhibit any significant interference peak current. This indicates the excellent selectivity of the modified electrode towards DA. As depicted in Figure 4.19, these materials had no significant effects on the DA sensing ability of the electrode at the tested concentrations; thus suggesting that the developed electrode has an outstanding selectivity toward DA determination.

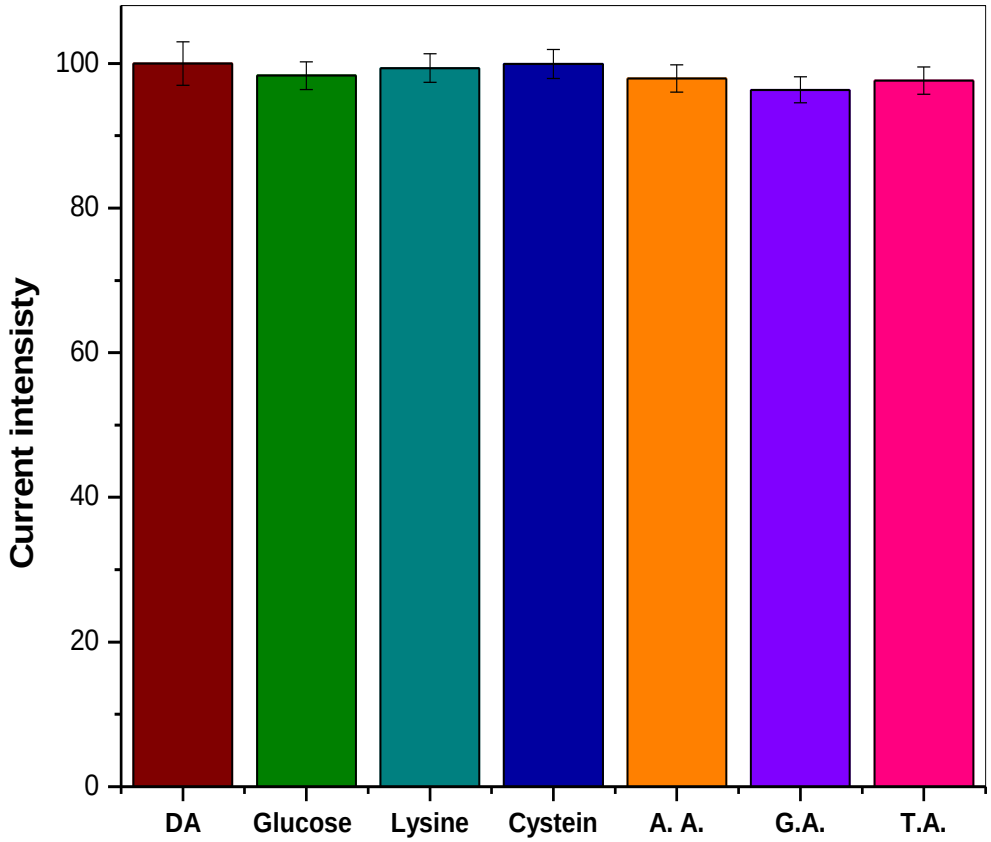

Figure 4.19: The variation of oxidation peak current intensity for interfering compounds concerning dopamine as a percentage by DPV at AC- Fe_3O_4/GF/GCE modified electrode in 0.1 M PBS at a scan rate of 50 mV s^{-1}.

4.4.7 Determination of Dopamine from the urine sample

To investigate the application of the prepared electrode in the real sample, a human urine sample was used. The electrochemical determinations were carried out to establish the application of the AC- Fe_3O_4/GF/GCE modified electrode toward dopamine in the urine sample. To determine the concentration of dopamine present in the urine sample, the differential pulse voltammetry technique was carried out under conditions that were optimized. The human sample was collected from a local hospital and stored in the refrigerator at - 4℃. Before experimental measurements, 15 mL of urine sample was filtered using filter paper. Then 10 mL of the filtrate was diluted 100-fold with 0.1 M PBS of pH 7.

A human urine sample was used to determine dopamine using the standard addition method. Each of the prepared concentrations of 25, 45, 65, and 85 µM of dopamine was spiked into the sample for 100 microliters, and the peak currents were recorded. When known concentrations were added, it was observed that the peak current responses increased. The peak currents were plotted against the concentrations and a linear equation was obtained. The dopamine concentration in a sample was estimated to be 1.52 µM using the equation of the straight line from the extrapolated plot. Therefore, the results show that the modified electrode that was prepared can be used in real-world sample analysis.

To determine the feasibility of the modified electrode, recovery tests were performed on urine samples spiked with dopamine at concentrations ranging from 10 to 30 µM. The prepared urine sample was spiked with 100 µL of each prepared concentration. The current responses were recorded and three determinations were made for each run. Table 4.9 summarizes the satisfactory recoveries that were obtained from the linear plot of peak current as a function of concentrations (101.0% - 104.75%). There are slightly higher than 100% recoveries, which could mean that the sample had some dopamine at a very low concentration. The sensor therefore could prove the presence of dopamine in human urine samples. As can be observed from standard addition method results, a human urine sample could have dopamine as a biological sample. The experimental results confirm that the AC- Fe_3O_4/GF as an electrochemical sensor can be used for the detection of DA in clinical health and or to diagnose human diseases related to a high level of DA.

Table 4.9: Determination of dopamine in human urine sample by differential pulse voltammetry.

Sample	**Spiked (µM)**	**Found [a] / (µM)**	**Recovery/ (%)**	**R.S.D. (%) (n = 4)**
Human urine	10.0	10.41	104.9	1.39
	20.0	20.95	104.75	0.497
	30.0	30.30	101.0	1.65

[a] Average value of four determinations**.**

4.4.8 Conclusion

The electrochemical detection of dopamine using differential pulse voltammetry with AC-Fe_3O_4/GF/GCE has been successfully demonstrated. The modified electrode gave promising current responses for the determination of dopamine in aqueous solutions. The interference experiments showed that the presence of activated carbon, graphene foam, and iron oxide during dopamine sensing did not suffer from the matrix effect. This shows that the developed electrode has an outstanding selectivity and sensitivity towards DA determination.

The electrochemical sensor demonstrated superior electrocatalytic activity and improved the electroactive surface area of the modified electrode. The experimental results confirm that the AC-Fe_3O_4/GF as an electrochemical sensor can be used for the detection of DA in clinical health.

4.5 Electrocatalytic studies of dopamine hydrochloride and uric acid

4.5.1 Electrocatalytic oxidation-reduction of dopamine and uric acid

The electrochemical behavior of the developed electrochemical sensor was investigated using cyclic voltammetry for the mixture of 200 µM uric acid and dopamine in a 0.1 M PBS of pH 6. The potential window of 0.1 to 0.5 V with reference Ag/AgCl satd'd KCl and scan rate of 50 mV s^{-1} were used. Figure 4.19 below shows the redox process of uric acid and dopamine at bare GCE and different modified electrodes. On a bare glassy carbon electrode (yellow voltammogram) redox peaks for DA were observed at 0.258 V (oxidation) and 0.192 V (reduction) and the oxidation peak for uric acid was observed at 0.394 V. When GCE was modified with graphene foam (violet voltammogram), the peak current intensities of both uric acid and dopamine increased relative to bare GCE. The peak currents for redox peaks were three times higher than that of unmodified GCE. There was a positive shift in the oxidation peak of dopamine at 0.262 V and uric acid at 0.405 V. On the reverse scan, a small reduction peak was observed for uric acid at around 0.344 V potential and also reduction peak for dopamine was observed at 0.191 V. In the presence of activated carbon-iron oxide/graphene foam (AC-Fe_3O_4/GF/GCE) electrochemical sensor (magenta voltammogram), the peak current responses were enhanced showing the catalytic efficiency of the sensor [34]. The redox peaks for dopamine were well defined and that of uric acid but with a small reduction peak on the reverse scan showing that the chemical reaction is faster than the redox process. The separated peaks of the two compounds were observed, and this could be due to high electrical conductivity and large effective surface area of AC-Fe_3O_4/GF leading to the enhanced electrocatalysis of the electrode surface. The modified electrode proved to have superior properties towards UA and DA. Therefore, this implies that the simultaneous determination of these two compounds of interest can be feasible.

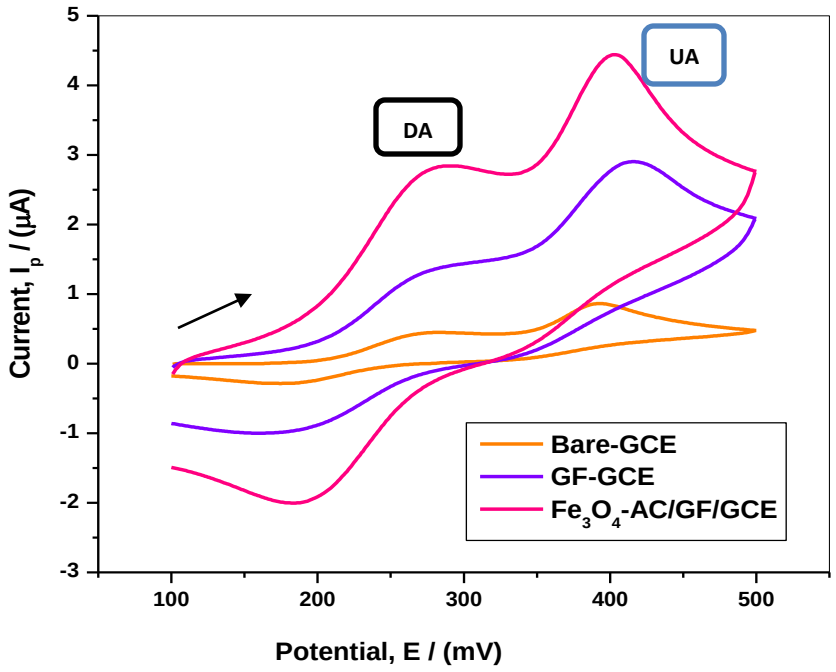

Figure 4.20: Cyclic voltammograms of 200 µM uric acid and dopamine using 0.1 M Phosphate buffer solution, pH 6, on bare GCE, GF/GCE, and AC- Fe_3O_4/GF/GCE at the scan rate of 50 mV s^{-1}**.**

4.5.2 Optimized instrumental parameters toward simultaneous detection of uric acid and dopamine

The instrumental parameters for differential pulse voltammetric measurements were optimized, these include the pulse amplitude 0.05 V, pulse width 0.05 s, sample width 0.017 s, potential window 0.0 to 0.4 V, scan rate 50 mV s^{-1}, and pulse period 0.2 s for simultaneous detection of dopamine and uric acid.

4.5.3 Effect of the scan rate on dopamine and uric acid oxidation-reduction process

Figure 4.20 **(a)** shows the cyclic voltammograms on 200 µM of DA and UA prepared in 0.1 M buffer solution of pH 6, at different scan rates on the AC-Fe_3O_4/GF/GCE modified electrode. The scan rate ranged from 5 to 300 mV s^{-1}. The oxidation peak currents gradually increase with increasing scan rate and also the peak potentials were slightly shifted to the positive direction. As

the scan rates increased, the oxidation peak currents also increased linearly. Figure 4.20 (**b**) displayed the anodic peak current as a function of the square root of the scan rate for uric acid and exhibited a linear response indicating that the charge transfer reaction was diffusion-controlled.

On the same note, figure 4.21 (**c**) shows the anodic and cathodic peak currents for dopamine were both proportional to the square root of the scan rate. This indicates that the electrode reaction of these two compounds was controlled by diffusion [35].

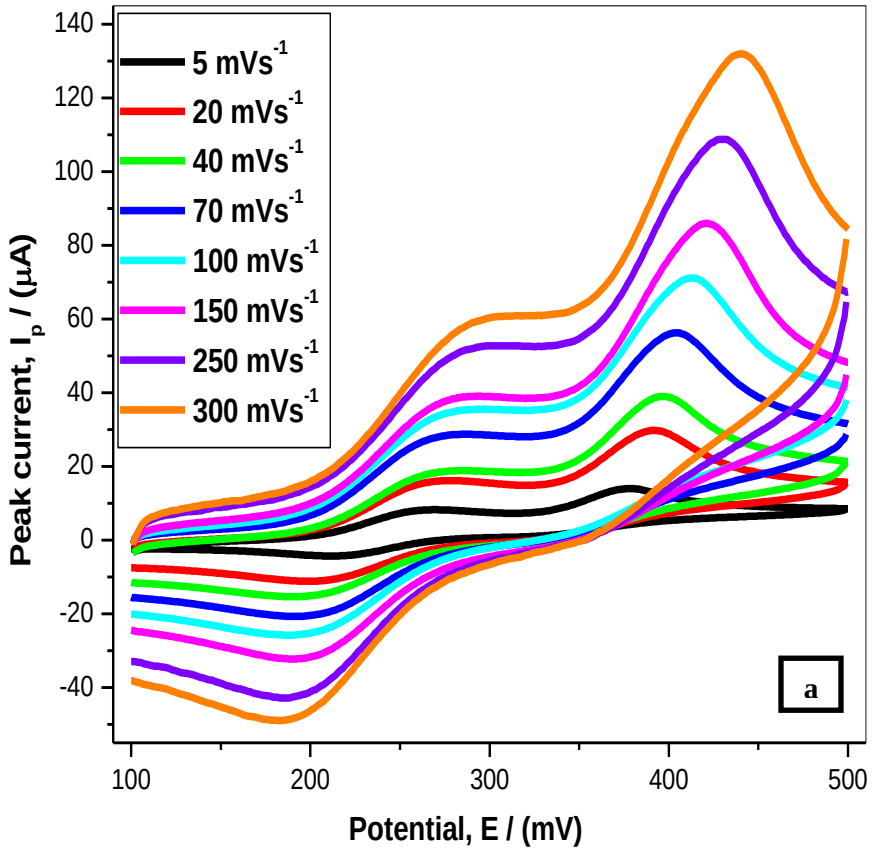

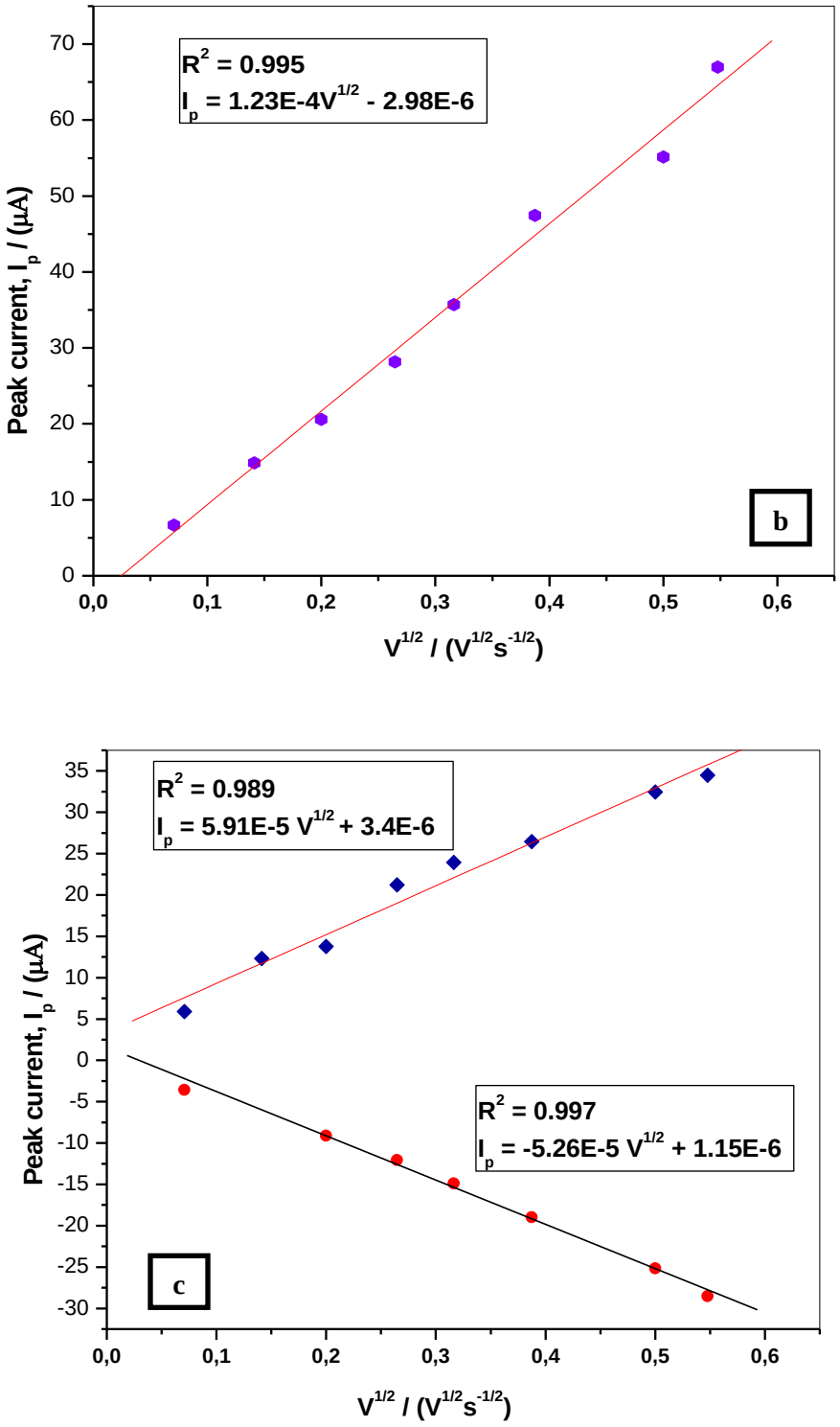

Figure 4.21: (a) Cyclic voltammograms of 200 µM DA and UA in 0.1 M phosphate buffer solution (pH 6) on AC-Fe_3O_4/GF/GCE at different scan rates. **(b)** The plot of the anodic peak current against the square root of the scan rate for uric acid (UA). **(c)** The plots of the anodic and cathodic peak currents as a function of the square root of the scan rate for dopamine (DA).

4.5.4 Influence of pH on dopamine and uric acid oxidation process

The influence of pH on the anodic peak current and peak potential of 200 μM UA and DA prepared in 0.1 M phosphate buffer solution at the modified electrode, AC-Fe_3O_4/GF/GCE, was investigated in the range of pH 4.0 to 8.0. The aqueous solutions of NaOH and HCl were used to adjust the desired pH. For determining how the pH of the supporting electrolyte system affects the electrochemical oxidation of uric acid and dopamine, and to achieve high sensitivity, differential pulse voltammetry was chosen as a more effective technique.

Figure 4.21 **(a)** shows the anodic peak currents of dopamine and uric acid against the pH. The plot shows that with increasing pH from 4 to 6.5, the oxidation peak current response of dopamine increases. After that, for pH 7 to 8, the anodic peak currents decrease. On the other hand, from pH 4 to 5, the oxidation peak current for uric acid was observed to increase with the increasing pH. For pH 5.5 to 8, there was a huge decline in terms of peak current. As a result, pH 5 and 6.5 produced the maximum anodic peak currents response for uric acid and dopamine respectively. Hence for the simultaneous determination of UA and DA, these pH values were chosen as the optimum pH values as the ideal pH for the electrochemical detection of DA and UA in the subsequent experiments due to their high oxidation peak currents. The maximum separation of individual oxidation peak potentials of DA and UA was observed under this condition. Furthermore, the electro-oxidation peak potentials shifted in the negative direction with the increasing pH indicating that the deprotonation step in the electrocatalytic oxidation processes occurs more easily with increasing pH [36].

In addition, the relationship between peak potential as a function of pH was obtained as: for DA: $E_{pa} = 0.604 - 0.0613$ pH ($R^2 = 0.995$), and for UA: $E_{pa} = 0.767 - 0.064$ pH ($R^2 = 0.9992$) as shown in Figure 4.21 (**b**). The slopes of DA, and UA were -61.3 $mVpH^{-1}$, and -64 $mVpH^{-1}$, respectively, which were close to the theoretical value -59 mV pH^{-1} [37], demonstrating that the electrode process is a two-proton and electron transfer process as shown by Schemes 4.1 and 4.2.

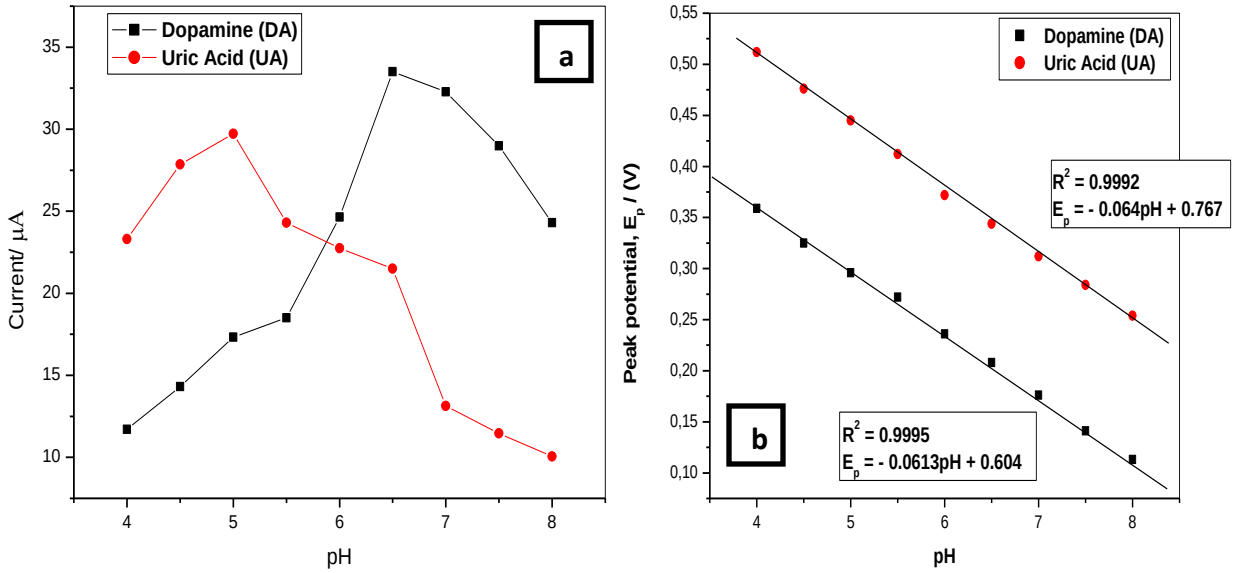

Figure 4.22: The plot of oxidation peak current for dopamine and uric acid in 0.1 M PBS containing (200 µM) of UA and DA at 50 mV s^{-1} scan rate as a function of pH. **(b)** The linear dependence of peak potentials for dopamine and uric acid against the pH.

4.5.5 Calibration curve and detection limits of dopamine and uric acid

To obtain the analytical utility of the AC-Fe_3O_4/GF/GCE, the simultaneous determination of each analyte in a mixture was investigated by DPV. Figure 4.22 displays DPV voltammograms of AC-Fe_3O_4/GF/GCE modified electrode for the simultaneous determination of dopamine and uric acid. The simultaneous electrochemical oxidation of dopamine and uric acid was observed at 0.2 V and 0.35 V and the peak separation between these two peaks was obtained to be 150 mV. This peak-to-peak separation was good enough to distinguish oxidative peak current for both uric acid and dopamine.

Figure 4.22 (**a**) shows the differential pulse voltammograms of dopamine at different concentrations in the presence of constant 60 µM UA concentration on AC-Fe_3O_4/GF/GCE modified GCE, at the scan rate of 50 mV s^{-1}. Different concentrations of DA ranging from 5.0 to 400 µM were prepared in 0.1 M PBS pH 6.5. The electro-oxidation peak current of dopamine was directly proportional to increasing concentrations as shown in Figure 4.23 (**b**). As illustrated in this Figure, the calibration curve was obtained with the linear equation: I_p = 0.1106 [DA] + 1.963

x 10^{-6}, and correlation coefficient (R^2 = 0.995). From this data, the limit of detection and quantification were calculated and the results were tabulated in Table 4.10.

These results demonstrated that changing the concentration of dopamine has no obvious influence on the oxidation of uric acid. Therefore simultaneous determination of this mixture is possible without uric acid oxidation peak current response affecting that of dopamine. Based on the optimized experimental conditions, Figure 4.22 (c) shows a differential pulse current response with increasing concentrations of uric acid ranging from 2.5 to 450 µM in the presence of 60 µM dopamine prepared in 0.1 M PBS of pH 5. The peak current increases linearly in the potential window from 0 to 0.5 V with increasing concentration as depicted in Figure 4.22 (c). From Figure 4.22 (c) calibration curve was obtained with the linear equation: I_p = 0.109 [DA] - 1.71 x 10^{-6}, and correlation coefficient (R^2 = 0.996). From this data, the limit of detection and quantification were calculated and the results were tabulated in Table 4.10. These were calculated using the following equations: LoD = 3.3 (**s**/**m**) and LoQ = 10 (**s**/**m**). Where ***s*** is the relative standard deviation of the intercept of the y-coordinate from the linear fit plot and **m** is the slope of the same line.

These results also demonstrated that changing the concentration of uric acid has no obvious influence on dopamine oxidation peak current. Therefore simultaneous determination of this mixture is possible without interference.

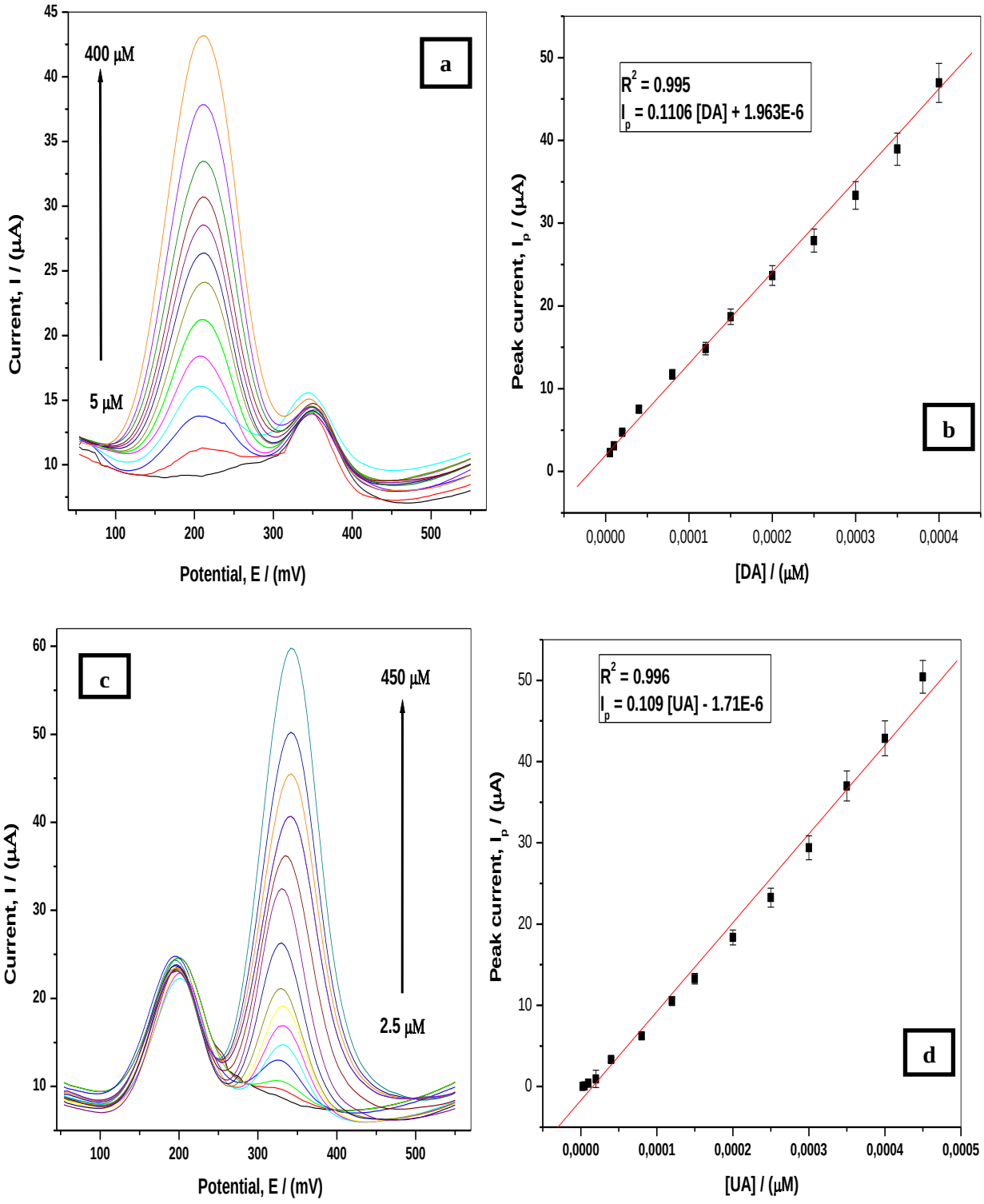

Figure 4.23: (a) and **(c)** Differential pulse voltammograms of 60.0 µM uric acid (UA) and different concentrations of dopamine (DA) (5.0 – 400) µM at pH = 6.5, 60.0 µM dopamine (DA) and different concentrations of uric acid (UA) (2.5 – 450) µM at pH 5, n = 3. **(b)** and **(d)**

The plots of peak current response for dopamine and uric acid as a function of concentrations respectively.

Table 4.10: Calibration curve parameters.

Differential pulse voltammetry (Parameters)	**Dopamine (DA)**	**Uric acid (UA)**
Concentration range / (mol.L^{-1})	400×10^{-6} - 5×10^{-6}	450×10^{-6} - 2.5×10^{-6}
Slope	0.1106	0.109
Intercept	1.963×10^{-6}	1.71×10^{-6}
Correlation coefficient (r)	0.995	0.996
LoD (mol.L^{-1})	2.7×10^{-6}	1.75×10^{-6}
LoQ (mol.L^{-1})	8.07×10^{-6}	5.84×10^{-6}

In comparison with the reported work conducted on the mixture of uric acid and dopamine, the AC-Fe_3O_4/GF/GCE modified electrode results are compared as shown in Table 4.11.

The detection limits were comparable to references [38] and [39] for uric acid but with a higher linear dynamic range as compared to references [38], [39], and [41]. For dopamine, the detection limit was lower than reference [39] and [41] but higher than reference [38] and [40]. However, the modified electrode possesses a good linear range as compared to reference [38], [39], and [41]. From the perspective of LoDs toward UA and linear range, AC-Fe_3O_4/GF /GCE still occupies a unique advantage in the simultaneous detection of DA and UA. It should also be noted that the literature on electrochemical detection of the mixture of DA and UA, the determination of electroactive surface area, and the diffusion coefficients of the analytes of interest were very scarce. Therefore, this signifies the novelty of this study, especially using AC- Fe_3O_4/GF/GCE as an electrochemical sensor.

Table 4.11: Comparison of the analytical performance of AC- Fe_3O_4/GF/GCE on the simultaneous determination of dopamine and uric acid with other reported sensors towards a mixture of dopamine and uric acid.

Sensor	Method	Linear range / (µM)		LoD / (µM)		Ref.
		UA	DA	UA	DA	
Au/rGO/GCE	DPV	8.8 - 53	6.8 - 41	1.4	1.8	[38]
GF/CNTs/GNPsGCE	DPV	0.1 - 48	0.5 - 60	1.36	33.03	[39]
PEDOT/rGO/GCE	DPV	0.1 - 901	0.1 - 701	0.6	0.2	[40]
OPEDOT-AuNPs/GCE	SWV	4 - 100	20 - 100	1.0	5.0	[41]
AC-Fe_3O_4/GF/GCE	DPV	2.5 - 450	5.0 - 400	1.75	2.7	This work

Abbreviations: MWCNT – multi-wall carbon nanotubes, GO - graphene oxide, Au- gold, AuNPS – gold nanoparticles, rGO – reduced graphene oxide, poly (3,4-ethylene dioxythiophene)-PEDOT, AC-activated carbon, GF-graphene foam, GNPs - graphene nanoparticles, Fe_3O_4- iron oxide, LoD – Limit of detection.

4.5.6 Interference study on uric acid and dopamine

Lastly, to evaluate the anti-interference ability of AC-Fe_3O_4/GF/GCE, the following are some foreign compounds that were used as potential interference substances; ascorbic acid, tartaric acid, glutamic acid, cysteine, lysine, and glucose.

Although the concentrations of both DA and UA mixture were the same, they possess different diffusion coefficients, and that signifies their different mass transportation from the electrolyte medium to the surface area of the electrode where the redox process takes place. Therefore we cannot anticipate getting the same electro-oxidation peak current for both dopamine and uric acid as depicted in Figure 4.24.

Figure 4.24 illustrates the variation of oxidation peak currents for interfering compounds concerning dopamine (DA), and uric acid (UA) at AC-Fe_3O_4/GF modified electrode in 60 µM of DA and UA mixture prepared in 0.1 M PBS of pH 6. Eighty µM of each interfering compound was prepared in a 0.1 M phosphate buffer of pH 6. The addition of 100 µL into a 10 mL buffer solution containing a 60 µM mixture was analyzed under differential pulse voltammetry. The modified electrode had anti-interfering behavior towards the electro-oxidation of dopamine and uric acid, in the presence of interfering compounds with an average of only a 1.4% and 3.04% current drop on the DPV current response for DA and UA respectively. While only a 0.63% current increase was observed for UA in the presence of the l-lysine compound.

Thus, these results indicate that the proposed sensor can be used to monitor real-time sample analysis, and another predominant factor is that the results do not exhibit any significant interference signals. This indicates the excellent selectivity of the modified electrode towards simultaneous electroanalysis of DA and UA. As depicted in Figure 4.24, these materials had no significant effects on the UA and DA sensing ability of the electrode at the tested concentrations; thus suggesting that the developed electrode has an outstanding selectivity toward both UA and DA determination.

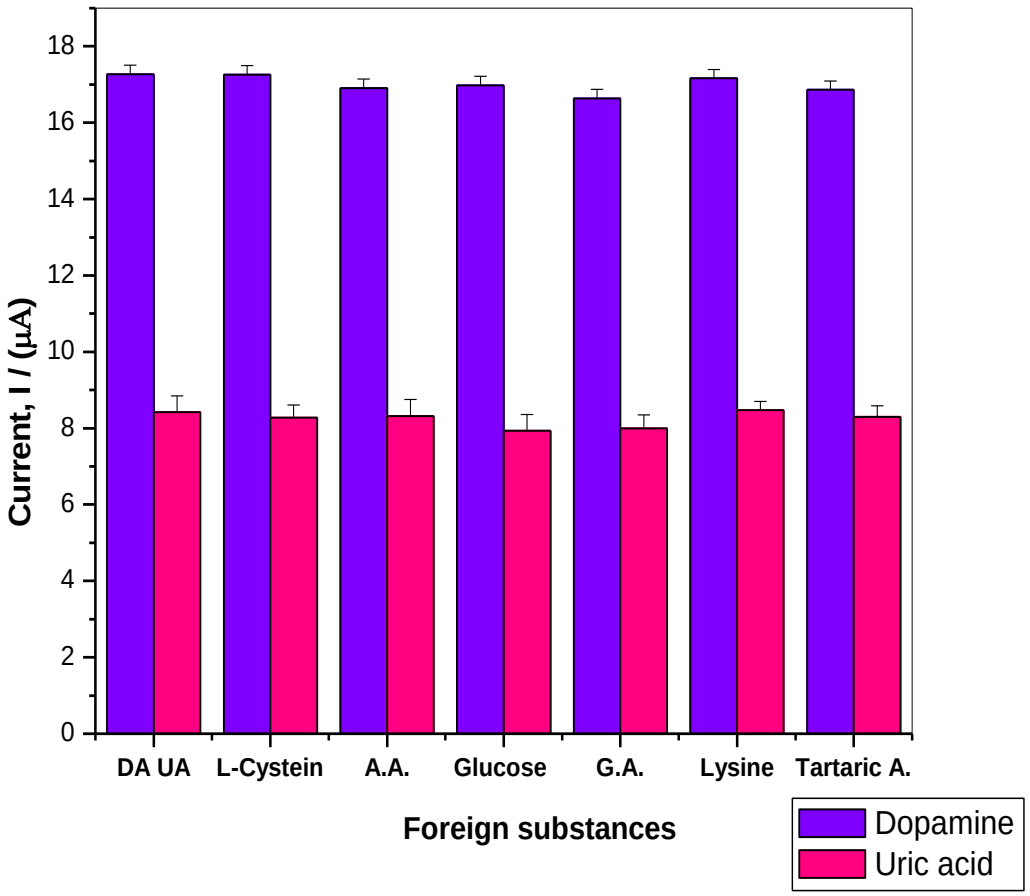

Figure 4.24: The variation of oxidation peak current intensity for interfering compounds concerning 60 µM dopamine and uric acid by DPV at AC-Fe_3O_4/GF/GCE modified electrode in 0.1 M PBS at a scan rate of 50 mV s^{-1}.

4.5.7 Determination of dopamine and uric acid in the urine sample

For the evolution of the applicability of the proposed sensor, DA and UA in human urine samples were analyzed at the AC-Fe_3O_4/GF /GCE. The differential pulse voltammetry method was used under optimized conditions to ascertain the dopamine and uric acid concentrations present in the urine sample.

The standard addition method was used to determine dopamine and uric acid concentrations from a human urine sample. The peak currents were recorded after each of the prepared concentrations of 20, 40, 60, and 80 µM of the mixture was spiked into the sample for 100 µL. The peak current

responses were observed to rise when known concentrations of the mixture were added. Linear equations were derived by plotting the oxidation peak currents against the concentrations. The straight-line equations from the extrapolated plots were used to estimate the sample's uric acid and dopamine concentrations to be 1.606 µM and 0.522 µM, respectively. As a result, the findings demonstrate that the prepared modified electrode can be utilized in actual sample analysis.

The prepared different concentrations of 10, 20, and 30 µM of DA and UA were each spiked into the prepared human serum samples, and the DPV experimental results are shown in Table 4.12. The recoveries of the spiked samples were detected within the range of 95.6% – 100.3%, indicating that the assay could be potentially used for the determination of dopamine and uric acid in real samples.

Table 4.12: Determination of dopamine and uric acid in human urine samples by differential pulse voltammetry less than 3.0%, indicating that the assay could be potentially used for the determination.

Sample	**Spiked / (µM)**	**Found [a] / (µM)**		**Recovery (%)**		**R.S.D. (%)**	
		DA	**UA**	**DA**	**UA**	**DA**	**UA**
Urine	10.0	9.56	9.75	95.6	97.5	0.58	1.25
	20.0	20.06	19.62	100.3	98.8	1.396	1.76
	30.0	28.84	29.74	96.13	99.13	2.94	3.94

a Average value of four determinations.

The application of AC- Fe_3O_4/GF/GCE for simultaneous determination of uric acid in urine samples (n = 3). All concentrations are in µM.

4.5.8 Conclusion

Uric acid and dopamine were simultaneously investigated using the modified glassy carbon electrode, AC-Fe_3O_4/GF/GCE. The oxidation of these two analytes was found to be resolved by both GF/GCE and AC-Fe_3O_4/GF/GCE, with the latter being superior in terms of its increased surface area and current sensitivity. The electroanalytical performance of the AC-Fe_3O_4/GF/GCE was evaluated in comparison to a bare GCE, and GF/GCE using cyclic voltammetry and other reported literature. The differential pulse voltammetry provided linear calibrations with detection limits of 1.75 µM for uric acid and 2.7 µM for dopamine. The modified electrode was found to be a good sensor for directly determining both dopamine and uric acid in real urine samples due to its high selectivity and good antifouling ability. A new sensor prototype that can selectively detect dopamine and or uric acid in a variety of foods, pharmaceuticals, and human serum samples is anticipated to emerge from the fabricated sensor.

References

1. Petcharoen, K., & Sirivat, A. J. (2012). Synthesis and characterization of magnetite nanoparticles via the chemical co-precipitation method. *Materials Science and Engineering*: *B*, *177*, 421-427.

2. Zakaria, R., Jamalluddin, N. A., & Bakar, M. Z. A. (2021). Effect of impregnation ratio and activation temperature on the yield and adsorption performance of mangrove based activated carbon for methylene blue removal. *Results in Materials*, *10*, 100183.

3. Mirghni A.A., Madito M.J., Masikhwa T.M., Oyedotun K.O., Bello A., Manyala N. (2017). Hydrothermal synthesis of manganese phosphate/graphene foam composite for electrochemical supercapacitor applications. *Journal of Colloid Interface Sci*. *15*, 325-337.

4. Ping, Y., Gong, Y., Fu, Q., & Pan, C. (2017). Preparation of three-dimensional graphene foam for high performance supercapacitors. *Progress in Natural Science: Materials International*, *27*, 177-181.

5. Ouyang, Z. W., Chen, E. C., & Wu, T. M. (2015). Thermal stability and magnetic properties of polyvinylidene fluoride/magnetite nanocomposites. *Materials*, *8*, 4553-4564.

6. Omri, A., & Benzina, M. (2012). Characterization of activated carbon prepared from a new raw lignocellulosic material: Ziziphus spina-christi seeds. *Journal de la Société Chimique de Tunisie*, *14*, 175-183.

7. Huang, M., Wang, C., Quan, L., Nguyen, T. H. Y., Zhang, H., Jiang, Y., ... & Ruoff, R. S. (2020). CVD growth of porous graphene foam in film form. *Matter*, *3*, 487-497.

8. Alam, S., Khan, M. S., Bibi, W., Zekker, I., Burlakovs, J., Ghangrekar, M. M., ... & Zahoor, M. (2021). Preparation of activated carbon from the wood of Paulownia tomentosa as an

efficient adsorbent for the removal of acid red 4 and methylene blue present in wastewater. *Water*, *13*, 1453.

9. Awwad, A. M., & Salem, N. M. (2012). A green and facile approach for synthesis of magnetite nanoparticles. *Nanoscience and Nanotechnology*, *2*, 208-213.

10. Idris, A. O., Orimolade, B. O., Mafa, P. J., Kuvarega, A. T., Feleni, U., & Mamba, B. B. (2022). Carbon-Nanodots modified glassy carbon electrode for the electroanalysis of selenium in water. *Results in Chemistry*, *4*, 100394.

11. Fernández, L., & Carrero, H. (2005). Electrochemical evaluation of ferrocene carboxylic acids confined on surfactant–clay modified glassy carbon electrodes: oxidation of ascorbic acid and uric acid. *Electrochimica Acta*, *50*, 1233-1240.

12. Movlaee, K., Norouzi, P., Beitollahi, H., Rezapour, M., & Larijani, B. (2017). Highly selective differential pulse voltammetric determination of uric acid using modified glassy carbon electrode. *International Journal of Electrochem. Sci*, *12*, 3241-3251.

13. Eteya, M. M., Rounaghi, G. H., & Deiminiat, B. (2019). Fabrication of a new electrochemical sensor based on AuPt bimetallic nanoparticles decorated multi-walled carbon nanotubes for determination of diclofenac. *Microchemical Journal*, *144*, 254-260.

14. Huang, X. J., Im, H. S., Yarimaga, O., Kim, J. H., Lee, D. H., Kim, H. S., & Choi, Y. K. (2006). Direct electrochemistry of uric acid at chemically assembled carboxylated single-walled carbon nanotubes netlike electrode. *The Journal of Physical Chemistry B*, *110*, 21850-21856.

15. Rajabi, H., Noroozifar, M., & Sabbaghi, N. (2017). Electrochemical determination of uric acid using nano resin modified carbon paste electrode as a new sensor. *J. Matter. Applied Sci*, *1*, 1002-1006.

16. Guan, J. F., Zou, J., Liu, Y. P., Jiang, X. Y., & Yu, J. G. (2020). Hybrid carbon nanotubes modified glassy carbon electrode for selective, sensitive and simultaneous detection of dopamine and uric acid. *Ecotoxicology and Environmental Safety*, *201*, 110872.

17. Kamyabi, M. A., & Shafiee, M. A. (2012). Electrocatalytic oxidation of dopamine, ascorbic acid and uric acid at poly2, 6 diaminopyridine on the surface of carbon nanotubes/gc electrodes. *Journal of the Brazilian Chemical Society*, *23*, 593-601.

18. Gupta, V.B. and Shrivastava, A. (2011) Methods for the Determination of Limit of Detection and Limit of Quantitation of the Analytical Methods. *Chronicles of Young Scientists*, *2*, 21-25

19. Esmail S., Elnaz M. K., Pantea R., Ebrahim N., Mehdi R. N., and Farhad A. (2020), Electrochemical sensor based on modified methylcellulose by graphene oxide and Fe3O4 nanoparticles: Application in the analysis of uric acid content in urine. *Journal of Electroanalytical Chemistry*, *877*, 1572-6657.

20. Song, H., Xue, G., Zhang, J., Wang, G., Ye, B. C., Sun, S., ... & Li, Y. (2017). Simultaneous voltammetric determination of dopamine and uric acid using carbon-encapsulated hollow Fe 3 O 4 nanoparticles anchored to an electrode modified with nanosheets of reduced graphene oxide. *Microchimica Acta*, *184*, 843-853.

21. Jiang, J., Wang, J., Wang, P., Lin, X., & Diao, G. (2023). Three-dimensional graphene foams with two hierarchical pore structures for metal-free electrochemical assays of

dopamine and uric acid from high concentration of ascorbic acid. *Journal of Electroanalytical Chemistry*, *928*, 117056 (1-8).

22. Beitollahi, H., Ebadinejad, F., Shojaie, F., & Torkzadeh-Mahani, M. (2016). A magnetic core–shell Fe_3O_4@ SiO_2/MWCNT nanocomposite modified carbon paste electrode for amplified electrochemical sensing of amlodipine and hydrochlorothiazide. *Analytical Methods, 8*, 6185-6193.

23. Maiuolo, J., Oppedisano, F., Gratteri, S., Muscoli, C., & Mollace, V. (2016). Regulation of uric acid metabolism and excretion. *International Journal of Cardiology*, *213*, 8-14.

24. Gao, F., Cai, X., Wang, X., Gao, C., Liu, S., Gao, F., & Wang, Q. (2013). Highly sensitive and selective detection of dopamine in the presence of ascorbic acid at graphene oxide modified electrode. *Sensors and Actuators B: Chemical*, *186*, 380-387.

25. Mazloum-Ardakani, M., Beitollahi, H., Ganjipour, B., Naeimi, H., & Nejati, M. (2009). Electrochemical and catalytic investigations of dopamine and uric acid by modified carbon nanotube paste electrode. *Bioelectrochemistry*, *75*, 1-8.

26. Ejaz, A., Joo, Y., & Jeon, S. (2017). Fabrication of 1, 4-bis (aminomethyl) benzene and cobalt hydroxide@ graphene oxide for selective detection of dopamine in the presence of ascorbic acid and serotonin. *Sensors and Actuators B: Chemical*, *240*, 297-307.

27. Łuczak, T. (2008). Electrochemical oxidation of dopamine in the presence of secondary amine. An alternative way for quantitative dopamine determination at a gold electrode. *Electroanalysis: An International Journal Devoted to Fundamental and Practical Aspects of Electroanalysis*, *20*, 1639-1646.

28. Zheng, A. L. T., Andou, Y., & Zawawi, R. M. (2017). Voltammetric determination of dopamine mediated by nanoparticle WO_3/MWCNT modified glassy carbon electrode. *Int. J. Appl. Chem*, *13*, 899-912.

29. Promsuwan, K., Soleh, A., Saisahas, K., Saichanapan, J., Kanatharana, P., Thavarungkul, P., ... & Limbut, W. (2021). Discrimination of dopamine by an electrode modified with negatively charged manganese dioxide nanoparticles decorated on a poly (3, 4 ethylenedioxythiophene)/reduced graphene oxide composite. *Journal of Colloid and Interface Science*, *597*, 314-324.

30. Bahrami, E., Amini, R., & Vardak, S. (2021). Electrochemical detection of dopamine via pencil graphite electrodes modified by Cu/CuxO nanoparticles. *Journal of Alloys and Compounds*, *855*, 157292.

31. Gao, F., Cai, X., Wang, X., Gao, C., Liu, S., Gao, F., & Wang, Q. (2013). Highly sensitive and selective detection of dopamine in the presence of ascorbic acid at graphene oxide modified electrode. *Sensors and Actuators B: Chemical*, *186*, 380-387.

32. Kim, Y. R., Bong, S., Kang, Y. J., Yang, Y., Mahajan, R. K., Kim, J. S., & Kim, H. (2010). Electrochemical detection of dopamine in the presence of ascorbic acid using graphene modified electrodes. *Biosensors and Bioelectronics*, *25*, 2366-2369.

33. Yue, H. Y., Zhang, H. J., Huang, S., Lu, X. X., Gao, X., Song, S. S., ... & Guan, E. H. (2020). Highly sensitive and selective dopamine biosensor using Au nanoparticles-ZnO nanocone arrays/graphene foam electrode. *Materials Science and Engineering: C*, *108*, 110490.

34. Arvand, M., & Ghodsi, N. (2014). Electrospun TiO_2 nanofiber/graphite oxide modified electrode for electrochemical detection of l-DOPA in human cerebrospinal fluid. *Sensors and Actuators B: Chemical*, *204*, 393-401.

35. Gupta, V.B. and Shrivastava, A. (2011) Methods for the Determination of Limit of Detection and Limit of Quantitation of the Analytical Methods. *Chronicles of Young Scientists, 2*, 21-25

36. Zheng, J., & Zhou, X. (2007). Sodium dodecyl sulfate-modified carbon paste electrodes for selective determination of dopamine in the presence of ascorbic acid. *Bioelectrochemistry*, *70*, 408-415.

37. Du, J., Yue, R., Yao, Z., Jiang, F., Du, Y., Yang, P., & Wang, C. (2013). Nonenzymatic uric acid electrochemical sensor based on graphene-modified carbon fiber electrode. *Colloids and Surfaces A: Physicochemical and Engineering Aspects*, *419*, 94-99.

38. Wang, C., Du, J., Wang, H., Zou, C. E., Jiang, F., Yang, P., & Du, Y. (2014). A facile electrochemical sensor based on reduced graphene oxide and Au nanoplates modified glassy carbon electrode for simultaneous detection of ascorbic acid, dopamine and uric acid. *Sensors and Actuators B: Chemical*, *204*, 302-309.

39. Huang, B., Liu, J., Lai, L., Yu, F., Ying, X., Ye, B. C., & Li, Y. (2017). A free-standing electrochemical sensor based on graphene foam-carbon nanotube composite coupled with gold nanoparticles and its sensing application for electrochemical determination of dopamine and uric acid. *Journal of Electroanalytical Chemistry*, *801*, 129-134.

40. Dinesh, B., Vilian, A. E., Kwak, C. H., Huh, Y. S., Saraswathi, R., & Han, Y. K. (2019). The facile and simple synthesis of poly (3, 4-ethylenedioxythiophene) anchored reduced graphene oxide nanocomposite for biochemical analysis. *Analytica Chimica Acta*, *1077*, 150-159.

41. Pan, J., Liu, M., Li, D., Zheng, H., & Zhang, D. (2021). Overoxidized poly (3, 4-ethylenedioxythiophene)–gold nanoparticles–graphene-modified electrode for the simultaneous detection of dopamine and uric acid in the presence of ascorbic acid. *Journal of Pharmaceutical Analysis*, *11*, 699-708.

Chapter 5
Conclusion and Recommendations

5.1 Conclusion

Through chemical vapor deposition of graphene foam (GF), co-precipitation of iron oxide (Fe_3O_4), and use of activated carbon (AC), the AC-Fe_3O_4/GF electrochemical sensor was successfully developed, resulting in a high product yield, cost-effectiveness, and environmentally green catalytic composite. This exploration work describes the fruitful fabrication of an electrochemical sensor based on activated carbon, iron oxide, and graphene foam-modified electrodes for the electrochemical detection of a few chosen biological molecules (uric acid and dopamine). Various characterization methods, such as Energy Dispersive X-ray Spectroscopy (EDS), Fourier Transform Infrared Spectroscopy (FT-IR), X-ray diffraction Spectroscopy (XRD), and Scanning Electron Microscopy (SEM), were used to investigate the AC-Fe_3O_4/GF composite's distinctive characteristics.

Cyclic voltammetry studies of a variety of modified electrodes revealed that, in contrast to the other electrodes, the AC-Fe_3O_4/GF/GCE electrode had well-defined peak resolution and peak separation in the ferrocyanide redox system, as well as rapid electron transfer. The voltammetry measurement of physiologically related molecules like uric acid and dopamine is made possible by the AC-Fe_3O_4/GF/GCE electrode's enhanced electrocatalytic performance.

The bare glassy carbon electrode (GCE) and the modified AC-Fe_3O_4/GF/GCE electrode had electroactive surface areas of 0.0596 cm^2 and 0.210 cm^2, respectively, indicating that the modified electrode was easier to transfer electrons. According to the voltammetric data that were obtained, the GF/GCE electrode had a lower ΔEp value of (114 mV), which lends credence to numerous publications' claims regarding graphene-based materials' demonstrated improved electron transport properties. However, the AC-Fe_3O_4/GF/GCE electrode's current response was the highest (125 µA).

The optimal buffer conditions (0.1 M phosphate buffer solution), pH, scan rate, and differential pulse voltammetry parameters were used to create this modified electrode for the dopamine and

uric acid sensors, allowing for a satisfactory current response and rapid detection of the target analytes.

The electrocatalytic redox process of the individual uric acid (UA) and dopamine (DA) was performed using the cyclic voltammetry technique and the redox peaks at the AC-Fe_3O_4/GF/GCE electrode were observed at 0.44 V for UA and (0.28 V and 0.21 V) for DA. That is, only an anodic peak current was observed for uric acid (5 mM) and both anodic and cathodic peak currents were observed for dopamine (185 µM). About 7.2 µA current response was observed for uric acid on AC-Fe_3O_4/GF/GCE while on bare electrode 3.4 µA current was observed. For dopamine electroanalysis, 22.5 µA anodic peak current and -16.5 µA cathodic peak current were observed on the modified electrode and 5 µA anodic and -4.8 µA were observed on bare GCE. The developed electrochemical sensor proved an outstanding high sensitivity and improved catalytic property of the modified GCE.

Cyclic voltammetry conducted a scan rate study on uric acid and dopamine, and linear graphs defined by equations were produced by plotting oxidation peak currents as a function of the square root of the scan rate: with correlation coefficients of $R^2 = 0.989$ and $R^2 = 0.994$, $I_p = -9.5 \times 10^{-6} V^{1/2} + 6.94 \times 10^{-5}$, $I_p = 2.42 \times 10^{-4} V^{1/2} - 3.28 \times 10^{-6}$, respectively. On the AC-Fe_3O_4/GF/GCE electrode, these relationships suggested a diffusion-controlled process for uric acid and dopamine. The modified electrode was used to calculate the diffusion coefficients for uric acid and dopamine,12.8×10^{-6} cm^2 s^{-1} for Uric acid, and 3.97×10^{-6} cm^2 s^{-1} for dopamine were obtained, which were comparable to the diffusion coefficients that were reported for these candidates using various modified electrodes.

Plots of current versus UA and DA concentrations using an AC-Fe_3O_4/GF/GCE electrode were used to determine the LoD (2.55 µM), LoQ (7.703 µM), and LoD (1.47 µM), LoQ (4.91 µM) respectively, for individual uric acid and dopamine detection. For these individual measurements, the linear range for UA was (1630 to 5 µM, and for DA, it was 2.5 to 450 µM). Again, differential pulse voltammetry (DPV) was used at the modified electrode to perform simultaneous uric acid and dopamine measurements. Uric acid's LoD (1.75 µM), LoQ (5.84 µM), and dopamine's LoD (2.7 µM) and LoQ (8.07 µM) were calculated. The measurement was made at concentrations ranging from 450 to 2.5 µM for UA and 400 to 5 µM for DA.

In addition, the proposed sensor demonstrated excellent selectivity and anti-interference behavior when it came to detecting selected biological samples even when some species were interfering. The real sample analysis was set up to see if the new AC-Fe_3O_4/GF/GCE sensor could be used in human urine samples. The constructed sensor's percentage recoveries for uric acid and dopamine concentrations indicate its potential for determining the analyte in urine samples.

5.2 Recommendations

- ✓ The adaptability of the modified electrode utilized in this research work can be additionally studied by applying it to various redox species.

- ✓ While metal oxide coupled with carbon-based materials used in this work enhanced the peak current of uric acid and dopamine, it will be good to try different types of carbon nanomaterials since they are economically accessible and possess lesser negative environmental effects.

- ✓ The development of inexpensive, simple, and readily available sensors that can detect biological molecules down to nanomolar concentrations with high selectivity can be a focus for future work.

- ✓ The effect of particle size on the materials used for electrode modification can also be studied for optimization.

Appendices

Formulae used:

- LoD = 3.3 (***s***/m)
- LoQ = 10 (***s***/m)
- $\Delta E_p = E_{pc} - E_{pa}$
- $I_p = 2.69 \times 10^5 \, n^{3/2} \, A \, C \, D^{1/2} \, V^{1/2}$, at 25^{o}C.